Using Movement Intention EEG In Rehabilitation

Usman Rashid

A thesis submitted to Auckland University of Technology
in partial fulfilment of the requirements for the degree of
Doctor of Philosophy (PhD)

2019

Health and Rehabilitation Research Institute

Copyright

Declaration

I hereby declare that this submission is my own work and that, to the best of my knowledge and belief, it contains no material previously published or written by another person nor material which to a substantial extent has been accepted for the qualification of any other degree or diploma of a university or other institution of higher learning.

_____

Signature of student

Acknowledgements

I would like to thank the participants who contributed their valuable time to this research by participating in my experimental studies. I deeply appreciate the multifaceted contributions of my supervisors; Prof. Denise Taylor, Dr. Nada Signal and Dr. Imran Khan Niazi; to my research and their support throughout my PhD journey. I am thankful to all the members of the Neurorehabilitation Research Team at Auckland University of Technology, New Zealand for adding value to my research with feedback and conducive discussions.

Special thanks to Professor Dario Farina (Imperial College London, U.K.), Mads Jochumsen (Centre for Sensory-Motor Interaction, Department of Health Science and Technology, Aalborg University, Denmark) and Laurens R. Krol (Technische Universitat Berlin, Berlin, Germany) for their invaluable feedback on parts of my research. I would like to acknowledge the advice given by Associate Professor Alain C. Vandal (Auckland University of Technology, New Zealand) on optimisation and statistical analysis methods.

I appreciate the time taken by Rasmus Nedergaard, Samran Navid (Aalborg University, Denmark), Sylvain Cremoux (University of Valenciennes and Hainaut-Cambresis, France) and Darko Bejakovich (Auckland University of Technology, New Zealand) for testing parts of the software developed and used in my PhD.

I am thankful to Sharon Olsen (Auckland University of Technology, New Zealand) for reviewing and proof reading parts of this thesis.

Dedication

I dedicate this study to my loving father, Rashid Ahmad Chattha.

Abstract

Stroke causes brain injury and is a major cause of long term disability in New Zealand and across the world. Scientific evidence shows that our nervous system is plastic and adapts itself to this injury in order to recover from disability. One promising research area which aims to enhance brain's plasticity for faster and greater recovery following stroke is an intervention which involves temporally associating repeated electrical stimulation to affected limb to coincide with the intention to move the limb. This intervention achieves temporal association by using a Brain Computer Interface (BCI) to interpret Movement-related Cortical Potentials (MRCPs) recorded with Electroencephalography (EEG) to identify the intention to move. There is an increasing body of laboratory based research evidence which supports this rehabilitation intervention. However for successful translation of this intervention into clinical practice, research to support the development of a mobile and usable medical device is required. In this thesis I have comprehensively examined the gaps in the scientific knowledge which hinder development of this intervention to support its uptake in clinical practice. To address the key gaps I have proposed a blueprint of a BCI which has potential to be developed into an affordable, mobile and usable rehabilitation medical device. I have proposed and evaluated the different components required for this BCI within three experimental studies. In the first study I have evaluated the performance of a low power small footprint cost effective analogue to digital converter in recording MRCPs against a laboratory based gold standard system. In the second study I have proposed a method

for automated labelling of MRCPs. In the third study I have proposed an optimisation method along with extending an existing algorithm for enhancing the detection of movement onset and offset from surface electromyography. Moreover, the conceptual blueprint and the evidence generated by this thesis contributed to the development of a prototype rehabilitation medical device at a national technology challenge. Future research should focus on how such a device can be embedded into clinical practice.

Publications

U. Rashid, I. K. Niazi, N. Signal, D. Taylor, An EEG Experimental Study Evaluating the Performance of Texas Instruments ADS1299, Sensors 18 (2018) 3721, doi:10.3390/s18113721

U. Rashid, I. K. Niazi, M. Jochumsen, L. R. Krol, N. Signal, D. Taylor, Automated Labeling of Movement-Related Cortical Potentials using Segmented Regression, IEEE Transactions on Neural Systems and Rehabilitation Engineering, April 2019, doi:10.1109/TNSRE.2019.2913880

U. Rashid, I. K. Niazi, N. Signal, D. Farina, D. Taylor, Optimal Automatic Detection of Muscle Activation Intervals, Journal of Electromyography and Kinesiology, June 2019, doi:10.1016/j.jelekin.2019.06.010

Candidate Contributions to Co-authored Papers

Contributions:

Rashid, U., Niazi, I., Signal, N., & Taylor, D. (2018). An eeg experimental study evaluating the performance of texas instruments ads1299. *Sensors*, *18*(11), 3721.	Rashid Niazi Signal Taylor	85% 5% 5% 5%
Rashid, U., Niazi, I. K., Jochumsen, M., Krol, L. R., Signal, N., & Taylor, D. (2019). Automated labelling of Movement-Related Cortical Potentials using Segmented Regression. *IEEE Transactions on Neural Systems and Rehabilitation Engineering*.	Rashid Niazi Jochumsen Krol Signal Taylor	80% 4% 4% 4% 4% 4%
Rashid, U., Niazi, I. K., Signal, N., Farina, D., & Taylor, D. (2019). Optimal Automatic Detection of Muscle Activation Intervals. *Journal of Electromyography and Kinesiology*.	Rashid Niazi Signal Farina Taylor	80% 5% 5% 5% 5%

Signatures:

Usman Rashid (Student)

Denise Taylor (Primary Supervisor)

Nada Signal (Secondary Supervisor)

Imran Khan Niazi (Tertiary Supervisor)

Mads Jochumsen (Collaborator)

Laurens Ruben Krol (Collaborator)

Dario Farina (Collaborator)

Contents

Glossary

assessment of motor training To quantify changes in cortical activity after a motor training task.. 31

PN Peak negative value in a MRCP. 50, 61

PNT Time of PN value. 61

prototype system The prototype system based on Texas Instruments ADS1299 on OpenBCI Cyton Board V3-32 and Compumedics Neuroscan Quick-Cap. 57

S/D Participant wise ratio of power values in step on/off to those in dorsiflexion. 66

Acronyms

ADC Analog to Digital Converter. 11, 34, 46, 51, 53, 79, 139

BCI Brain Computer Interface. 20, 23, 31, 139

BCIs Brain Computer Interfaces. 10, 20, 31, 50, 55, 139

BP Bereitschaftspotential. 24

BP1 Early Bereitschaftspotential. 24, 42, 50

BP2 Late Bereitschaftspotential. 24, 25, 42, 50

CNV Contingent Negative Variation. 23, 25

dB Decibels. 60

EEG Electroencephalography. 20, 23

GS Gold Standard System. 57

ICA Independent Component Analysis. 59, 60

MRCP Movement-related Cortical Potential. 20, 23, 26

MRCPs Movement-related Cortical Potentials. 20–23, 138, 140

PMN Pre-movement Noise. 60

r Cosine Similarity. 62

RMS Root Mean Square. 60

sEMG Surface Electromyography. 30, 33, 58, 80, 81, 137, 140, 141

SNR Signal to Noise Ratio. 61

List of Tables

List of Figures

Chapter 1

Introduction

1.1 Statement of the Problem

Stroke is a leading cause of disability with more than 80 million stroke survivors worldwide (Johnson et al., 2019; Gorelick, 2019). In New Zealand over 7,000 people experience a stroke each year (Feigin et al., 2015; Ministry of Health, 2009; Dyall et al., 2008). Approximately two-thirds of stroke survivors have residual neurological deficits that impair function and approximately 50% are left with disabilities that render them dependent on others for activities of daily living (Donnan et al., 2008; Schweizer & Macdonald, 2014). Complete recovery after stroke occurs in only 15% of people (Hendricks et al., 2002). Thus there is a pressing need for continued development of effective rehabilitation interventions which maximise recovery for stroke survivors.

Neural plasticity is the main driver of recovery after stroke (Kleim & Jones, 2008). It is the ability of the nervous system to modify its structure and function in response to demand or experience (von Bernhardi et al., 2017). Evidence from studies conducted in both animals and humans suggests that neural plasticity may lead to a faster and greater recovery after stroke (Hara, 2015). However a review of neurorehabilitation research findings suggest that substantial amount of movement practice is required for

improved recovery outcomes (Lang et al., 2015). Observational studies indicate that the physical therapy and the use of affected limbs during daily activities in stroke patients is lower than required for improved recovery (Bernhardt et al., 2007; McLaren et al., 2019). Some researchers have attributed the lower levels of physical therapy to its increasing cost and have hypothesised that evidence-based cost-effective technologies may help close the gap between the required amount of therapy and the status quo (Reinkensmeyer et al., 2004). Lower levels of activity have been linked to boredom and the use of technology may increase engagement (Langan et al., 2017). More importantly evidence-based technologies which aim to enhance motor learning using the principles of neural plasticity may lead to long term functional recovery (Knotkova & Rasche, 2015; Clayton et al., 2016).

Some of the most promising evidence-based technologies for post-stroke rehabilitation include robotic-assisted therapies (Morone et al., 2017) and Brain Computer Interfaces (BCIs) (Cervera et al., 2018). Although extensive analysis of the cost and effectiveness of these technologies is required, an argument can be made in favour of BCIs as these can be made from inexpensive components (Chiesi et al., 2019; McCrimmon et al., 2017). BCIs can also be combined with rehabilitation robotics and proprioceptive feedback with potential for better outcomes (Formaggio et al., 2013; Ramos-Murguialday et al., 2012).

Recent work shows that adaptive neuroplastic changes can be induced by repetitive electrical stimulation of a peripheral nerve timed by a BCI to arrive at the peak negativity of a Movement-related Cortical Potential (MRCP) (Mrachacz-Kersting et al., 2012; Niazi et al., 2012; Olsen et al., 2017; Jochumsen et al., 2018). MRCPs are low frequency changes in Electroencephalography (EEG) recordings associated with the planning, execution and feedback of voluntary movements (Shibasaki & Hallett, 2006; Walter et al., 1964). This neuromodulatory intervention is a type of paired associative stimulation which modulates long-term potentiation in the human motor cortex (Krames et al.,

2009; Suppa et al., 2017). The advantage of this intervention is that it removes the need to directly stimulate the cortex, as is done in some of the other neuromodulatory techniques such as Repetitive Transcranial Magnetic Stimulation (rTMS) (Lewis et al., 2016). As advised by guidelines, TMS is contraindicated in people with stroke who have co-existing medical problems or are using heart implants, have metal-ware in their heads or are taking seizure lowering medication (Rossi et al., 2009). Thus the MRCP based neuromodulatory intervention may have a wider clinical adoption as it has fewer contraindications.

There is a growing body of evidence which supports the hypothesis that the MRCP based neuromodulatory intervention not only induces neuroplastic changes, but may also boost functional recovery after stroke (Mrachacz-Kersting et al., 2016, 2019). Although this is early evidence based on initial results from small sample studies in stroke population, it is promising and warrants research in translation of the MRCP based neuromodulatory intervention from laboratory to clinical practice. One aspect of this translation is the further research in development of the BCI used to deliver the intervention. This involves research dedicated to both hardware and software development to overcome the limitations of bulky laboratory equipment, noisy signal recording from the brain and muscles, real-time processing of these signals and the ability to adapt to enormous variability across patients in the specifics of their disability (López-Larraz et al., 2018).

1.2 Aims

The primary aim of my research is to investigate and overcome the key limitations of both the hardware and the software required for the BCI used to deliver the MRCP based neuromodulatory intervention. A secondary aim of my research is to refine the computational methods which are currently used in the processing of MRCPs.

1.3 Thesis Structure

A detailed review of the literature and the key limitations in the scientific knowledge of the BCI used to deliver the MRCP based neuromodulatory intervention is presented in Chapter 2. A conceptual blueprint of a BCI which can be developed into a prototype rehabilitation medical device is also presented in Chapter 2. In Chapter 3 details of my contributions to the development and validation of hardware proposed to address the key limitations are presented. The computational methods that I proposed for processing of MRCPs are presented in Chapter 4. Discussion on my findings, their wider implications and avenues for future research are presented in Chapter 5. The ethics approval letter, the participant information sheet and the consent form used for data collection purposes during the experimental studies are presented in Appendix A.

1.4 Delimitations of the Study

This thesis does not attempt to address the following.

- **Efficacy of the intervention:** The efficacy of the MRCP based intervention, tuning of its parameters and selection of movements are important and demanding questions. However these questions are not addressed in this thesis. Moreover, a comparative analysis of neuromodulatory interventions based on the MRCP and other brain or muscle signals is not dealt with in this thesis.

- **Invasive technologies**: Although invasive technologies have shown greater efficiency in measurement of brain and muscle signals (López-Larraz et al., 2018), the focus of this thesis is non-invasive technologies.

Chapter 2

Literature Review

This chapter begins with a brief overview of the Movement-related Cortical Potential (MRCP), the Contingent Negative Variation (CNV) and the differences in defining these terms among different authors. The chapter then introduces the three MRCP based rehabilitation paradigms. The Brain Computer Interface (BCI) used in the laboratory for these paradigms is described along with the limitations which hinder its translation from laboratory to clinical practice. Then the concept of a mobile BCI is introduced along with a feasible blueprint for a BCI which can be developed into a medical device for MRCP based rehabilitation paradigms. The requirements of this BCI, the design constraints imposed by current technology, available options for its components, the currently used computational methods and their limitations are discussed in detail. The chapter concludes by highlighting the key gaps in the scientific knowledge which need to be addressed for developing the BCI into a usable rehabilitation medical device.

2.1 Movement-related Cortical Potentials

MRCPs are low frequency changes in Electroencephalography (EEG) recordings associated with the planning, execution and feedback of voluntary movements (Kornhuber

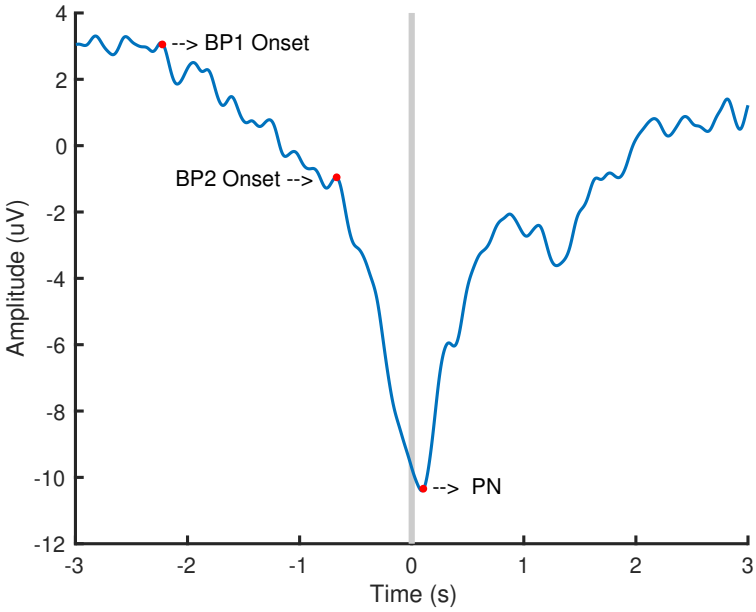

Figure 2.1: An example movement-related cortical potential
An example MRCP obtained from averaging of EEG activity over fifty right foot ballistic dorsiflexions performed by a healthy person. '0' seconds represents time of the movement onset detected from two electrodes placed on the right Tibialis Anterior (TA) muscle.

& Deecke, 1965; Hallett, 1994; Sakamoto et al., 2009). An example MRCP is shown in Figure 2.1. From an MRCP three notable features can be identified. The Bereitschaft-spotential (BP) starts around 2.0 seconds before the movement onset. At approximately 0.4 seconds before the movement onset, its slope abruptly becomes steeper. Based on these two different slopes compared to the baseline EEG activity, the BP is characterised as Early Bereitschaftspotential (BP1) and Late Bereitschaftspotential (BP2) (Shibasaki & Hallett, 2006). The third notable feature is the negative peak (PN) which is observed in the close vicinity of the movement onset. These potentials have been studied across both healthy and pathological populations (Kim et al., 2017; Patil et al., 2017; Wright et al., 2011).

2.1.1 Contingent Negative Variation

A similar brain potential is Contingent Negative Variation (CNV). It is slow negative shift in EEG recordings elicited between a warning (S1) and an imperative (S2) stimuli when a motor response to S2 is required (Walter et al., 1964; Hamano et al., 1997). Hamano et al. (1997) concluded in their study of BP and CNV in people with intractable epilepsy patients that Late CNV and BP2 are not the same as they have different cortical sources. However other authors regard Late CNV and BP2 as equivalent (J. W. Rohrbaugh & Gaillard, 1983; J. Rohrbaugh et al., 1976).

2.1.2 Differences in MRCP Definition

Different authors define the MRCP with slight differences. Oishi et al. (1995); Ikeda et al. (1997); Sakamoto et al. (2009); Sur & Sinha (2009); Ichiro et al. (2012) define MRCP and CNV as two different potentials. For these authors MRCPs are recorded preceding self-initiated voluntary movement, reflect movement preparation, processing and do not involve cognitive processing for an imperative stimulus (Sakamoto et al., 2009; Shibasaki & Hallett, 2006). Whereas their definition of CNV is slow negative shift in EEG recordings elicited between a warning (S1) and an imperative (S2) stimuli when motor response to S2 is required. Thus for these authors MRCP is the negative shift observed in EEG in a self-paced task and CNV is the negative shift observed in EEG in a S1/S2 type cued task.

Jankelowitz & Colebatch (2002) studied EEG signals related to cued, self-paced and imagined movements and called BP and CNV as movement-related potentials (MRPs) while acknowledging that the concepts of CNV and MRP have been developed independent of each other. Do Nascimento & Farina (2008) studied the rate of torque development in imaginary and real isometric plantar flexions. In this work they used a combination of an auditory and a visual cue. They termed the EEG recordings during

these tasks as MRCPs and did not mention CNV. The definition of MRCP was further blurred with CNV in a work published by Mrachacz-Kersting et al. (2012). According to Mrachacz-Kersting et al. (2012), "If a warning stimulus is provided followed by a cue to start the movement the MRCP is generally termed the contingent negative variation (p. 1670)." Some succeeding authors have also given similar definitions of MRCP and CNV (Shakeel et al., 2015; Jiang et al., 2014; Jochumsen, 2015).

In light of these differences, this thesis acknowledges both the classical definition of the MRCP and the fact that definitions evolve with time. Thus in agreement with the later authors, the word MRCP is used as an umbrella term for both the traditional MRCP and the CNV with greater emphasis placed on the paradigm (self-paced or cued) used to record the signal.

2.2 MRCP based Rehabilitation Paradigms

There are three MRCP based rehabilitation paradigms which have scientific evidence for their potential translation from the research laboratory to implementation in clinical practice. The first two paradigms are neuromodulatory interventions whereas the third is the assessment of changes in motor control in response to motor training. These paradigms are briefly introduced in the following sections.

2.2.1 Neuromodulatory Intervention

Neuromodulation involves alteration of nerve activity by employing targeted delivery of stimulus to specific neurological sites in the body Luan et al. (2014). Recent work shows that adaptive neuroplastic changes can be induced by repetitive electrical stimulation of the peripheral nerve timed to arrive at the peak negativity of a MRCP (Mrachacz-Kersting et al., 2012). This intervention modulates the brain activity by pairing the peripheral stimulation with the intention to move (Olsen et al., 2017). Thus

it follows a modified version of the paired associative stimulation (PAS) protocol (Suppa et al., 2017). In the original PAS protocol, the electrical stimulation of the peripheral nerve is timed with the electromagnetic stimulation of the motor cortex which leads to long term potentiation (LTP). LTP is the strengthening of the synaptic connections which lasts longer than the application of the stimulus. Rather than using an exogenous electromagnetic signal, the MRCP-based protocol uses the peak negativity of the MRCP as an endogenous signal from the motor cortex. The advantage of this approach is that it eliminates the need to externally stimulate the brain. The MRCP-based protocol enhances the cortical excitability with the underlying hypothesis that increased excitability may lead to improved long term functional recovery (Jochumsen et al., 2018). Although extensive research is required to test this hypothesis in a stroke population and to fine tune the different parameters of the intervention, there is some early evidence from studies in stroke population which support its efficacy (Mrachacz-Kersting et al., 2016, 2019).

This neuromodulatory intervention has an offline version and an online version (Mrachacz-Kersting & Aliakbaryhosseinabadi, 2018; Niazi et al., 2012; Jochumsen et al., 2019). In both the versions, the participant is seated comfortably in a chair and perform multiple repetitions of a movement. An illustration of the laboratory setup used for this intervention can be seen in Figure 2.2. There are two phases of the intervention: training phase and stimulation phase. The online and offline versions have different protocols for the training and stimulation phases.

Figure 2.2: Laboratory setup used for delivering the MRCP based intervention The participant can be seen wearing an EEG headset and stimulation electrodes on his left leg. The participant is facing the cue screen.

2.2.1.1 Offline Version

In the offline version a screen is placed in front of the participants to display a cue (Mrachacz-Kersting et al., 2012). Participants are requested to follow the cue shown in Figure 2.3. In the training phase they perform fifty cued repetitions of a movement. In most of the past studies involving this intervention, participants performed ballistic ankle dorsiflexions. The cue consists of three repeating windows: focus, go and rest. During the focus window shown in Figure 2.3 (a), the participants are requested to stay focused and try not to make any voluntary movement. During the go window shown in Figure 2.3 (b), there is a vertical line which sweeps from left to right and the participants are advised to start the movement as soon as the moving line hits a second stationary line in the middle of the window. As the moving line goes past the stationary line, the participants are advised to hold the movement. During the go window, the participants are also advised not to blink their eyes as it may contribute to artefacts in the EEG data.

During the rest window shown in Figure 2.3 (c), the participants may blink their eyes and move their arms or legs if they want to. Generally the time interval for the focus, go and rest windows is set at 1.5, 4.5 and 3 seconds respectively.

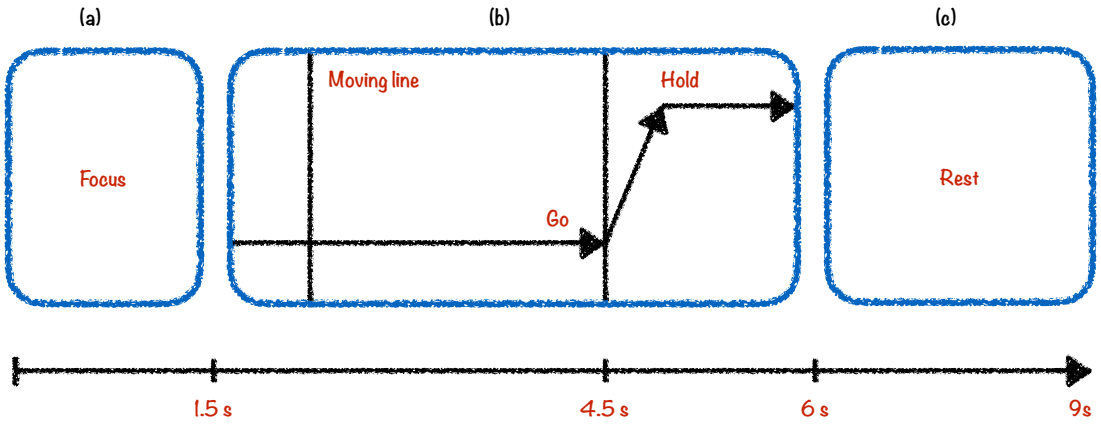

Figure 2.3: An illustration of the cue used for the offline version of the MRCP based neuromodulatory intervention in the laboratory
Note: (a), (b) and (c) represent the 'Focus', 'Go' and 'Rest' windows respectively.

Electrical stimulus is not applied during these repetitions in the training phase. EEG data is filtered and it is separated into epochs which are time locked with the time at which the go window's moving line hits the stationary line. These epochs are plotted one by one. An expert accepts or rejects these epochs based on the quality of the signal. The accepted epochs are averaged to obtain a single grand average MRCP signal. The time of the negative peak in this MRCP is defined by the expert and its time relative to go cue is calculated.

Next, the stimulation phase starts. The participants perform several repetitions of the movement and their peripheral nerve is electrically stimulated with a single pulse at the time of the negative peak calculated in the training phase with respect to the go cue. In the case of the right ankle ballistic dorsiflexion, stimulation is applied to the deep branch of their right common peroneal nerve (Jochumsen et al., 2019). The stimulus is applied 50 milliseconds prior to the time of the negative peak with respect to the cue due to the conduction time of the afferent stimulus and central processing delays in the

brain (Mrachacz-Kersting et al., 2012). The nerve is stimulated at the motor threshold which is defined as the smallest level of current that elicits a palpable response in the tibialis anterior tendon. EEG data is not recorded during this phase.

2.2.1.2 Online Version

Similar to the offline version the electrical stimulus is not applied during the training phase in the online version. Surface Electromyography (sEMG) electrodes are placed on one of the muscles involved in the selected movement to detect the onset of the movement. Instead of following a cue, the participants are advised to perform 50 repetitions of the movement at their own pace with a delay of at least 10 seconds between consecutive repetitions. EEG and EMG data from this phase is used by the computer to build a participant specific model of the MRCP using an algorithm (Niazi et al., 2012).

During the stimulation phase, the participants perform multiple movement repetitions again at their own pace. During each repetition, the computer using the built participant specific model, detects the movement intention from the negative shift in the MRCP and fires the electrical stimulus just before the negative peak in the MRCP. Thus instead of relying on the assumption that the participants perform the movement with the same strategy during each repetition, this version tries to adapt to the changes in repetition performance over time. There is some evidence to suggest that this version results in higher cortical excitability compared to the offline version (Jochumsen et al., 2019).

2.2.2 Assessment of Motor Training

The third MRCP based rehabilitation paradigm is not an intervention but a technique to quantify neurophysiological changes in response to motor training. The motivation

for using EEG in general and MRCP in particular is the hypothesis that these methods may be more sensitive to changes in response to motor training compared to current techniques used in the clinic (Jochumsen et al., 2017). Moreover, EEG data may provide a low cost and simple method to quantify these changes compared to other approaches such as functional magnetic resonance imaging, magnetoencephalography, and transcranial magnetic stimulation (Jochumsen et al., 2017). A potential advantage of a more sensitive measure may be that it can better inform the patient and the clinician to follow their current rehabilitation program or modify it for improved recovery.

In assessment of motor training protocol, MRCP is recorded from multiple movement repetitions both before and after a motor trining session (Kim et al., 2017; Patil et al., 2017; Wright et al., 2011). The differences observed in the morphology of the MRCP before and after the training are then investigated in relation to improvement in motor performance. Although the efficacy of the MRCP in quantifying small changes in motor performance requires investigation in a stroke population, in this thesis I have attempted to address the limitations of the computational methods which are currently used to process the MRCP.

2.3 MRCP based Brain Computer Interfaces (BCIs)

A block diagram representation of the laboratory based system shown in Figure 2.2 is presented in Figure 2.4. Although all the hardware components are interconnected and work together, they can be grouped as four distinct subsystems. The subsystems are the EEG/sEMG system, the Cue display system, the Stimulation system and the Processing system. The EEG/sEMG system and the Processing system are the Brain Computer Interface (BCI) subsystems in this setup.

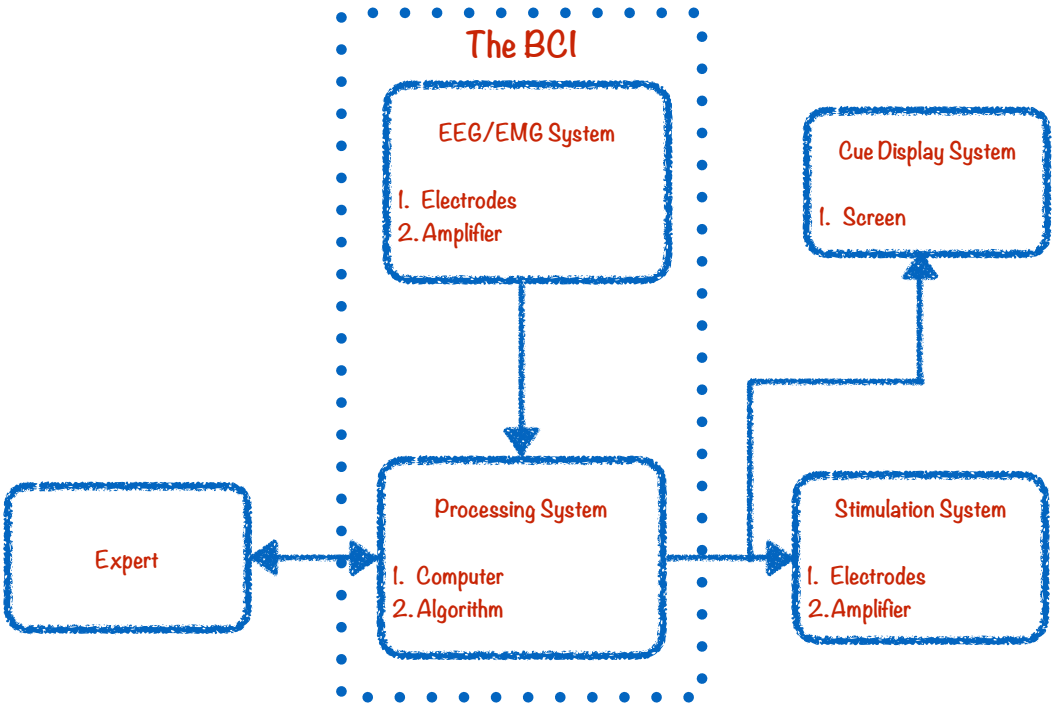

Figure 2.4: Four subsystems of the laboratory based setup along with the expert The arrows represent wiring and direction of information flow in the system.

2.3.1 Limitations of the Current BCI

The laboratory BCI used for the MRCP based intervention and assessment of motor training in earlier studies (Mrachacz-Kersting et al., 2012; Niazi et al., 2012; Jochumsen et al., 2017) is built from laboratory grade devices and imposes following limitations.

1. **Participant and Clinician centered Design:** As the current system is used in the laboratory and the primary focus of the experiments is the investigation of the efficacy of the intervention, limited attention is paid towards participant and clinician centered design. This is the most important limitation which hinder the translation of the neuromodulatory intervention from the laboratory into clinical practice. These factors include clinical requirements, effectiveness and usability (Signal et al., 2019). For example, the time and cost spent in relation to the benefit to their patients is an important factor for clinicians to consider a novel

intervention. Moreover, the intervention in its current form is delivered in a single joint movement while sitting in a chair. Thus the patients may prefer to spend that time practicing a functional task to improve their ability to participate in daily activities. Some of the factors which contribute to this limitation are technological as discussed below.

2. **EEG Expert:** An EEG expert is required to setup the equipment and make a number of decisions in data processing such as accepting and rejecting the epochs based on signal quality. Thus there is a need for making the connections between different components invisible and automating this process to minimise the input from the clinician or the patient.

3. **Bulky Hardware:** All the hardware components used for the setup are research grade tools designed for laboratory use. For example, the EEG headset and its amplifier are state-of-the-art equipment for EEG research in a laboratory. Similarly a high specifications desktop computer is used for processing and a monitor is used for displaying the cue. The stimulator amplifier is also a versatile device for wide ranging laboratory experiments. Thus research in specialising and miniaturising these components for the neuromodulatory intervention is required.

4. **Sticky Gel based Electrodes:** Currently wet gel-based electrodes are used for EEG, sEMG and the application of electrical stimulus as they deliver better signal quality. However these electrodes require longer application time and cause inconvenience to the participant. The technological challenges which impose this limitation are discussed at length later in Section 2.5.1.

5. **Cost:** As all the components of the BCI are state-of-the-art and designed for research, a large sum is required for setting up this intervention in a clinic.

2.4 Blueprint of a Mobile, Affordable and Usable BCI

The limitations discussed in the above section dictate that a mobile, affordable and usable BCI which can eventually be developed into a certified medical device for the MRCP based rehabilitation applications should have features which address the needs of the clinicians and the patients. In the following paragraphs, the technological components are listed for the blueprint for a possible system which may address some of these features.

1. **Electrodes (EEG/sEMG):** A minimum number of electrodes which have good quality to cost ratio for EEG recording. It should be possible to fabricate these electrodes into a customisable headset. At least one pair of sEMG electrodes is also required for detection of movement onset.

2. **Analog to Digital Converter (ADC):** A low cost small footprint EEG/sEMG ADC to connect the electrodes to the microprocessor.

3. **Embedded Computer:** A mobile microprocessor capable of running real-time algorithms and communicate with peripheral devices. The amplifier, the ADC and the microprocessor should have small form factor and it should be possible to fabricate the components on a small single circuit board.

4. **Power Electronics for the Stimulator:** Energy and area efficient power electronics are required for the electrical stimulator which can be packed with the sEMG circuitry.

5. **Wireless Communication:** The different components should be able to communicate wirelessly with each other. The BCI components should be able to communicate with a mobile device for control and cue display.

6. **Algorithms and Software:** A wide range of energy efficient algorithms are required to filter, remove artefacts, model and label the recorded data. Reliable and well tested software which packages these algorithms with hardware interfaces is also required.

7. **Control Application:** A control and feedback mobile application is required which may allow the clinicians and the patients to set the parameters for the intervention and keep track of the past sessions.

The overall block diagram which shows the interconnection of the components is presented in Figure 2.5.

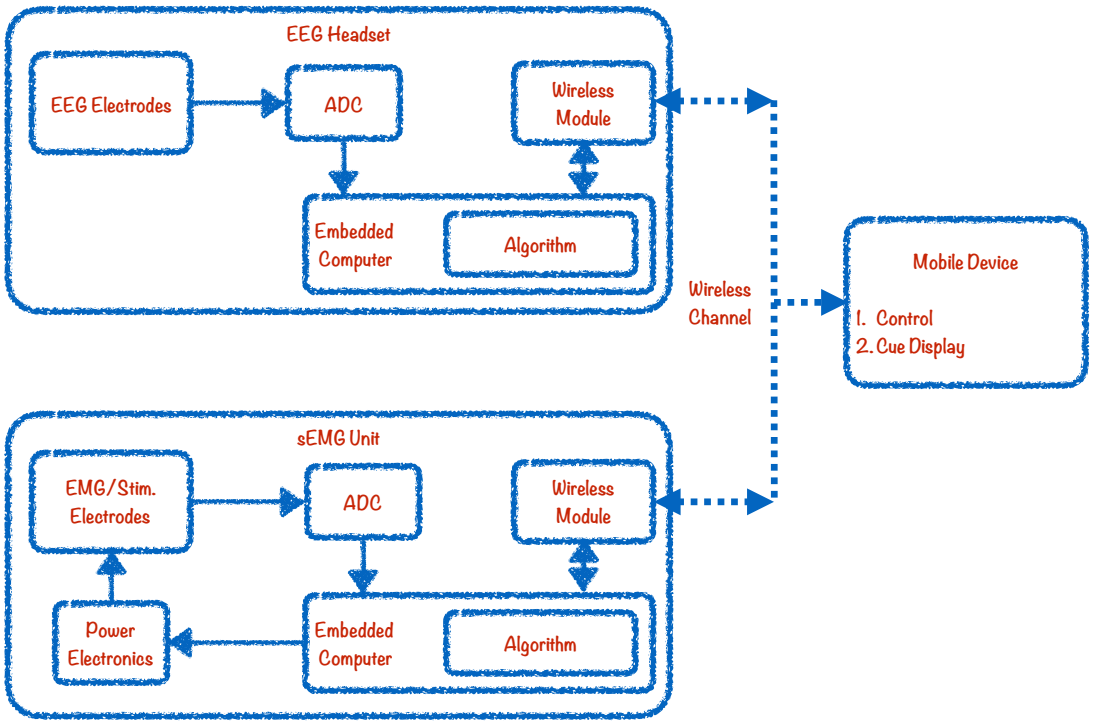

Figure 2.5: Blueprint of a mobile BCI for MRCP based rehabilitation applications
Note: Stim. stands for electrical stimulator.

2.5 Constraints and Options for the Components of the Blueprint BCI

In this section each technological component for the BCI is evaluated as per the guidelines in the previous section by evaluating the relevant theory and available options. In some cases a particular option is selected for a component whereas in other cases gaps in scientific knowledge are identified which need to be addressed through further research.

2.5.1 Electrodes

Electrodes act as the interface between the scalp and the measuring device. This interface does not behave like a simple electrical contact between two materials rather it behaves like an electrode-electrolyte interface in electrolysis as the electrode is usually a metal with electrons as the charge carriers and the scalp is a tissue with ions as the charge carriers. Two types of currents pass through this interface: a displacement current and an electrolytic current (Webster, 2009). The electrolytic current results from the oxidation and reduction of scalp ions on the electrode, thus giving up electrons or taking electrons from the electrode. This phenomenon can be modelled by an electric resistor. The displacement current results from push and pull of the electrons in the electrode by the ions in the scalp and vice versa. This phenomenon can be modelled as an electric capacitor which makes the impedance of the interface frequency dependent.

When an electrode is placed in an electrolyte, there is a transfer of charge across the boundary due to difference in concentration of ions in the two materials. Thus a double layer of charge is formed. This double layer causes an electric potential across the boundary called polarisation potential. This potential can be modelled by a voltage source. The polarisation potential is much larger than the potential

caused by neural activity. As a result a DC offset can be seen in EEG recordings (Niedermeyer & da Silva, 2005). This offset can be easily removed by applying high pass filtering. However relative displacement between the scalp and the electrodes cannot be eliminated entirely which causes movement artefact. This displacement disturbs the double layer equilibrium potential and results in sharp jumps in EEG recordings. A major component of this artefact is at low frequencies (Webster, 2009). This noise cannot be filtered without losing the useful low frequency information. This artefact can be minimised by using non-polarisable electrodes and placing a gel between the electrode and the scalp. An electrode which approaches the ideal non-polarisable behaviour is Ag-AgCl electrode which has become the gold standard in EEG instrumentation (Lopez-Gordo et al., 2014). Compared to other metallic and compound electrodes, it has lower impedance and lower noise at low frequencies (Das & Webster, 1980; Geddes & Baker, 1977). A gel containing Cl^- as the principle anion is used with the Ag-AgCl electrode for a steady electrical and mechanical contact. The wet sintered non-contact Ag-AgCl electrode gives best signal quality in the low frequency band (Tallgren et al., 2005).

The reference electrode is generally placed on ipsilateral or contralateral earlobe or mastoid. The reason behind using earlobe/mastoid as the reference has more to do with convention than absence of cortical activity (Nunez & Srinivasan, 2006). An additional electrode called ground (GND) is also used in EEG recordings. It helps reject the common mode noise. An earlobe electrode is generally used as the ground.

2.5.1.1 Electrical Model of Electrode-Scalp Interface

The electrical model of the interface between the electrode, gel and the scalp is shown in Figure 2.6. E_{hc}, E_{se}, E_p are the polarisation potentials for electrode-gel interface, gel-epidermis interface and gel-sweat glands interface respectively.

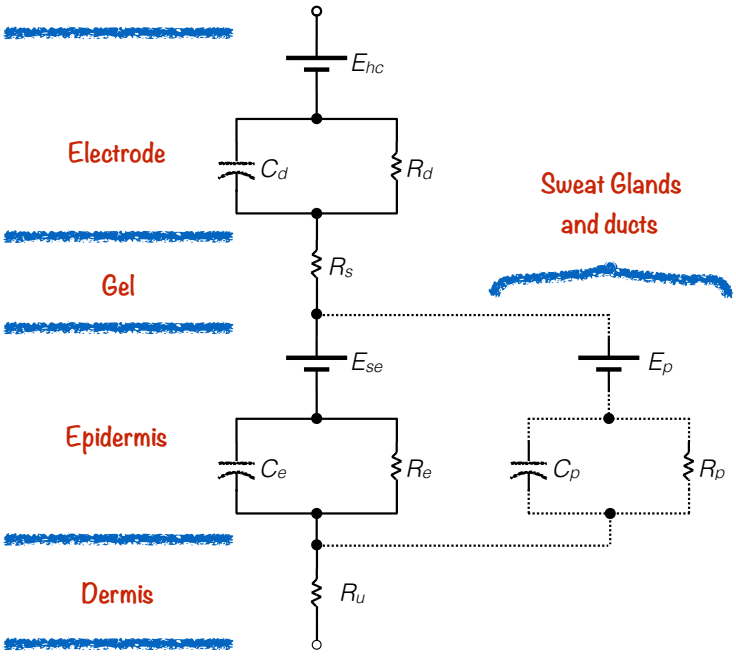

Figure 2.6: Electrical model of electrode and scalp interface

2.5.1.2 Selection of EEG/sEMG Electrodes

The most critical factor affecting the MRCP recording is the movement artefact as both have low frequency characteristics. The best electrode available to counter the effects of movement artefact is wet sintered non-contact Ag-AgCl electrode. The problem with wet electrodes is that the gel dries out over time and the application of gel is inconvenient for the participant (Lopez-Gordo et al., 2014). These problems can be avoided by using dry electrodes. A number of active and passive dry EEG electrodes and caps are available in the market (Lopez-Gordo et al., 2014). Development of new dry electrodes is an active area of research (Chi et al., 2010; Fiedler et al., 2014). However with current technology, the quality of EEG recording with dry electrodes at low frequencies is very poor (Oliveira et al., 2016). Thus wet sintered non-contact Ag-AgCl electrodes will be used for prototyping. As the application of individual EEG electrodes is very cumbersome, Quick-Cap (Compumedics Neuroscan, Dresden,

Germany) will be used. It is an EEG cap built per 10-20 international system using wet sintered non-contact Ag-AgCl electrodes. For EMG recording, Ambu BlueSensor N (Ambu®, Bayan Lepas, Malaysia) electrodes will be used. These are also gel based Ag-AgCl electrodes.

2.5.1.3 EEG Electrode Placement

The placement of electrodes on the scalp plays an important role in EEG recording. Different tasks involve activation of different areas of the brain. Research has shown that EEG collected from different places on the scalp is different (Adrian & Matthews, 1934). Therefore it is important to use a well-informed standard placement of electrodes for specific movements. To fully appreciate the origin of differences in EEG recording, motor physiology is discussed briefly in Section 2.5.1.3.1 It provides evidence for placement of electrodes over the motor cortex. However to specify the exact location of electrodes, a standard for electrode placement is introduced. Using this standard, evidence for choice of electrode placement for self-paced and cued movements is presented directly from MRCP research in Section 2.5.1.3.2.

2.5.1.3.1 Evidence from Physiology of Motor Control Motor control is defined as the ability to regulate or direct the mechanisms essential to movement (Shumway-Cook & Woollacott, 2007). It involves processing, integration of sensory information and muscle activation, as well as coordination between different muscles. In the central nervous system, the area highly associated with motor planning and execution is called motor cortex. It has several different processing areas including primary motor cortex and premotor areas, labelled as 4 and 6 in Figure 2.7 respectively.

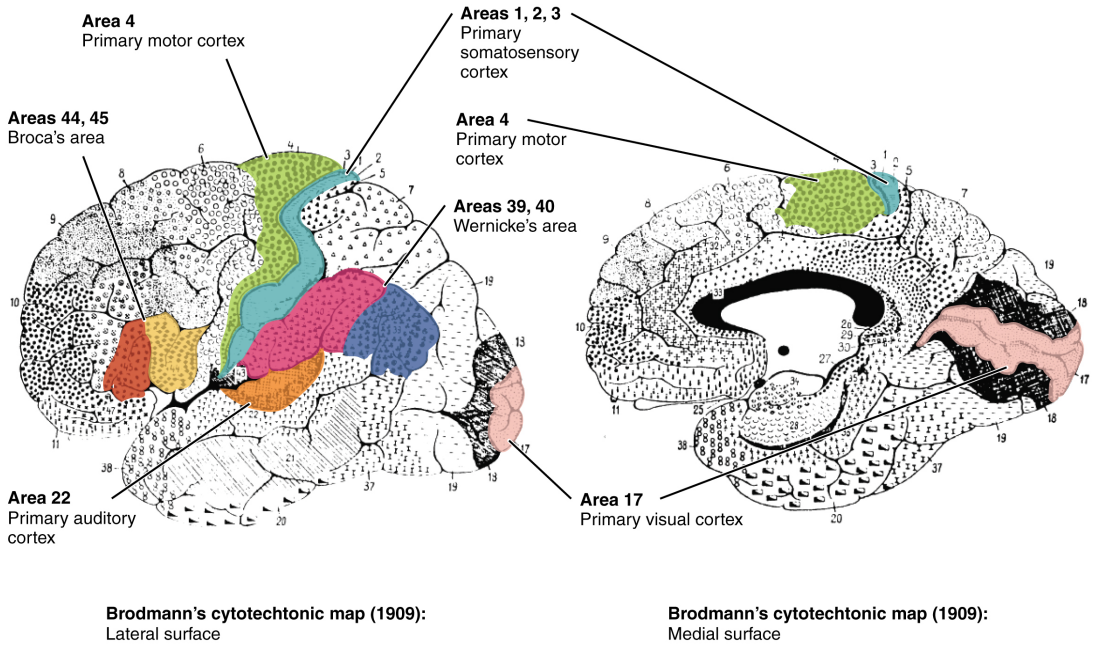

Figure 2.7: Labelling of various cerebral areas by Brodmann (1909)
Figure obtained from openstax book Anatomy and Physiology licensed under Creative Commons Attribution 4.0. The book is available at https://cnx.org.

Thus the theoretic probability of obtaining "better quality" MRCP is much higher if the electrodes are placed over the motor cortex and premotor areas rather on the frontal cortex (areas 8 and 9 in Figure 2.7). For recording MRCP during a lower limb task, the electrodes should be place at the centre of the head and for upper limb task, the electrodes should be place laterally to the temporal lobe on the contralateral side as suggested by the schematic in Figure 2.8.

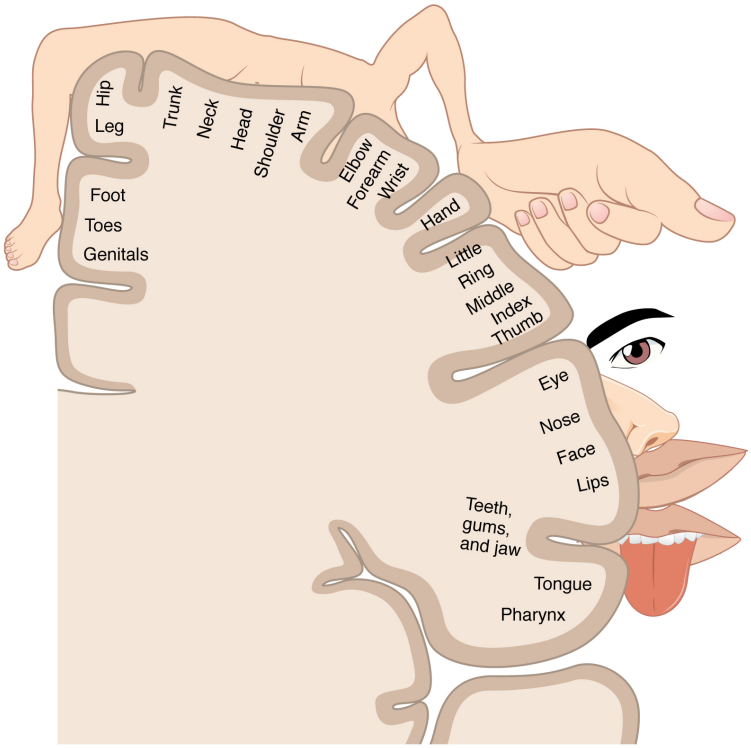

Figure 2.8: Schematic representation of the location of different body parts within the primary motor cortex
The divisions for each body part are overlapped, thus, care should be taken while interpreting this diagram (Solodkin et al., 2007). Figure obtained from openstax book Anatomy and Physiology licensed under Creative Commons Attribution 4.0. The book is available at https://cnx.org.

To adopt a more precise and uniform placement of electrodes, the international 10-20 system will be used. The international 10-20 system uses the length from Nasion (bridge of the nose) to the Inion (occipital protuberance) as the base measure. The electrodes are separated by 10% or 20% of the base measure. A visual representation of the 10-20 system is shown in Figure 2.9.

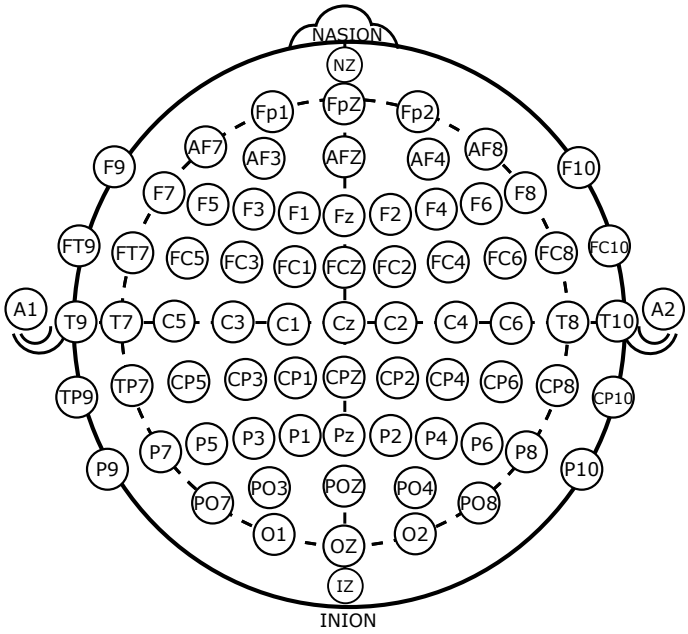

Figure 2.9: International 10-20 system for placement of EEG electrodes
Note: 'F', 'C', 'O', 'P' and 'T' stand for frontal, central, parietal, occipital and temporal, respectively.

2.5.1.3.2 Evidence from MRCP Research In self paced movements, BP1 of the MRCP is maximum at the midline centro-parietal area and symmetrically and widely distributed over the scalp regardless of whether the movement is in the upper or the lower limb. BP2, however, is maximal over the contralateral central area – approximately Cz in the lower limb and C1 or C2 in the upper limb (Shibasaki et al., 1981).

In the cued movements, Early CNV originates from prefrontal area and supplementary sensorimotor area (SSMA). While the Late CNV originates from the prefrontal area, M1, S1, temporal area, occipital area, and SSMA (Hamano et al., 1997).

2.5.1.3.3 Selection for EEG Electrode Placement In agreement with the previous research , data will be recorded from following electrodes: Fp1, F3, F4, FC3, FCZ, FC4, C3, CZ, C4, CP3, CPZ, CP4, P3, P4 (Mrachacz-Kersting et al., 2012; Niazi et al., 2012). It is still unclear what is the minimum set of electrodes required for a particular MRCP rehabilitation paradigm.

There is no true reference in EEG recording and any electrode can be made a reference using signal processing (Nunez & Srinivasan, 2006). We will use the right mastoid as the reference. The reason for choosing mastoid is that it will be relatively easy to hardwire an electrode for this location in the final prototype. The AF2 electrode of the 10-20 system will be used as the ground.

2.5.1.4 sEMG Electrode Placement

sEMG electrodes will be placed in accordance with the Surface Electromyography for the Non-Invasive Assessment of Muscles (SENIAM) guidelines (Hermens et al., 2000) on the muscle which is the first activated muscle in the selected movement.

2.5.2 Analog to Digital Converter

To store and process EEG/sEMG signals on a digital computer, they should be converted from voltage levels to sequences of binary numbers. This is achieved by using an analog to digital converter. Modern day EEG/sEMG instruments have several differential amplification stages as brain signals are only a few microvolts.

2.5.2.1 Amplifier

The back-bone of these stages is the operational amplifier (op-amp) shown in Figure 2.10.

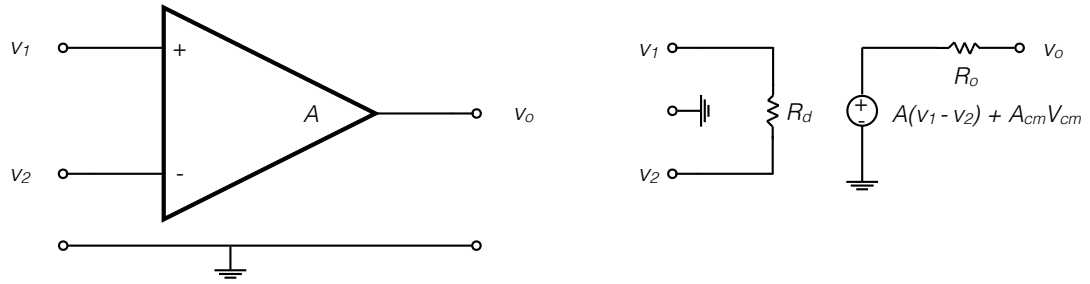

Figure 2.10: Circuit symbol and equivalent circuit of an op-amp

The theoretical amplifiers amplify the signal without distorting it in any way. The real op-amps, however, does distort the input signal to some extent. Different measures are used to quantify the quality of amplifiers. For EEG recordings, input impedance, common mode rejection ratio and input referred noise are the most important measures. A higher input impedance means that little current is drawn from the electrodes making the electrode impedance irrelevant. The common mode rejection ensures that the signal which appears on both electrodes will be eliminated. This is very important for EEG as muscle artefacts, Electrocardiogram (ECG) and environment noise (50/60 Hz power frequency) affect all electrodes equally. The common mode rejection ability of an op-amp is quantified by the Common Mode Rejection Ratio (CMMR). Input referred noise is the signal we get when there is no input applied to the amplifier. In other words, the minimum signal that the amplifier will be used to sense should be greater than input referred noise for accurate measurement. A simplified model of an instrumentation amplifier connected with two electrodes is shown in Figure 2.11.

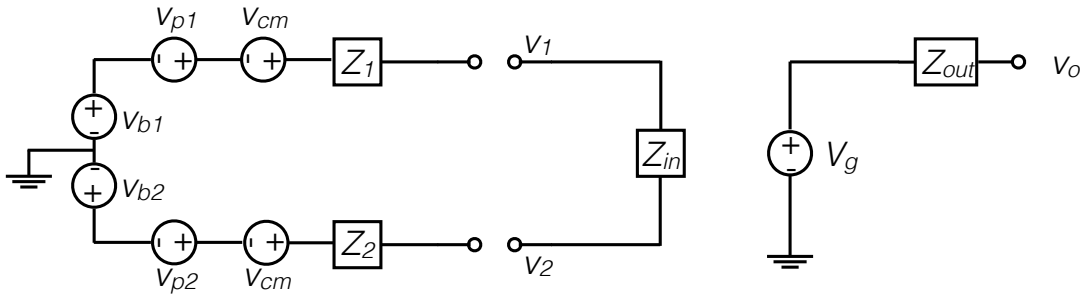

Figure 2.11: Electrical circuit of two electrodes connected with an instrumentation amplifier
Note: Z_l and Z_l are electrode impedances obtained by lumping together all the impedance components in Figure 2.6. Z_{in} and Z_{out} are the input and output impedances of the amplifier. V_{p1} and V_{p2} are polarisation potentials for the electrodes. V_{cm} is the common signal present on both electrodes. V_{b1} and V_{b2} are the cortical potentials recorded by the electrodes.

A good approximate relationship between the amplifier output V_o and the scalp potentials is given by Equation 2.1 (Ferree et al., 2001).

$$V_o = \Big(1 - \frac{Z_1 + Z_2}{2Z_{in}}\Big)[V_{b1} - V_{b2}] + \Big(1 - \frac{Z_1 + Z_2}{2Z_{in}}\Big)[V_{p1} - V_{p2}] + \Big(\frac{Z_1 - Z_2}{Z_{in}}\Big)V_{cm} \quad (2.1)$$

2.5.2.2 Impedance Requirements

Analysis of Equation 2.1 yields following observations about effects of electrode impedance on the resulting EEG signal.

1. Small electrode impedance means better rejection of common mode noise and less attenuation of cortical potentials. However in the case of modern amplifiers which have an input impedance of around 200 MΩ, large electrode impedances do not result in considerable signal attenuation. At an impedance of 50 kΩfor each electrode, the signal loss is only 0.025% (Ferree et al., 2001). Therefore there is no need to puncture the skin under the electrode to reduce impedance.

2. A large difference in impedance across electrodes has serious consequences on signal quality. If one of the electrodes has large impedance, the common mode noise will not be attenuated adequately.

3. Both the polarisation potentials and the cortical potentials are amplified by the same factor. As the polarisation potential is much larger than the cortical potential, a large DC offset can be seen in EEG signals. Thus it is very important that the polarisation potential remains constant. A non-polarisable electrode such as Ag-AgCl has a small steady polarisation potential. However the epidermis and sweat glands result in constantly changing skin potentials (E_{se} and E_p from Figure 2.6). To reduce the noise from these potentials it is, therefore, necessary to lightly abrade the skin under the electrode (Ferree et al., 2001).

2.5.2.3 Selection of Analog to Digital Converter (ADC)

To find a suitable ADC, a search was conducted on the online stores of ten semiconductor companies[1] for "biopotential amplifier OR eeg" using their store search function. Their catalogs was also browsed manually. Table 2.1 summarises the results.

Table 2.1: Results of search for "biopotential amplifier OR eeg" and catalog browsing on the online stores of semiconductor companies
Note: 'n' stands for internal noise and 'c' stands for number of channels.

Manufacturer	Products
Intel	Nil
Samsung Electronics	Nil
SK Hynix	Nil
Qualcomm	Nil
Micron	Nil
Texas Instruments	ADS1194/96/98 (n: 12 µV, c: 8) ADS1291/92/92R (n: 8 µV, c: 2) ADS1294/96/98 (n: 4 µV, c: 8) ADS1299-4/6/ (n: 1 µV, c: 4/6/8)
Toushiba	Nil
Broadcom	Nil
STMicroelectronics	HM301D (n: NA, c: 3)
Infineon Technologies	Nil

Texas Instruments ADS1299 front end is specifically designed for EEG applications and was selected. It satisfies the design requirements in Section 2.4 and it is affordable. In Table 2.2, its key features are presented.

[1] See a list at https://en.wikipedia.org/wiki/Semiconductor_industry

Table 2.2: Technical specifications of Texas Instruments ADS1299

Feature	Specification	Comment
Cost	36-56 USD[2]	
Development tools	OpenBCI development kit[3]	The ADS1299 is being used by OpenBCI to develop their open source hardware and software platform for BCIs. This development kit can be modified as required and the modified form can be commercialised. It is licensed under MIT license[4]. This development kit will be used for initial prototyping.
Input impedance	1000 MΩ at 0 Hz	The impedance stays well above the required limit of 500 MΩ (Ferree et al., 2001).
CMMR	110 dB at 50 Hz	This number means that the common mode noise will be attenuated by a factor of 300000 compared to the signal at 50 Hz. The CMMR decreases as the frequency increases, thus, it is even higher at low frequencies.
Input referred noise	1 microvolt peak to peak from 0.01 Hz to 70 Hz at gain 24 and sampling rate 250	The peak negative value of MRCP is usually 8-10 microvolts (Shibasaki & Hallett, 2006). A noise of 1 microvolt can affect the MRCP quality. This effect will be quantified during analysis.
Effective bandwidth	0.01 – 65 Hz at gain 24 and sampling rate 250	Although different bandwidth ranges can be achieved by selecting different gain and sampling rates, this range is most suitable for MRCP recording. Lower gain and higher sampling rate result in higher input referred noise. This bandwidth is not, however, ideal for sEMG recording as sEMG signal ranges from 5 Hz to 400 Hz with peak activity in 25 to 75 Hz band. However, in this work sEMG is only used for detecting the movement onset.
Impedance measurement	Yes	The ADS1299 can measure electrode impedance and can also detect a lead-off/connection break.

Driven right leg circuit (DRL)	Yes ('Bias' pin on OpenBCI and 'Ground' electrode in EEG montage)	The human body acts as an antenna collecting surrounding electrical activity especially power frequency. DRL actively attenuates these common mode signals (B. B. Winter & Webster, 1983).
Number of channels	4, 6, 8, 16, 24, 32	ADS1299-4 and ADS1299-6 offer same specifications with 4 and 6 channel packages. Two and more ADS1299 can be interfaced together to record data from more than 8 channels. OpenBCI kit provides 16 channels for recording.

[2]https://store.ti.com/ADS1299IPAGR.aspx
[3]www.openbci.com
[4]https://opensource.org/licenses/MIT

2.5.3 Algorithms

The three MRCP based rehabilitation paradigms discussed in Section 2.2 require a wide range of cleaning, processing, detection and feature extraction algorithms. One common shortcoming of the literature on MRCP algorithms is that a time and memory complexity analysis is not presented (Wegener, 2005). Such an analysis is critical to selection of the hardware on which these algorithms are deployed for a mobile device (Ahmadi et al., 2012). In the following paragraphs, algorithms required for each paradigm are briefly discussed.

For the offline version of the neuromodulatory intervention, an algorithm is required which can clean the recorded MRCP epochs, reject the noisy epochs and automatically obtain the time of the negative peak. Although these steps have been clearly delineated in past research (Mrachacz-Kersting et al., 2012; Mrachacz-Kersting & Aliakbary-hosseinabadi, 2018) and a number of general purpose automated cleaning pipelines are available in the literature (Gabard-Durnam et al., 2018; Ojeda et al., 2019), an efficient implementation of such a pipeline and its testing for offline neuromodulatory intervention is still missing.

For the online version of the neuromodulatory intervention, an algorithm is required which can detect an MRCP in real-time and send a signal to the stimulator. A detailed review of MRCP detection algorithms is available (Shakeel et al., 2015). Among the reviewed publications, Matched Filter (Niazi et al., 2011), Linear Discriminant Analysis (Lew, 2012) and Independent Component Analysis (Jiang et al., 2015) are of special interest as they have reported latency in addition to detection accuracy. All these algorithms, however, involve building a participant specific model. This step relies on the assumption that either EMG is available and can be reliably detected or the participants can follow a cue. If EMG is used, efficient algorithms are required for detecting onsets of muscle activations. Thus for a purely online system, there is a need

for a MRCP detection algorithm which can work without the initial participant specific model.

For assessment of motor training, in addition to an algorithm for cleaning of epochs, an automated feature extraction algorithm is required. A number of features are extracted from the MRCPs to evaluate the neurophysiological changes in response to motor training (Taylor, 1978; W. Lang et al., 1983; Niemann et al., 1991; Wright et al., 2012b; M.-K. Lu et al., 2011; Jochumsen et al., 2017). In some of these studies, onsets of BP1 and BP2 were specified a priori from previous research and their amplitudes were obtained for evaluation (Taylor, 1978; M.-K. Lu et al., 2011; Fattapposta et al., 1996). Whereas in other studies, BP1, BP2 and PN were identified from the MRCP with visual inspection by single or multiple human experts (Kita et al., 2001; Wright et al., 2012a). The limitation of these methods is manual identification and subjective onset specification. Therefore an algorithm for automating this process is required.

2.5.4 Embedded Computer

The specifications of the embedded computer depend on the time and memory complexity of the chosen algorithms. In the past, researchers have used both microprocessors (e.g. 32-bit ARM core microcontroller) and Field Programmable Gate Arrays (FPGA) in their proposed mobile BCIs (McCrimmon et al., 2017; Belwafi et al., 2018). Both these approaches have their own pros and cons (Bezerra & Gough, 2000). For a MRCP based BCI, a definitive choice of an embedded computer can only be made once a comprehensive time and memory complexity analysis of the required algorithms is available. This has already been identified as a gap in the current scientific literature on algorithms for MRCP based rehabilitation paradigms.

2.5.5 Wireless Communication

The selection of wireless communication channel is also dependent on the underlying timing requirements of the algorithm and the selection of the supported peripheral devices (e.g. an iPad). The most obvious choice is Bluetooth Low Energy (BLE) as it can support multiple connections and a latency as low as 676 micro-seconds (Gomez et al., 2012).

2.6 MRCP based Rehabilitation Medical Devices: Objectives for Further Research

This section presents a summary of the research objectives identified in the literature review. These objectives require further research for development of the MRCP based rehabilitation medical devices for their uptake in clinical practice.

1. **Evaluation of dry EEG electrodes for MRCPs:** One important objective is the development and evaluation of dry EEG electrodes for MRCP recording with adequate signal quality.

2. **Evaluation of portable ADC:** The evaluation of the performance of Texas Instruments ADS1299, identified as a cost-effective small footprint ADC in the literature review, for recording MRCPs is required.

3. **Algorithm for cued intervention:** A fully automated method for processing MRCPs for delivery of the offline version of the intervention is needed.

4. **Algorithms for self-paced intervention:** First, a fully automated method of detecting muscle onsets and offsets in complex movements for delivery of the online version of the intervention. It is needed when muscle activity onset is used

as the movement onset for building a participant specific model. Second, a fully automated algorithm for processing MRCPs which does not require an initial participant specific model for delivery of the online version of the intervention.

5. **Algorithm for feature extraction from MRCPs:** A fully automated method for feature extraction from MRCPs.

6. **Usability testing:** The usability testing of the prototype medical devices with clinicians and patients is required. Any novel findings of the usability testing should update the design of the prototypes.

2.7 Summary

In summary, movement-related cortical potentials are electroencephalographic activity related to voluntary movement. Past laboratory based research has proposed movement rehabilitation paradigms based on MRCPs. Although further research is required, there is enough evidence to warrant research in development of mobile medical devices for clinical and home use. For this purpose, a number of objectives are identified in terms of the hardware, software and usability testing for further research. In the next two chapters, I have detailed my contributions towards achieving some of these objectives.

Chapter 3

Evaluation of a Cost-effective Small Footprint ADC for MRCPs

This chapter presents my contribution towards achieving objective 2 in section 2.6 which was to evaluate the MRCP recording performance of a low cost, portable off the shelf Analog to Digital Converter (ADC). An experimental study was conducted and its results were published in a peer-reviewed journal. The published article is presented here with no content modifications and minor formating modifications to facilitate reading[1]. The ethics approval for this study was obtained from Health and Disability Ethics Committees (HDEC). The ethics approval letter, participant information sheet and consent form are available in Appendix A.

[1]Original article: U. Rashid, I. K. Niazi, N. Signal, D. Taylor, An eeg experimental study evaluating the performance of texas instruments ads1299, Sensors 18 (2018) 3721. doi:10.3390/s18113721

Start of Published Manuscript 1

3.1 An EEG Experimental Study Evaluating the Performance of Texas Instruments ADS1299

3.1.1 Abstract

Texas Instruments ADS1299 is an attractive choice for low cost Electroencephalography (EEG) devices owing to its low power consumption and low input referred noise. To date, there have been no rigorous evaluations of its performance. In this EEG experimental study we evaluated the performance of the ADS1299 against a high quality laboratory based system. Two self-paced lower limb motor tasks were performed by 22 healthy participants. Recorded power across delta, theta, alpha and beta EEG bands, power ratio across the motor tasks, pre-movement noise, and signal to noise ratio were obtained for evaluation. The amplitude and time of the negative peak in the Movement Related Cortical Potentials (MRCPs) extracted from the EEG data were also obtained. Using linear mixed models, no statistically significant differences ($p > 0.05$) were found in any of these measures across the two systems. These findings were further supported by evaluation of cosine similarity, waveform differences and topographic maps. There were statistically significant differences in MRCPs across the motor tasks in both systems. We conclude that the performance of the ADS1299 in combination with wet Ag/AgCl electrodes is analogous to that of a laboratory based system in low frequency (< 40 Hz) EEG recording.

3.1.2 Introduction

Texas Instruments ADS1299 is a System on Chip (SOC) specifically designed for biopotential applications including Electroencephalography (EEG) and Electrocardiography (ECG). It has attractive electrical characteristics such as low input referred noise (1 μV_{pp}), low power consumption (5 mW/channel), test signals for impedance measurement, and a SPI™ compatible interface (Instruments, 2012). In recent years, it has attracted considerable attention from the biomedical research community, both for clinical research and the development of mobile Brain Computer Interfaces (BCIs).

ADS1299 has been used in multiple studies to evaluate hardware and software for EEG. These include testing 3D printed electrodes (Krachunov & Casson, 2016), ultra high impedance active electrodes (F. N. Guerrero & Spinelli, 2018), finger based dry electrodes (Nathan & Jafari, 2015), and artefact rejection algorithms (Zou et al., 2016; Qian et al., 2017). It has also been used in EEG experimental research to study neurophysiology in both humans (Kaongoen et al., 2017; Beauchene et al., 2016; Jindal et al., 2015; Zhao et al., 2017) and mice (Ssentongo et al., 2017). Importantly, these studies are making decisions about the relative merits of these technologies and experimental outcomes based on parameters of the EEG recorded with the ADS1299.

With an increased interest in mobile brain computer interfaces (Kranczioch et al., 2014; Wolpaw et al., 2002; Lalor et al., 2005), engineers and researchers have sought front-ends which are low cost, have a small form factor and possess good electrical characteristics (Uktveris & Jusas, 2018). Consequently, in the past two years alone, it has appeared in six novel BCIs including an interactive care system for aged patients with dementia (Dang et al., 2017), a modular hybrid BCI based on EEG and near infra-red spectroscopy (NIRS) (von Lühmann et al., 2017), a plug and play BCI for active and assisted living control (Mora et al., 2016), a hybrid BCI combining P300 and Auditory Steady State Response (ASSR) (Kaongoen & Jo, 2017), an embedded

BCI for classification of event related synchronisation/desynchronisation (Belwafi et al., 2018), and a study of stimuli design for a BCI based on Steady State Evoked Potentials (SSVEP) (Jukiewicz & Cysewska-Sobusiak, 2016). However, these BCIs have been tested in only a small number of participants and evaluations of the signal quality have relied on comparisons to past literature.

The breadth of research using the ADS1299 illustrates its appeal for both clinical research and end-user devices. None of these studies has evaluated the EEG recording performance of the ADS1299 in comparison with a high quality system in absence of other variables such as novel electrodes, an algorithm or a BCI paradigm. Researchers have emphasised the need for objective evaluation of EEG signals from devices intended to be used in BCI applications (Oliveira et al., 2016; Radüntz, 2018; Ries et al., 2014). Thus, there is a pressing need for an an independent evaluation of the ADS1299 with a robust experimental design. The aim of this research is to evaluate its performance in EEG against a high quality laboratory based system while controlling for participants, paradigm, tasks performed, electrodes used, and data processing methods. Also, this research aims to evaluate the performance of the ADS1299 in both single joint (dorsiflexion while sitting) and multi-joint (step on/off while standing) motor tasks.

3.1.3 Materials and Methods

This within-participants experimental study was conducted at Auckland University of Technology, New Zealand. Ethical approval for the study (17/CEN/133) was obtained from Central Health and Disability Ethics Committee (HDEC), New Zealand in accordance with the Declaration of Helsinki.

3.1.3.1 Participants

Twenty two healthy participants (Average age: 36 ± 6 years, 10 female) were recruited through professional networks and local advertising. Participants were excluded if they had a history of any neurological disorders or epilepsy. All the participants signed a written consent form before data collection.

3.1.3.2 EEG Systems

3.1.3.2.1 Prototype For evaluation of the ADS1299, a prototype system was built using OpenBCI (OpenBCI, New York, NY, USA) V3-32 board along with a V3 Daisy module for supporting up to 16 channels, a 4N25 optocoupler and required connectors. The firmware of the OpenBCI board was modified from version 3.0.0[2] (refer to supplementary files). The data was saved on the onboard SD card. The sampling rate was set at 250 Hz and Programmable Gain (PGA) at 24, as these settings result in minimum peak-to-peak input referred noise (Instruments, 2012).

3.1.3.2.2 Gold Standard NuAmps (Compumedics Neuroscan, Dresden, Germany) was used as the Gold Standard System (GS) (Cravo et al., 2011; Nascimento et al., 2004; Gu et al., 2009; Niazi et al., 2011; van Deursen et al., 2009). A search on Google Scholar for the keywords "Compumedics Neuroscan NuAmps" returned 395 results. It was connected to a computer via a USB cable and data was recorded with the Acquire software (Compumedics Neuroscan, Dresden, Germany). As per standard data collection protocols, the sampling rate was set at 500 Hz (Cravo et al., 2011; Nascimento et al., 2004; Gu et al., 2009; Niazi et al., 2011; van Deursen et al., 2009).

3.1.3.2.3 Electrodes With both the systems, a 32 channel Quick-Cap with Ag/AgCl wet electrodes (Compumedics Neuroscan, Dresden, Germany) was used for EEG and

[2]Available on GitHub at: https://github.com/OpenBCI/OpenBCI_32bit_Library/releases/tag/v3.0.0

disposable BlueSensor N (Ambu®, Bayan Lepas, Malaysia) electrodes were used for Surface Electromyography (sEMG). A 37 pin D-subminiature connector was used to connect the prototype to the Quick-Cap.

3.1.3.3 Experiment Protocol

For each of the 22 participants, data was collected over two sessions on consecutive days. In each session, participants performed two motor tasks using a single system. The order of the systems and the order of the motor tasks was randomised across the participants. Thus, all the participants performed both the tasks using both the systems, however, the order in which they performed these tasks and the choice of the system used on a given day was random. This pair-wise matching of the participants across the two systems and the two tasks allowed for the paired statistical analysis. This within-participant protocol is in agreement with the previous research evaluating EEG hardware (Oliveira et al., 2016; Radüntz, 2018).

In each session, the participants executed 50 right foot ballistic dorsiflexions while seated and 50 repetitions of right foot step on and off a step-stool (approximately 23 cm high) placed at a comfortable distance while standing. Participants were asked to place their right foot on the step-stool and immediately bring it back to the ground. They executed the tasks at their own pace while pausing for at least five seconds between each repetition. The order of the tasks was chosen at random and data was recorded separately for each task.

EEG data was collected from 14 10-20 system locations (Fp1, F3, F4, FC3, FCz, FC4, C3, Cz, C4, CP3, CPz, CP4, P3, P4) using either the gold standard or the prototype depending on the randomisation schedule. A single reference electrode from Quick-Cap was used which was located on the right mastoid. Electrodes were prepared using Quick-Gel (Compumedics Neuroscan, Dresden, Germany). For sEMG, two electrodes were placed on the right Tibialis Anterior (TA) muscle. Preparation included shaving,

exfoliating with the Nuprep Gel (Weaver and Company, Aurora, CO, USA), and cleansing with disposable alcohol swabs. Acquire software (Compumedics Neuroscan) was used in combination with NuAmps to monitor impedance for both EEG and sEMG, and was accepted when below 10 kΩ. During data collection the systems were placed on a desk next to the participant.

3.1.3.4 Data Processing

The data was processed on MATLAB 2017b (MathWorks, Inc., Natick, MA, USA) using a combination of custom code[3] and EEGLAB (version 14.1.1) functions (Delorme & Makeig, 2004). Movement onsets from rectified sEMG data were detected using an extended version of the double thresholding algorithm (Bonato et al., 1998). These onsets were then visually checked and adjusted. Using 2nd order, zero-phase, Butterworth filters, sEMG data was filtered with a high pass cut-off at 10 Hz, and low pass cut-off at 200 Hz and at 100 Hz for the gold standard and the prototype, respectively. As sEMG was used only for identifying the movement onsets, these cut-offs were considered adequate (Ives & Wigglesworth, 2003; Boxtel et al., 1993).

3.1.3.4.1 EEG Processing EEG channels were filtered with 2nd order, zero phase, Butterworth filters with a highpass filter cut-off at 0.05 Hz, a low pass filter cut-off at 40 Hz and a notch filter from 49 to 51 Hz. These filtered EEG channels were visually inspected along with their frequency spectrum and histograms. The channels which were missing or had very large transients were removed and interpolated with EEGLAB *pop_interp* function using the *spherical* interpolation method. The data was then down sampled to 125 Hz and epochs were derived by including data from 3 seconds before and after the sEMG onset.

Then, epochs with large or very fast transients were removed and Independent

[3]The data processing pipeline is available on GitHub at: https://github.com/GallVp/evalMRCP

Component Analysis (ICA) was performed with EEGLAB *pop_runica* function using the *runica* algorithm (Makeig et al., 1996). Components corresponding to eye blinks, or limited to only one electrode and a few epochs, were removed. The remaining components were remixed (back projected to sensor space) and epochs with amplitude above 125 μV_{pp} across any channel were removed to obtain clean EEG epochs. MRCP epochs were obtained from these cleaned EEG epochs by applying a small spatial filter across FC3, FCz, FC4, C3, Cz, C4, CP3, CPz, CP4 channels with center at Cz (McFarland et al., 1997). The spatial filter was followed by a 2^{nd} order, zero phase, Butterworth filter with a low pass cut-off at 5 Hz. By taking the mean across the epochs, the averaged MRCP was obtained.

3.1.3.5 Performance Measures

In order to compare the two systems, the following performance measures were obtained from the EEG epochs and the averaged MRCP for each participant.

3.1.3.5.1 EEG Specific Measures

a Power across EEG Bands: Power across four EEG bands (delta [0.05–3 Hz], theta [3–8 Hz], alpha [8–12 Hz] and beta [12–38 Hz]) was obtained separately from each epoch for all the channels using MATLAB *bandpower* function. The obtained power was converted to Decibels (dB), and then averaged across epochs and channels for each band (Oliveira et al., 2016).

b Pre-movement Noise (PMN): The EEG activity from two to three seconds before the sEMG onset was regarded as baseline (Shibasaki & Hallett, 2006). The Root Mean Square (RMS) value of the baseline was calculated separately from each epoch for all the channels and then averaged across channels and epochs to obtain pre-movement noise (Vos et al., 2014).

3.1.3.5.2 MRCP Specific Measures

a Signal to Noise Ratio (SNR): The signal to noise ratio was defined as the ratio of peak negative amplitude to the RMS value in the baseline segment of the averaged MRCP, expressed in decibels.

b Amplitude and Time of Negative Peak (PN, PNT): The amplitude of the negative peak in the 1 second before and after the sEMG onset was obtained from the averaged MRCP using a local peak algorithm (Luck, 2014). The time of the peak negative amplitude was expressed in milli-seconds; where a negative value represents occurrence before, and a positive value after, the sEMG onset. The peak negative value is one of the most important features of the MRCP as it has been widely studied in relation with rehabilitation and motor learning (Jochumsen et al., 2017; Mrachacz-Kersting et al., 2012).

3.1.3.6 Statistical Analysis

Statistical analysis was performed[4] in R (R Foundation for Statistical Computing) version 3.5.0. Means are given with the standard deviations. Based on an apriori statistical analysis, the performance of the prototype was assessed against the gold standard for power across EEG bands, power ratio, pre-movement noise, signal to noise ratio, and the amplitude and time of the negative peak using linear mixed models or generalised linear mixed models as appropriate (B. Winter, 2013). *lme4* package version 1.1-17 was used for fitting the models (Bates et al., 2015). The detailed setup of the models is given in the corresponding result sections. Analysis of deviance tables for the models were obtained using the *Anova* function from *car* package version 3.0-0 (Fox & Weisberg, 2011). Significance level was set at 0.05. For main effects and interactions, Type II Wald Chi-square tests are reported. In case of significant interactions, pair-wise

[4]The statistical analysis pipeline is also available on GitHub at: https://github.com/GallVp/evalMRCP

comparisons were performed with Tuckey's HSD (Honestly Significant Differences) method using the *lsmeans* function from the *lsmeans* package version 2.27-62 (Lenth, 2016). For the pair-wise comparisons, Cohen's d effect size using pooled variance was calculated. It was interpreted as small (0.20), medium (0.5), or large (0.8) effect (Lakens, 2013). Cosine Similarity (r) was also assessed for the averaged MRCPs across the two systems. The MRCPs from the two systems were treated as vectors and their cosine similarity was defined as follows (Dehak et al., 2010).

$$r = \frac{\mathbf{u}.\mathbf{v}}{\|\mathbf{u}\| \times \|\mathbf{v}\|} \tag{3.1}$$

Where, **u**, **v** represent the two MRCPs as vectors. '**.**' represents the dot product between the two vectors, and $\|.\|$ represents the L_2 norm of the vector. Two additional analyses which were not part of the apriori analysis plan were also performed. First, grand average MRCPs for the gold standard and the prototype were obtained in dorsiflexion and step on/off from the averaged MRCPs of the participants. These grand average MRCPs were plotted along with their differences and 95% confidence intervals. Differences were evaluated by applying sample wise repeated measure t-tests and interpreted based on Bonferroni corrected p-values. Second, interpolated topographic maps were also obtained at different latencies by task and system wise pooling of all the cleaned EEG epochs. The *pop_topoplot* function from EEGLAB was used for this purpose. Differences were evaluated by obtaining the maps from absolute difference of the channels.

3.1.4 Results

3.1.4.1 Data Loss and Artefacts

In case of the gold standard system, there was no loss of data. For the prototype, the data from dorsiflexion of one participant was lost as the sEMG channels were recorded for only the first repetition. The EEG data from this repetition was rejected due to the presence of large transients. The prototype's data had occasional single sample very large amplitude (> 1000 µV) artefacts in some channels as shown in Figure 3.1. The incidence of these artefacts was approximately 1 in 10,000 samples. It was removed using an automatic detection algorithm and replaced with the average of the fifth sample from its left and right.

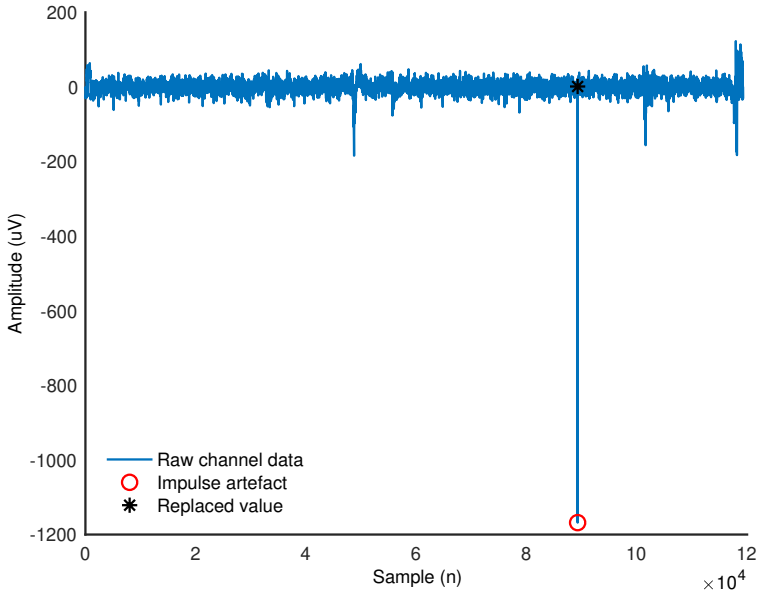

Figure 3.1: An example of the artefact detected in the prototype data

3.1.4.2 Rejection of Channels, ICA Components and Epochs

For the gold standard system, on average 0.5 ± 0.8 and 0.7 ± 1.5 channels were interpolated in dorsiflexion and step on/off respectively, across the participants. For the prototype, 0.3 ± 0.6 and 0.4 ± 0.7 channels were interpolated. During the ICA analysis,

components corresponding to eye blinks, or limited to only one electrode and a few epochs, were removed. For the gold standard 3.0 ± 1.9 and 3.8 ± 2.1 components were rejected in dorsiflexion and step on/off respectively. For the prototype, 3.4 ± 2.2 and 3.3 ± 1.8 components were removed. The number of interpolated channels and rejected components appear to be similar across systems and higher in step on/off compared to dorsiflexion.

Two sets of 50 EEG epochs corresponding to the two systems were obtained for each task from the sEMG onsets. The epoch rejection rate was calculated as the ratio of the number of epochs rejected manually and with thresholding to number of sEMG onsets used for creating epochs. This ratio was expressed as percentage. The mean rejection rate at 125 μV_{pp} ranged from 4.9 to 7.6%. However, when 75 μV_{pp} threshold was applied, it ranged from 31.9 to 52.5% across tasks and systems, refer to Table 3.1. Whilst the standard deviation of the dorsiflexion rejection rate appears higher in the prototype, this can be explained by the rejection of 1 out of 1 epoch for the participant whose sEMG data was lost as explained earlier in Section 3.1.4.1.

Table 3.1: Means and standard deviations for percentage epoch rejection rates at 75 μV_{pp} and 125 μV_{pp}

Task	System	Rejection at 75 μV_{pp} (%)	Rejection at 125 μV_{pp} (%)
Dorsiflexion	GS	31.9 ± 26.4	6.1 ± 7.0
	Proto	34.7 ± 31.7	7.6 ± 20.9
Step on/off	GS	52.5 ± 35.6	5.7 ± 6.2
	Proto	43.6 ± 34.1	4.9 ± 4.0

3.1.4.3 EEG Specific Measures

3.1.4.3.1 Power across EEG Bands Separate linear mixed models were setup to compare EEG power in dorsiflexion and step on/off respectively. Systems, bands, and an interaction term for systems and bands was entered as fixed effects. For participants, a random intercept term was also entered. The setup of the linear mixed model is given

in R formula syntax as follows (Bates et al., 2015).

```
Power ~ System + EEGBand + System * EEGBand + (1|
    Participant)
```

In dorsiflexion, there was no interaction between the systems and EEG bands ($\chi^2[3] = 1.82$, $p = 0.61$). Also, there was no significant difference across systems ($\chi^2[1] = 0.01$, $p = 0.91$). There was a significant difference in power across bands ($\chi^2[3] = 554.42$, $p < 0.001$). Similar results were obtained in step on/off. There was no interaction between the systems and EEG bands ($\chi^2[3] = 0.57$, $p = 0.90$). There was no significant difference across systems ($\chi^2[1] = 0.13$, $p = 0.72$). There was a significant difference across the bands ($\chi^2[3] = 508.33$, $p < 0.001$), refer to Figure 3.2 (A, B) and Table 3.2. These results indicate that the prototype system is comparable to the gold standard system with respect to power.

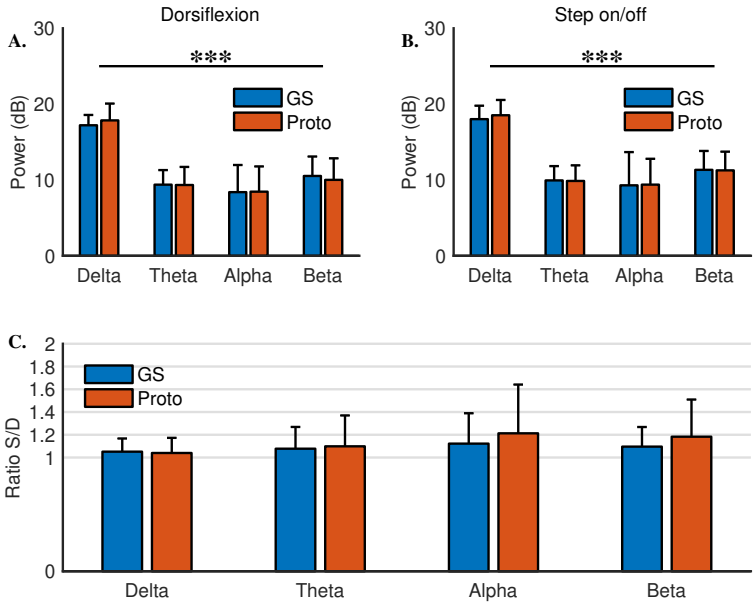

Figure 3.2: Power recorded across four EEG bands in dorsiflexion and step on/off
Note: '***' represents p-value less than 0.001.

Table 3.2: Means and standard deviation for power values in decibels (dB) across four EEG bands in dorsiflexion and step on/off

Task	System	Delta (dB)	Theta (dB)	Alpha (dB)	Beta (dB)
Dorsiflexion	GS	17.2 ± 1.4	9.4 ± 1.9	8.4 ± 3.5	10.5 ± 2.6
	Proto	17.9 ± 2.2	9.3 ± 2.4	8.5 ± 3.3	10.0 ± 2.8
Step on/off	GS	18.0 ± 1.8	9.9 ± 1.9	9.3 ± 4.4	11.3 ±2.5
	Proto	18.5 ± 2.0	9.9 ± 2.1	9.4 ± 3.4	11.3 ±2.5

In order to assess the sensitivity of the systems to detect differences in power across tasks, a participant wise ratio of power values from step on/off to dorsiflexion (S/D) was obtained, as shown in Figure 3.2, C. For the delta band the power ratios for the gold standard and the prototype were 1.05 ± 0.12 and 1.04 ± 0.13 respectively. The power ratios for the prototype in theta, alpha and beta bands were 1.1 ± 0.27, 1.2 ± 0.43 and 1.18 ± 0.33 respectively. For the gold standard, the ratios for the theta, alpha, and beta bands were 1.08 ± 0.19, 1.12 ± 0.27 and 1.1 ± 0.17 respectively. A linear mixed model with systems, bands, and interaction term for systems and bands as fixed effects was setup. A random intercept term for the participants was also entered. Significant interaction between the bands and the systems on the power ratio was not detected ($\chi^2[3] = 1.51$, $p = 0.68$). There were no significant differences across bands ($\chi^2[3] = 6.8$, $p = 0.08$) or systems ($\chi^2[1] = 1.94$, $p = 0.16$). These results suggest that both systems have similar sensitivity to power differences in EEG bands across different motor tasks.

3.1.4.3.2 Pre-movement Noise Pre-movement noise in dorsiflexion was 8.82 ± 1.57 µVrms and 8.85 ± 2.00 µVrms for the gold standard and the prototype respectively. In step on/off the values for the two systems were 9.87 ± 1.91 µVrms and 10.11 ± 2.54 µVrms. To evaluate differences across systems and tasks in the pre-movement noise, a generalised linear mixed model with Gamma family and log link was setup as the data had skew with a long tail. Systems, tasks and an interaction term for systems and tasks were entered as fixed effects. A random intercept term for the participants was

also entered. The setup of the generalised linear mixed model is given in R formula syntax as follows (Bates et al., 2015).

```
Noise ~ System + Task + System * Task  + (1|Participant)
```

There was no significant interaction between systems and tasks on pre-movement noise ($\chi^2[1] = 0.09$, $p = 0.77$). There was no significant difference across the systems ($\chi^2[1] = 0.05$, $p = 0.83$). A significant difference was detected across the tasks ($\chi^2[1] = 14.12$, $p < 0.001$). These results suggest that the prototype system's susceptibility to noise is similar to the gold standard system. However, both systems have higher noise in step on/off compared to dorsiflexion, refer to Figure 3.3, A.

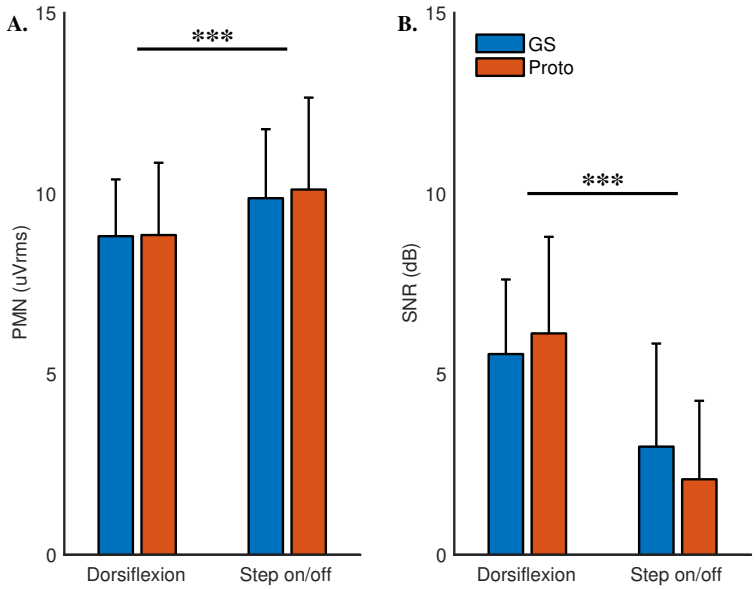

Figure 3.3: Means and standard deviations for pre-movement noise and signal to noise ratio
Note: '***' represents p-value less than 0.001.

3.1.4.4 MRCP Specific Measures

3.1.4.4.1 Signal to Noise Ratio Signal to noise ratio in dorsiflexion was 5.56 ± 2.06 dB and 6.13 ± 2.67 dB for the gold standard and the prototype respectively. In step on/off the values for the two systems were 2.99 ± 2.85 dB and 2.09 ± 2.17 dB. A linear mixed model with systems, tasks and an interaction term for systems and tasks as

fixed effects was setup. A random intercept term for the participants was also entered. Significant interaction between the systems and the tasks was not detected ($\chi^2[1] = 2.32$, $p = 0.13$). No significant differences were detected across the systems ($\chi^2[1] = 0.111$, $p = 0.74$). However, a significant difference was detected across the tasks ($\chi^2[1] = 44.75$, $p < 0.001$). These results indicate that the signal to noise ratio of the prototype is comparable to that of the gold standard, refer to Figure 3.3, B.

3.1.4.4.2 Amplitude and Time of the Negative Peak Peak negative value in dorsiflexion for the gold standard and the prototype system was -4.44 ± 2.17 µV and -4.29 ± 2.00 µV respectively. In step on/off the PN amplitude was -2.36 ± 1.34 µV and -2.75 ± 1.50 µV. A linear mixed model with systems, tasks and an interaction term for systems and tasks as fixed effects was setup. A random intercept term for the participants was also entered. Interaction between the systems and the tasks on the PN amplitude was not significant ($\chi^2[1] = 1.04$, $p = 0.31$). There were no significant differences across the systems ($\chi^2[1] = 0.23$, $p = 0.63$). A significant difference across the tasks was detected ($\chi^2[1] = 47.61$, $p < 0.001$).

The time of the peak negative amplitude in dorsiflexion was 261.09 ± 139.32 ms and 256.00 ± 181.73 ms for the gold standard and the prototype system respectively. In case of step on/off, the time for the systems was 284 ± 340.24 ms and 397.82 ± 344.05 ms. A linear mixed model with systems, tasks and an interaction term for systems and tasks as fixed effects was setup. A random intercept term for the participants was also entered. Interaction between the systems and the tasks on the time of the peak negative amplitude was not significant ($\chi^2[1] = 1.23$, $p = 0.27$). There were no significant differences across the systems ($\chi^2[1] = 1.11$, $p = 0.29$) and the tasks ($\chi^2[1] = 2.31$, $p = 0.13$).

The systems were comparable with respect to the time and the amplitude of the negative peak in the MRCP. The amplitude of the negative peak differed significantly between the motor tasks, refer to Figure 3.4.

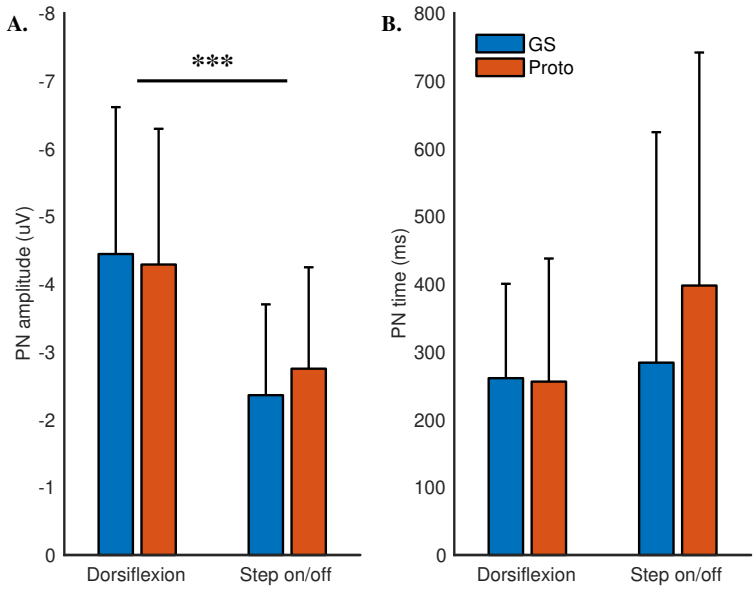

Figure 3.4: Means and standard deviations for the peak negative value and its time for the two systems across the tasks
Note: '***' represents p-value less than 0.001.

3.1.4.5 Cosine Similarity

The mean similarity in dorsiflexion across the two systems was 0.84 ± 0.14 and 0.75 ± 0.28 in step on/off. Averaged MRCPs from the two systems along with cosine similarity are given in Figure 3.5 and 3.6. The results indicate a strong cosine similarity between the MRCP signals recorded by the two systems, suggesting that the prototype is comparable to the gold standard.

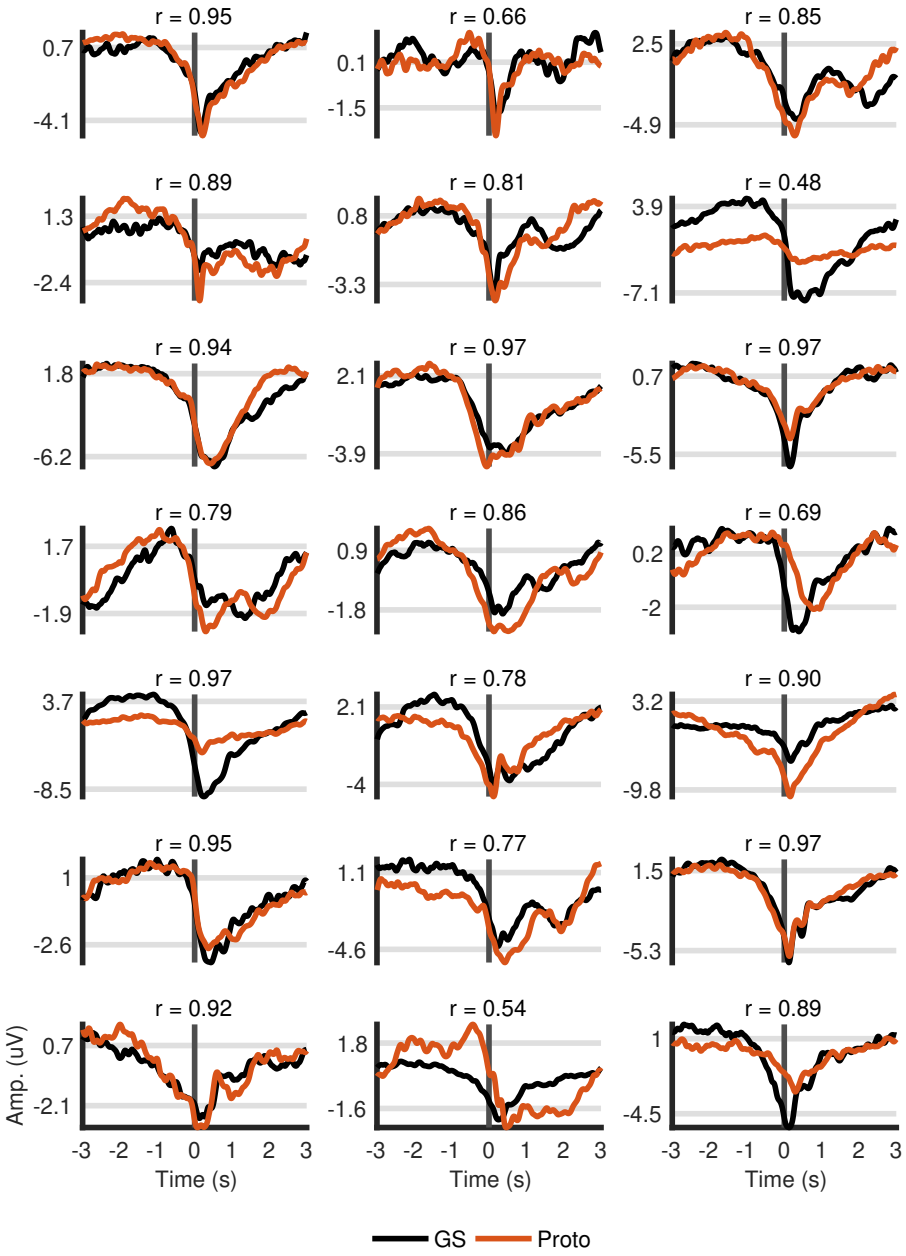

Figure 3.5: Averaged MRCPs for 21 participants in dorsiflexion
Averaged MRCPs for 21 participants in dorsiflexion from gold standard and the prototype along with cosine similarity (r). GS and Proto stand for the gold standard and the prototype system respectively.

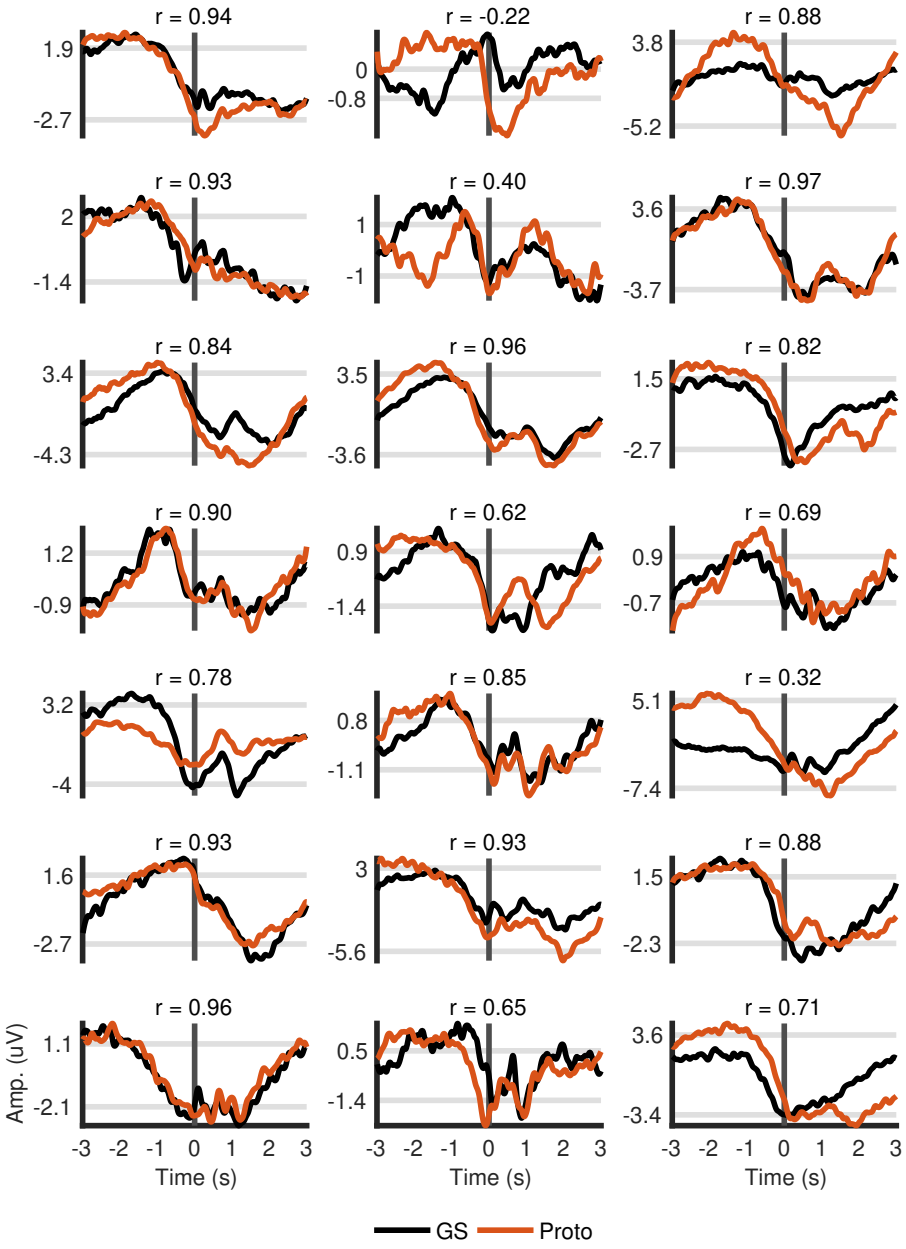

Figure 3.6: Averaged MRCPs for 21 participants in step on/off
Averaged MRCPs for 21 participants in step on/off from gold standard and the prototype along with cosine similarity (r). GS and Proto stand for the gold standard and the prototype system respectively.

3.1.4.6 Grand Average of Participant MRCPs

Grand averages and difference waveforms with 95% confidence intervals obtained from the averaged MRCPs of the individual participants are shown in Figures 3.7 and 3.8.

The grand average MRCPs were similar for the two systems in both the tasks. The confidence intervals were uniform, overlapping, and their size was smaller than ±1 µV. There were no significant differences across the systems. These results indicate agreement between the averaged MRCPs recorded by the two systems.

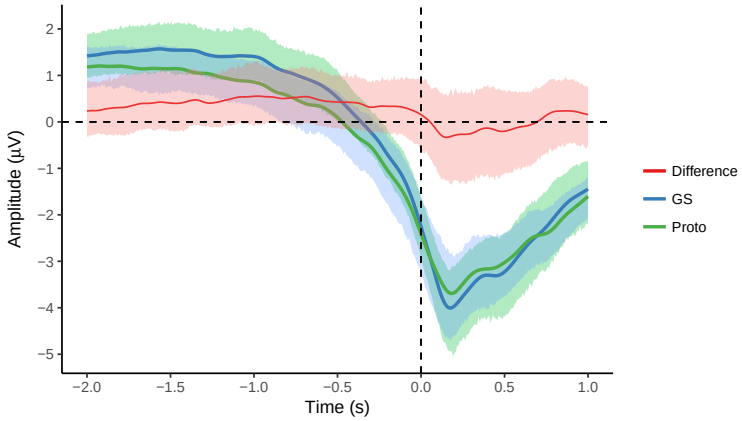

Figure 3.7: Grand averages and difference (GS - Proto) in dorsiflexion
Grand averages and difference (GS - Proto) along with 95% confidence intervals for the averaged MRCPs (n = 21). Time at 0 seconds corresponds to the movement onset.

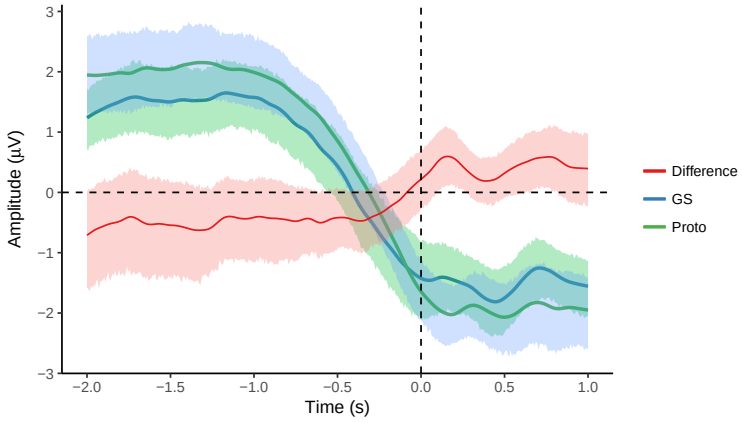

Figure 3.8: Grand averages and difference (GS - Proto) in step on/off
Grand averages and difference (GS - Proto) along with 95% confidence intervals for the averaged MRCPs (n = 22). Time at 0 seconds corresponds to the movement onset.

3.1.4.7 Topographic Maps

Interpolated topographic maps obtained from cleaned EEG epochs of the 14 EEG channels are shown in Figures 3.9 and 3.10 for dorsiflexion and step on/off respectively. These maps suggest that in both tasks, the spatial distribution of cortical activity was similar and the differences across the systems are negligible. At movement onset, cortical activations are centered around CPz and Cz in both systems. These results also indicate that both the systems record similar EEG.

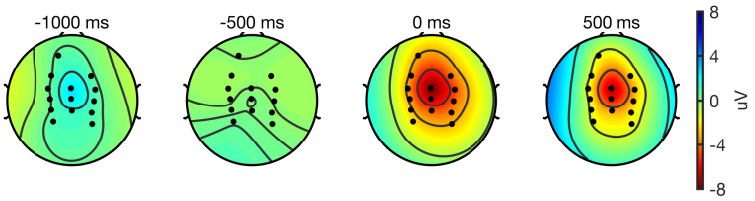

(a) GS

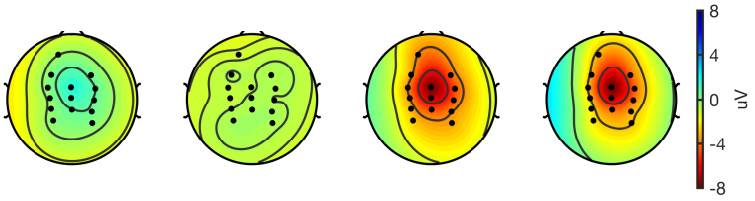

(b) Proto

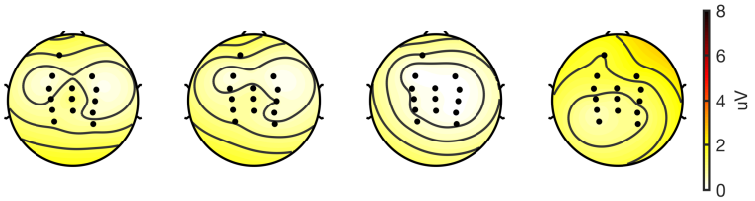

(c) Absolute difference of channels from (a) and (b)

Figure 3.9: Interpolated topographic maps for dorsiflexion
Interpolated topographic maps obtained at different latencies with respect to the movement onset form cleaned EEG epochs (n = 21). 977, 1007 epochs were used for the gold standard and the prototype respectively. Time at 0 milli-seconds corresponds to the movement onset.

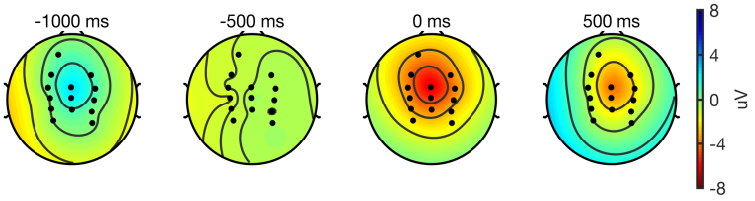

(a) GS

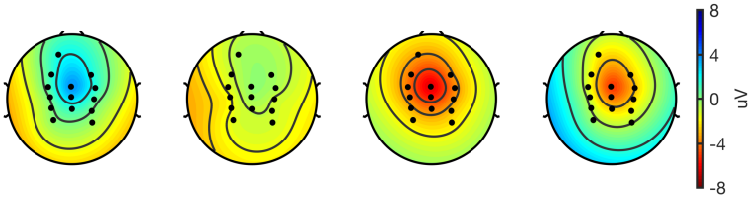

(b) Proto

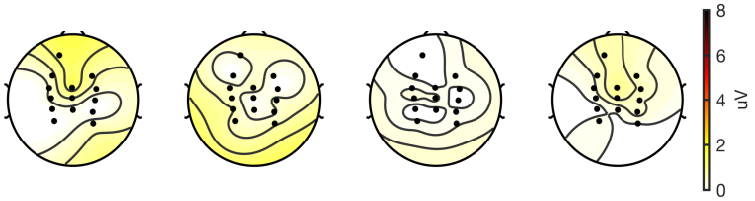

(c) Absolute difference of channels from (a) and (b)

Figure 3.10: Interpolated topographic maps for step on/off
Interpolated topographic maps obtained at different latencies with respect to the movement onset form cleaned EEG epochs (n = 22). 1022, 1028 epochs were used for the gold standard and the prototype respectively. Time at 0 milli-seconds corresponds to the movement onset.

3.1.5 Discussion

This experimental study has rigorously evaluated the EEG recording performance of ADS1299 in comparison to a high quality laboratory based system whilst controlling for participants, paradigm, tasks performed, electrodes used, and data processing methods in a large sample of healthy participants. The main finding of this research are that the ADS1299 is comparable with respect to power across EEG bands, power ratio, pre-movement noise of the EEG, and the signal to noise ratio, the amplitude and time of the negative peak, and cosine similarity of the MRCPs. The validity of these findings are

supported by the large sample size, and the robust statistical analysis which accounted for between participant variance. These results are discussed in detail below.

We computed the average power in delta, theta, alpha and beta bands from all the included epochs of all the recorded channels. Thus, the obtained value included both the evoked and the induced power. Within both motor tasks, there were no significant differences between the laboratory based system and the ADS1299. The sensitivity to power changes across different tasks was evaluated with the ratio of step on/off power to dorsiflexion. There were no differences in the power ratio across the systems or the bands. Therefore, in EEG studies where spectral features during motor tasks are of interest (Kamavuako et al., 2015; Ramos-Murguialday & Birbaumer, 2015; Trammell et al., 2017), ADS1299 can be used with confidence.

Another important measure of EEG device quality is the level of noise present in the baseline. Similar to past studies (Vos et al., 2014; Oliveira et al., 2016), this was quantified by the root mean square value in the baseline EEG from epochs of all channels. There were no differences across the two systems. The noise was higher in case of step on/off compared to dorsiflexion. The most likely sources of this noise are cable sway (Symeonidou et al., 2018), head movements (Mihajlovic et al., 2014), or physiological differences. In this research, the experimental protocol and the requirement to standaradise the setup across the systems necessitated that the ADS1299 was placed on a desk. However, in mobile BCI applications the effects of head movements and cable sway may be mitigated by the use of an inertial measurement unit and by mounting it closer to the electrodes (O'Regan et al., 2013). Comparable noise levels in both the systems is a strong indicator of the quality of EEG recorded by the ADS1299.

Two notable differences between the systems were revealed during data pre-processing. First, the prototype data exhibited a single sample, very large value artefact. This problem most likely originated from the way data was stored on the SD card using the OpenBCI board, as the error was also found in the raw data file before conversion from

hexadecimal values. The artefact could not be removed with a low pass filter as this resulted in large transients. However, the artefact sample could easily be substituted with an averaged value. The second difference between the systems was that in one prototype file sEMG data was missing. The source of this problem is most likely that the Daisy board was disconnected from the main OpenBCI board and failed to reconnect during recording. In future studies, this problem can be avoided by ensuring a more robust connection between the two boards.

Comparable number of interpolated channels, rejected ICA components and epoch rejection rates indicate that the ADS1299 records EEG reliably. We explored epoch rejection rates at traditional 75 uVpp and 125 uVpp thresholds. At 75 uVpp both systems had rejection rates of 40 – 50% during step on/off, which is similar to those reported by Oliveira et. al. for Biosemi system and Cognionics wet system during a walking task (Oliveira et al., 2016). At 125 uVpp, the ADS1299 epoch rejection rate was below 10%, supporting its use in EEG devices.

MRCPs are slow moving potentials which start before the movement onset and continue during and after the movement (Shibasaki & Hallett, 2006). In this research MRCPs were recorded in motor tasks undertaken while sitting and standing. The fact that they are challenging to record and process as they are found in the delta band and are highly susceptible to movement artefacts and other sources of noise makes them an excellent test case for evaluating EGG devices. Based on the findings of this research it can be asserted that the ADS1299 is an excellent choice for recording MRCPs. This assertion is supported by the equivalence of signal to noise ratio, time and amplitude of the negative peak, and the cosine similarity, the waveform differences of the MRCP with that of the laboratory based system. Also, the topographic maps showed that the cortical distribution of EEG was similar across the two systems in both tasks and concordant with previous research (Nascimento et al., 2004; Shibasaki & Hallett, 2006). These findings have implications for the translation of MRCP based BCI paradigms to

real world applications (Niazi et al., 2012; Jochumsen et al., 2017; R. Xu et al., 2016).

Reflecting on the differences between the MRCP in the two motor tasks highlighted some important findings which have implications for researchers interested in MRCP based brain computer interfaces targeted towards both single joint movements such as dorsiflexion and functional movements such as walking (Sburlea et al., 2015) or sitting/standing (Bulea et al., 2014). The signal to noise ratio was significantly lower in step on/off, due to higher noise in baseline EEG and a smaller negative peak in the MRCP. The decrease in the peak negative value in step on/off maybe explained by the torque generated in the two tasks (Nascimento et al., 2004), although other task parameters may have also influenced. This observation is supported by the fact that the time of the negative peak was same across both tasks, although it had larger variability in step on/off. The differences across the tasks were found in both the systems suggesting that the ADS1299 is sensitive enough to discern these variances.

The findings of this research should be considered in light of a number of limitations. First, EEG and EMG data was not recorded simultaneously with both the systems. Rather, a single system was used in a given recording session in a randomised order on different days. This protocol is in line with the research comparing different EEG devices using within-participant designs (Oliveira et al., 2016; Ries et al., 2014; Radüntz, 2018). Second, the performance of an EEG recording system depends not only on the amplification chip, but also on the quality of the electrode system and the design of the printed circuit board (PCB). Thus, the performance evaluation of the ADS199 performed in this research should be interpreted in relation with the used electrode system (Compumedics Neuroscan Quick-Cap) and the circuit board (OpenBCI Cyton V3-32 board). Third, the sample rate used for ADS1299 was 250 Hz and PGA gain was 24 as these setting result in minimum input referred noise (Instruments, 2012). On the other hand, in agreement with the past research, the sampling rate was set at 500 Hz for the NuAmps (Cravo et al., 2011; Nascimento et al., 2004)(Gu et al., 2009; Niazi et al.,

2011; van Deursen et al., 2009). To address this, data from both the systems was down sampled to 125 Hz before analysis. Fourth, the features studied in this research only represented the lower range (< 40 Hz) of the EEG spectrum. Thus, further research is required to investigate the quality of EEG recording with ADS1299 in the higher frequency bands.

3.1.6 Conclusion

This study has comprehensively demonstrated that the ADS1299 records low frequency (< 40 Hz) EEG at a level comparable to a laboratory based system. Using a robust experimental design with pre-planned statistical analysis we found no significant differences across the two systems in both EEG specific measures such as power across bands, power ratio across bands, pre-movement noise, and MRCP specific measures such as signal to noise ratio, time and amplitude of the negative peak. In addition, this study illustrated differences in the MRCP of the two motor tasks, one single joint and the other multi-joint. We conclude that ADS1299 in combination with wet Ag/AgCl electrodes is a good choice for both clinical research and the development of mobile BCIs based on low frequency (< 40 Hz) EEG.

End of Published Manuscript 1

3.2 Summary

In summary, Texas Instruments ADS1299 chip was selected and evaluated to provide a portable ADC for medical devices for MRCP based rehabilitation paradigms. We found strong evidence for its ability to record MRCPs at a quality analogous to that of a laboratory based system (Rashid et al., 2018). This fully addresses objective number 2 listed in section 2.6, which was to establish the performance of a cost-effective small footprint ADC for recording MRCPs.

Chapter 4

Contributions to Computational Methods

This chapter presents three computational methods which I proposed to bring closer the goal of building a medical device for MRCP based rehabilitation paradigms. The first method was proposed to address the objective numbered 5 in section 2.6 which was to automate the feature extraction from the movement-related cortical potential. The original study was published in a peer reviewed journal. The published article is presented in section 4.1 with no content modifications and minor formating modifications to facilitate reading[1].

As it was introduced in chapter 2 section 2.5.3, an important component of the brain computer interface used for delivering the online neuromodulatory intervention is the algorithm which detects the MRCP in real-time. The existing MRCP detection algorithms either use movement onsets obtained from sEMG data to construct a person specific model of the brain activity, or the timing of the cue presented on a screen. Thus, the use of these algorithms is predicated on the quality of the sEMG signal which can be

[1]Original article: U. Rashid, I. K. Niazi, M. Jochumsen, L. R. Krol, N. Signal, D. Taylor, Automated Labeling of Movement Related Cortical Potentials using Segmented Regression, April 2019, doi: 10.1109/TNSRE.2019.2913880

recorded from a person with a movement disability and the efficiency of an EMG onset detection algorithm. This is where the second and the third proposed computational methods fit. These methods aimed to address objective numbered 4 in section 2.6. The first method, Extended Double Thresholding Algorithm (eDTA), is a sEMG movement onset detection algorithm specifically designed for functional movements which have two or more components. For example, stepping on and off a step-stool is a functional movement with two components, stepping on and then stepping off. The second method is an optimisation technique, *nOptim*, which can be used to improve the quality of the results produced by eDTA or any other sEMG onset detection algorithm. These methods were conceived to solve very specific problems in the processing pipeline of the brain computer interface used for MRCP based rehabilitation paradigms. However we realised that these methods are likely to have a much wider application. Thus to make these methods more accessible to the research community at large, they were published together and presented as a solution for the challenging problem of accurate identification of onsets and offsets of muscle activations in general. The original study was published in a peer reviewed journal. The published article is presented in section 4.2 with no content modifications and minor formating modifications to facilitate reading[2].

[2]Original article: U. Rashid, I. K. Niazi, N. Signal, D. Farina, D. Taylor, Optimal Automatic Detection of Muscle Activation Intervals, Journal of Electromyography and Kinesiology, June 2019, doi:10.1016/j.jelekin.2019.06.010

Start of Published Manuscript 2

4.1 Automated Labeling of Movement-Related Cortical Potentials using Segmented Regression

4.1.1 Abstract

The movement-related cortical potential (MRCP) is a brain signal related to planning and execution of motor tasks. From a MRCP, three notable features can be identified: the early Bereitschaftspotential (BP1), the late Bereitschaftspotential (BP2), and the negative peak (PN). These features have been used in past studies to quantify neurophysiological changes in response to motor training. Currently, either manual labelling or *a priori* specification of time points is used to extract these features. The limitation of these methods is the inability to fully model the features. This study proposes segmented regression along with a local peak method for automated labelling of the features. The proposed method derives the onsets, amplitudes at onsets and slopes of BP1, BP2 along with time and amplitude of the negative peak in a typical average MRCP. To choose the most suitable regression technique bounded segmented regression method, a change point method and multivariate adaptive regression splines were evaluated using root-mean-square error on a dataset of 6000 simulated MRCPs. The best performing regression technique combined with the local peak method was then applied to a smaller set of 123 simulated MRCPs. Error in onsets of BP1, BP2, and time of PN were compared with errors in manual labelling by an expert. The performance of the proposed method was also evaluated on an experimental dataset of MRCPs derived from electroencephalography (EEG) recorded across two sessions from 22 healthy participants during a lower limb task. Bland-Altman plots were used to evaluate the

absolute reliability of the proposed method. On experimental data, the proposed method was also compared to manual labelling by an expert. Bounded segmented regression produced the smallest error on the simulation data. For the experimental data, our proposed method did not exhibit statistically significant bias in any of the modelled features. Furthermore, its performance was comparable to manual labelling by experts. We conclude that the proposed method be used to automatically obtain robust estimates for the MRCP features with known measurement error.

4.1.2 Introduction

Movement-related cortical potentials (MRCPs) represent the cortical activity related to motor preparation and execution (Kornhuber & Deecke, 1965; Hallett, 1994; Sakamoto et al., 2009). From a MRCP, three notable features can be identified: the early Bereitschaftspotential (BP1), the late Bereitschaftspotential (BP2), and the negative peak (PN). The Bereitschaftspotential (BP) starts around 2.0 seconds before the movement onset. Around 0.4 seconds before the onset, its slope abruptly steepens. These two slopes are characterised with reference to the baseline electroencephalography (EEG) activity as BP1 and BP2 (Shibasaki & Hallett, 2006). These components of the MRCP have been studied across many different populations (Kim et al., 2017; Patil et al., 2017; Wright et al., 2011), notably in the context of motor training (Taylor, 1978; W. Lang et al., 1983; Niemann et al., 1991; Wright et al., 2012b; M.-K. Lu et al., 2011). One motivation to use EEG data is to provide a low cost and simple method to quantify motor training compared to other approaches such as functional magnetic resonance imaging, magnetoencephalography, and transcranial magnetic stimulation (Jochumsen et al., 2017). For EEG data based quantification, measures of BP1, BP2, and PN play an important role.

4.1.2.1 Problem Statement

A range of methods have been employed to obtain BP1, BP2, and PN. In some of the past studies, onsets of BP1 and BP2 were specified *a priori* from previous research and their amplitudes were obtained for evaluation (Taylor, 1978; M.-K. Lu et al., 2011; Fattapposta et al., 1996). Whereas in other studies, BP1, BP2 and PN were identified from the MRCP with visual inspection by single or multiple experts (Kita et al., 2001; Wright et al., 2012a) who applied their knowledge of MRCPs to label points of interest on the signals. The limitation of the first method is that it limits the analysis to amplitudes as onsets are pre-specified. The limitation of the second method is that it cannot be applied automatically.

Another limitation of these methods is that after specifying or labelling the onsets of BP1 and BP2, their amplitudes were obtained by taking an average over a range of the signal (Wright et al., 2012a,b). Averaging over a range reduces the variability due to the local noise present in the signal. However, it discounts the negative slopes of BP1 and BP2 (Shibasaki & Hallett, 2006), as the mean statistic can only partially model a linear trend which has both a non-zero slope and a non-zero intercept. In yet another approach, the difference in amplitudes at two time points was used (Kita et al., 2001), which partially captures the change over time aspect of the slopes but the amplitudes taken at single time points from the signal are susceptible to local noise. Thus, there is a need for an automated method of identifying the MRCP features, which fully captures the underlying signal and is not susceptible to local noise.

4.1.2.2 Related Work

In the context of Lateralised Readiness Potential (LRP) which is another movement-related potential, there has been an effort to propose an automatic detector for its onset. Schwarzenau and Falkenstein proposed a novel method based on segmented regression

for estimating the onset of LRPs (Schwarzenau et al., 1998). Their method fitted two straight line segments to the LRP and labelled the LRP onset at the intersection of the two fitted lines. Alternatively, Miller, Patterson and Ulrich proposed the use of a set voltage threshold for the onset detection of the LRP from the group grand average followed by a jack-knifing procedure to obtain a standard error for the estimated onset (Miller et al., 1998). Later, their jack-knifing method was further improved by Smulders (Smulders, 2010). A detailed investigation of these methods for detection of the LRP onset was conducted by Mordkoff and Gianaros (Mordkoff & Gianaros, 2000). They suggested that regression based methods should be used and the best performing method was the one which only allowed the slope of the second line to vary (Mordkoff & Gianaros, 2000). The obvious disadvantage of using the jack-knifing approach is that the onset and its standard error is computed for the entire group and an arbitrary threshold voltage has to be specified *a priori*. As these methods were proposed and applied to label a single onset of LRP, these methods can not be directly applied to label the two distinct onsets of BP1 and BP2 in a MRCP.

4.1.2.3 Novel Contributions

The aim of this research was to propose an automated method for the identification of BP1, BP2, and PN from a MRCP. To achieve this aim, we propose a local peak method for labelling of PN, and segmented regression for labelling of BP1, BP2. To choose the most suitable regression technique, we present a novel bounded segmented regression method which uses particle swarm optimisation and evaluate it against a change point method and multivariate regression splines. To evaluate these techniques, we also propose a method to simulate MRCPs.

The simulation provides datasets of MRCPs in which the onsets and amplitudes of BP1, BP2 and PN are known. The simulation results are used to select the most suitable regression method for labelling of BP1 and BP2. The selected regression

method combined with the local peak method are proposed for the identification of BP1, BP2, and PN from a MRCP. The performance of the proposed method was then evaluated both on simulated and experimental MRCP data and compared to manual labelling by experts. We also validated the simulated MRCPs against experimental MRCPs.

4.1.3 Methods

Based on the comprehensive discussion of MRCPs found in "What is the Bereitschaft-spotential?" by Shibasaki and Hallet (Shibasaki & Hallett, 2006), we make the following assumptions about the MRCP. Refer to Figure 4.1 for an example signal.

a. BP1 and BP2 can be modelled by two straight lines with non-zero slopes and intercepts.

b. PN can be modelled as a negative peak and is in close vicinity to the movement onset.

c. EEG activity before the onset of BP1 can be modelled as a straight line with a zero slope but a non-zero intercept.

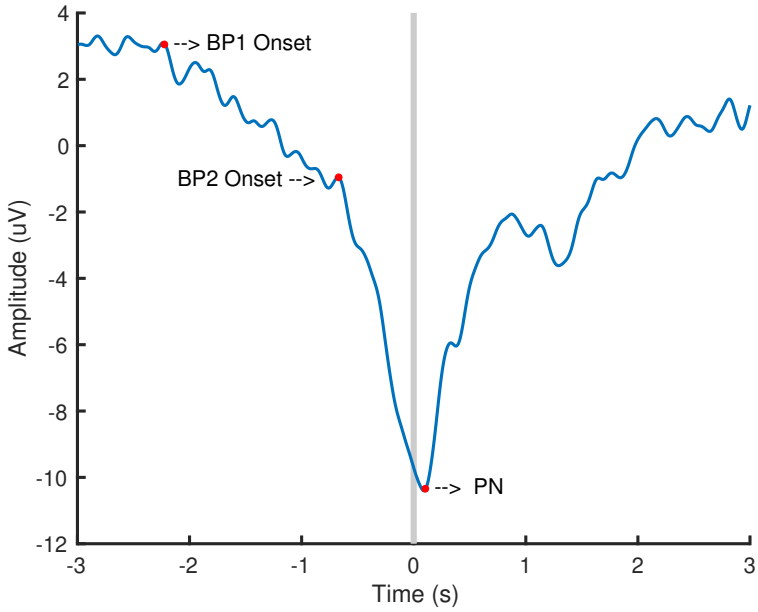

Figure 4.1: An example movement-related cortical potential
An example MRCP obtained from averaging of EEG activity over fifty right foot ballistic dorsiflexions performed by a healthy person. '0' seconds represents time of the movement onset detected from two sEMG electrodes placed on the right Tibialis Anterior (TA) muscle.

4.1.3.1 Methods for Labelling MRCPs

In order to label the PN in a MRCP, we used the local peak method (LPM), which in addition to finding the minimum value, also ensures that the adjacent samples are at higher values (Luck, 2014). LPM finds the PN in the vicinity of the movement onset. We defined this vicinity as a 1 second window before and after the movement onset to cater to the large variation across MRCPs. *findpeaks* function from MATLAB 2017b was used to apply this method.

4.1.3.1.1 Labelling of BP1 and BP2 In order to label the onsets of BP1 and BP2, we used the MRCP signal from 3.0 seconds before the movement onset up to PN, represented by $y(n)$. To this signal, we fitted three line segments. The first segment corresponds to the baseline activity, the second to BP1 and the third to BP2, as given

below.

$$\hat{y}(n) = \begin{cases} b_1 & n \leq n_1 \\ m_2 n + b_2 & n_1 < n \leq n_2 \\ m_3 n + b_3 & otherwise \end{cases} \tag{4.1}$$

Where n is the sample number, $\hat{y}(n)$ is the fitted value of the MRCP signal at sample number n, $[m_2, m_3]$ and $[b_1, b_2, b_3]$ are the slopes and the intercepts of the three segments respectively; and n_1 and n_2 are the onsets of BP1 and BP2. The first segment has only an intercept term as it represents the baseline EEG which is assumed as such. For known n_1 and n_2, the coefficients of this model were obtained with least squares linear regression. To find n_1 and n_2, we evaluated the following three methods.

Bounded Segmented Regression (BSR) To fit the model defined by Equation 4.1, we set up the following optimisation problem.

$$\begin{aligned} \min_{n_1,n_2} \quad & \sum_{n=1}^{n_1} |b_1 - y(n)| + \\ & \sum_{n=n_1+1}^{n_2} |m_2 n + b_2 - y(n)| + \\ & \sum_{n=n_2+1}^{L} |m_3 n + b_3 - y(n)| \\ & n_1^l \leq n_1 \leq n_1^u \\ & n_2^l \leq n_2 \leq n_2^u \end{aligned} \tag{4.2}$$

This problem finds n_1 and n_2 corresponding to BP1 and BP2 within the provided bounds for the three straight line segments fitted to the recorded signal $y(n)$ which has L number of samples. Given a set of n_1, n_2, it also computes the coefficients (b_1, m_2, b_2, m_3, b_3) of the three line segments. Thus, this problem encompasses two optimisation problems. (i) Finding n_1 and n_2. (ii) Nested inside (i), the second problem is finding the best fit line segments on intervals defined by n_1 and n_2.

The first problem is defined as minimising the sum of L^1 norms of errors over the

three segments. This formulation for finding n_1, n_2 does not allow guaranteed global optimum. Therefore, to increase the chances of finding the global or a near-global optimal solution, we used particle swarm optimisation algorithm (PSO) which is a global approach to optimisation (Eberhart & Kennedy, 1995). PSO has been found to produce better results compared to traditional approaches in solving similar non-linear regression problems (Adibifard et al., 2016; Erdoğmuş & Ekiz, 2016; N. Lu et al., 2009). Furthermore, the optimisation was run twice starting at randomly chosen n_1, n_2, and the solution with the smaller cost was selected to increase the chances of finding the global optimal or a near-global optimal solution. *particleswarm* function from MATLAB 2017b was used for this purpose. Swarm size was set to 6. The lower and upper bounds for n_1 were set at sample numbers corresponding to -2.5 seconds and -1.0 seconds with respect to the movement onset respectively. The bounds for n_2 were set at -1.0 seconds to the time of PN with respect to the movement onset. These are reasonably large bounds keeping in mind the variations across MRCPs.

The second problem is finding three best fit line segments on intervals defined by n_1 and n_2. These three problems were solved by using least squares regression. This minimises the L^2 norm of the errors and it is a convex optimisation problem with a guaranteed global optimum. *mldivide* function from MATLAB 2017b was used for this purpose.

Change Point Method (CPM) This method was selected from the change point literature. It uses an exhaustive algorithm based on dynamic programming to find n_1 and n_2 while minimising a linear function for the underlying segments (Lavielle, 2005; Killick et al., 2012). The advantage of this method is that it is exhaustive while providing fast convergence. It has two disadvantages. First, it is unbounded and thus can find n_1 and n_2 at any point in $y(n)$. Second, it does not fully satisfy the third assumption which is that the baseline has a zero slope. Rather, it fits a line which

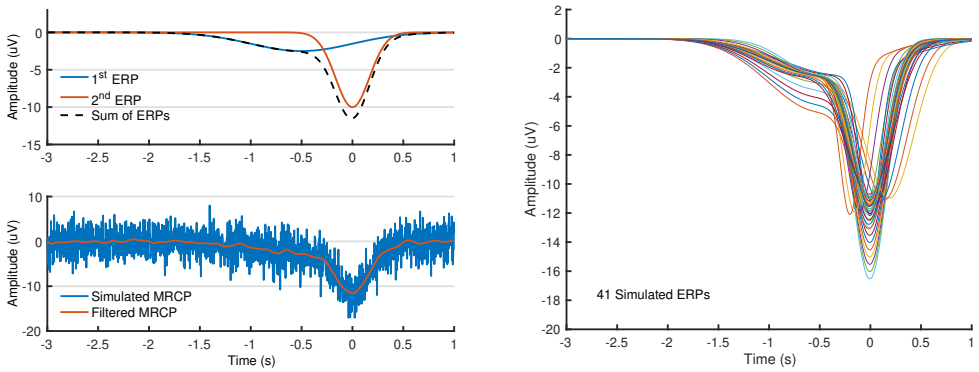

Figure 4.2: An example simulated MRCP obtained with SEREEGA/MATLAB
Note: On the left, a simulated MRCP obtained with SEREEGA/MATLAB by adding two ERPs and white noise (6 dB). On the right, the simulated ERPs derived by applying the 41 variations.

has a non-zero slope to the baseline. To run this method, *findchangepts* function from MATLAB 2017b was used with linear statistic and maximum number of change points set to 2.

Multivariate Adaptive Regression Splines (MRS) Multivariate adaptive regression splines with two knots corresponding to the onsets of BP1 and BP2 was also evaluated. This method fits a piece-wise linear function with three segments to $y(n)$. Traditionally the fitted model is stated in the following form.

$$\hat{y}(n) = a_0 + a_1 max(0, n - n_1) + a_2 max(0, n - n_2) \tag{4.3}$$

Where $[a_0, a_1, a_2]$ are the coefficients of the fitted model. Although it satisfies the third assumption, like the change point method it is also unbounded. To determine n_1 and n_2, ARESLab: Adaptive Regression Splines toolbox version 1.13.0 was used (Friedman, 1991; Jekabsons, 2016).

4.1.3.2 Proposed Method for Simulation of MRCPs

For appraisal of the above methods, we set up the simulation of MRCPs in SEREEGA (Krol et al., 2018). It is a MATLAB based open-source toolbox dedicated to the generation of simulated epochs of event-related EEG data.

We simulated a typical average MRCP by summing together two separate event-related potentials (ERPs) modelled using a gaussian function. The peak latency, peak amplitude, and total width of the first ERP was set at -0.5 seconds, -2.5 uV and 3.0 seconds respectively. The second ERP was added at 0 seconds, with a peak amplitude of -10 uV and total width of 1.0 seconds. Summed together, these resulted in a MRCP with BP1 onset at -1.5 seconds, BP2 onset at -0.5 seconds, and PN at 0 seconds, as shown in Figure 4.2. The parameters of the simulation were based on the variability reported in the past research. Shibasaki and Hallet reported that BP1 starts around 2.0 seconds before the movement onset, followed by BP2 which starts around 0.4 seconds before the movement onset (Shibasaki & Hallett, 2006). Wright et. al. in a study on motor planning reported that BP1 started around -1.79 ± SD 0.28 seconds and BP2 started around -0.72 ± SD 0.21 seconds in a group of non-musicians (Wright et al., 2012a). In the past, means and standard deviations for different features were not always stated explicitly. Thus, the values for these parameters were derived from the figures in these articles (Shibasaki & Hallett, 2006; Wright et al., 2011, 2012a,b; Jochumsen et al., 2017; Kita et al., 2001). Following 41 random variations were added to the simulation. These variations are also shown in Figure 4.2. Only one variation was applied to each simulated MRCP.

a. BP1 onset. The onset of BP1 was varied from -1.5 to -2.0 seconds with a step of 0.1 seconds. This variation was applied by changing the width of the first ERP in the simulation.

b. BP2 onset. The onset of BP2 was varied from -0.3 to -0.7 seconds with a step

of 0.05 seconds. It was applied by changing the latency of the first ERP. An equal change was also applied to the width of both ERPs to keep the remaining potentials at the same latencies.

c. PN time. The time of PN was varied from -0.2 to 0.2 seconds with a step of 0.05 seconds. It was applied by changing the latency of the second ERP. An equal change was also applied to the width of the second ERP to keep the remaining potentials at the same latencies.

d. BP2 amplitude. To produce variation in the amplitude of BP2, the peak amplitude of the first ERP was varied from -2.5 to -5 uV with a step of 0.5 uV.

e. PN amplitude. To produce variation in the amplitude of PN, the peak amplitude of the second ERP was varied from -10 to -15 uV with a step of 0.5 uV.

The latencies of BP1, BP2 and PN, and the amplitudes of BP1, BP2, PN obtained from the sum of the two ERPs at the latencies of BP1, BP2, time of PN provided the ground-truth data. A white noise was added to the sum of ERPs to produce simulated MRCPs under 3 signal to noise ratios (SNR) (6 dB, 3 dB, 0 dB) (Rashid et al., 2018). The signal to noise ratio was set by changing the root-mean-square value of the white noise with respect to the peak amplitude of the second ERP which corresponds to amplitude of PN. The simulated MRCPs were filtered with a low pass, 2^{nd} order, zero-phase Butterworth filter with cut-off at 5 Hz. These filtered MRCPs were used for further analysis. Thus, in the subsequent text, a simulated MRCP refers to the simulated MRCP obtained at the end of the filtering process.

4.1.3.3 Simulated MRCPs

Three sets of MRCPs were simulated. Set I contained 2000 MRCPs for each SNR condition with random variations. Set II contained 41 MRCPs for each SNR condition

with one MRCP corresponding to each variation. Set III was simulated in order to evaluate the validity of the simulated MRCPs. This set consisted of 42 simulated MRCPs, whose BP1, BP2 and PN latencies and amplitudes were copied from expert labels of experimental MRCPs (discussed next). To account for potential MRCPs with non-zero baselines, without having an explicit measure of baseline amplitude, BP1 amplitude was first subtracted from BP2 and PN amplitudes before simulation, and BP1 amplitude was subsequently added to the entire simulated MRCP after lowpass filtering. The simulation procedure was otherwise identical. This set allowed us to investigate the extent to which simulated MRCPs match experimental ones, as described in section 4.1.3.6.3.

4.1.3.4 Experimental MRCPs

The experimental MRCPs used in this research were recorded from 22 healthy participants (Average age: 36 ± 6 years, 10 female) who were recruited through professional networks and local advertising (Rashid et al., 2018). Participants were excluded if they had a history of any neurological disorders or epilepsy. All the participants signed a written consent form before data collection. Ethical approval for the study (17/CEN/133) was obtained from Central Health and Disability Ethics Committee (HDEC), New Zealand in accordance with the Declaration of Helsinki.

The participants performed 50 self-paced ballistic dorsiflexions in two data collection sessions over two days. The laboratory setup is illustrated in Figure 4.3. The data was bifurcated into session I and II across the two recording days. Thus, session I corresponds to recording on the first day and session II corresponds to recording on the second day.

Figure 4.3: An illustration of the laboratory setup for recording of EEG and sEMG data
An illustration of the laboratory setup for recording of EEG and sEMG data from a participant performing self-paced ballistic dorsiflexions.

Movement onsets were obtained from two surface electromyography (sEMG) electrodes placed on the right Tibialis Anterior (TA) muscle. EEG data was cleaned with filtering, channel interpolation, manual and automatic epoch rejection, and independent component analysis (ICA) in EEGLAB/MATLAB. 47.1 ± 10.6 and 48.8 ± 1.5 epochs were retained after rejection at 125 uVpp threshold for session I and II respectively. Whilst the standard deviation of the rejection rate appears higher in session I, this can be explained by the rejection of all the epochs for one of the participants whose sEMG data was lost. During the ICA analysis, components corresponding to eye blinks, or limited to only one electrode and a few epochs, were removed. *runica* algorithm was used and 3 components were removed on average. MRCPs were obtained from FC3, FCz, FC4, C3, Cz, C4, CP3, CPz, CP4 channels by applying a small laplacian filter with centre at Cz, followed by a 2^{nd} order, zero-phase, Butterworth filter with a low pass cut-off at 5 Hz, and averaging across epochs. SNR for the MRCPs in session I and II was 6.00 ± 2.39 dB and 5.70 ± 2.40 dB, respectively.

4.1.3.5 Manual Labelling of MRCPs

For comparison of the proposed method against experts, simulated MRCPs from set II (n = 123) and the experimental MRCPs were manually labelled. Experts with 3-8 years of experience working with MRCPs, manually labelled both the simulated and the experimental MRCPs using a custom MATLAB 2017b (MathWorks, Inc.) graphical user interface tool. This tool presented a MRCP as a 6 second epoch centered at the movement onset, with 3 seconds of data before and after the movement onset as shown in Figure 4.1. The experts labelled the onsets of BP1, BP2 and the PN using the mouse pointer. BP1 onset was labelled at the beginning of the negative slope, BP2 onset was labelled at the time when the slope increased abruptly, and PN was labelled at the time of the most negative amplitude. Amplitudes at the onsets of BP1, BP2 and the time of PN were obtained from the labelled time points. The slopes of BP1 and BP2 were mathematically computed from these time points and amplitudes.

4.1.3.6 Statistical Analysis

The analysis was performed in MATLAB 2017b (MathWorks, Inc.). We used root-mean-square error (RMSE) to compare errors incurred by different methods on both the simulated and experimental datasets. RMSE was interpreted as the accuracy of the method with the ideal value being zero (Mordkoff & Gianaros, 2000; Chai & Draxler, 2014). RMSE was used instead of sample mean as RMSE incorporates both the central tendency and the variability of the data. Pair-wise permutation test was used to evaluate statistical differences in RMSE across different methods (Butar & Park, 2008). Beside the validity of the measure under consideration, a permutation test requires that the assumption of exchangeability is satisfied (Berger, 2000). As in our case errors were obtained by different methods from the same data, the assumption of exchangeability required that the errors from the same pair be randomly permuted (Simpson et al., 2013).

Significance level was set at 0.05.

4.1.3.6.1 Evaluation on Simulated MRCPs For evaluation of LPM, CPM, MRS and BSR techniques set I of the simulated MRCPs was used (n = 6000). Failure rate, RMSE for the onsets of BP1, BP2 and time of PN were obtained for comparison. RMSEs were also obtained for the amplitudes of MRCPs at the onsets of BP1, BP2 and time of PN both from the simulated signals and the fitted models. From the fitted models, the amplitudes at the onsets of BP1, BP2 and time of PN were obtained from Equation 4.1 as b_1, $m_2n_2+b_2$ and m_3L+b_3, respectively. This comparison was performed based on the hypothesis that the amplitudes obtained at single points from the simulated MRCPs would have larger error compared to the amplitudes obtained at single points from the fitted models. Essentially, this allowed us to see how much closer the model came to the ground-truth (pre-noise MRCP), compared to the simulated signal (noise added filtered MRCP). Using the results from these analyses, better performing techniques were combined to formulate our proposed method for automated labelling of the MRCPs.

From set II of the simulated MRCPs (n = 123), onsets of BP1, BP2 and time of PN were obtained using the proposed method and compared against those labelled by an expert. The error for the time points was obtained by subtracting the ground-truth from the labelled time. RMSE was used for comparison.

4.1.3.6.2 Evaluation on Experimental MRCPs Onsets, amplitudes at onset and slopes of BP1, BP2, and time and amplitude of PN were obtained for the experimental MRCPs (n = 22 × 2) using the proposed method. Absolute reliability of the proposed method to identify these features across the two sessions was evaluated using Bland-Altman plots (Vaz et al., 2013). Bias, t-test for bias equal to zero, and coefficient of repeatability (CR) were reported. Bias was calculated as the mean of differences across the two sessions and interpreted as the systematic difference in the feature across the

two sessions. Significance level for the t-test was set at 0.05. CR was calculated as 1.96 times the standard deviation of differences and interpreted as the measurement error below which the absolute differences between two sessions would lie with 0.95 probability (Vaz et al., 2013).

The proposed method was compared to manual labelling by an expert in terms of the error across sessions in the onsets, amplitudes at onsets and slopes of BP1, BP2 along with time and amplitude of PN. This comparison was performed based on the hypothesis that the automated method would result in smaller error as compared to the manual labelling method. RMSEs was obtained for this comparison.

4.1.3.6.3 Validation of Simulated MRCPs To evaluate the validity of the simulated MRCPs, the experimental MRCPs were compared to their simulated copies in Set III. Cosine similarity between the experimental MRCPs and their simulated versions up to the negative peak was obtained as follows (Dehak et al., 2010).

$$r = \frac{\mathbf{u}.\mathbf{v}}{\|\mathbf{u}\| \times \|\mathbf{v}\|} \tag{4.4}$$

Where **u**, **v** represent the two MRCPs as vectors. '**.**' represents the dot product between the two vectors, and $\|.\|$ represents the L^2 norm of a vector.

4.1.4 Results

4.1.4.1 Evaluation on Simulated MRCPs

4.1.4.1.1 Failure rate The evaluated techniques did not always succeed in fitting a model. LPM was successful in finding PN in all cases under the three SNR conditions. Similarly, BSR was also successful in all cases under all the SNR conditions. The failure rate for CPM was 0%, 2.2% and 11.3% for 6 dB, 3 dB and 0 dB, respectively. For MRS, the failure rate was 0.35%, 1.25% and 1.95% for SNR at 6 dB, 3 dB and 0

Table 4.1: RMSEs in seconds for onsets of BP1, BP2 and time of PN for simulated data

RMSEs in seconds for onsets of BP1, BP2 and time of PN with respect to the movement onset under different SNR conditions in simulated MRCPs. Sim. Var. and Sim. Step stand for the simulated variability and the simulated step. H_0 stands for null hypothesis.

SNR	Potential	Method				Sim.	Sim.	p-value
		MRS	CPM	BSR	LPM	Var.	Step	H_0: BSR = CPM
6 dB	BP1	1.133	0.548	0.442	–	0.5	0.1	<0.001
	BP2	0.289	0.163	0.164	–	0.4	0.05	0.090
	PN	–	–	–	0.021	0.4	0.05	–
3 dB	BP1	0.919	0.627	0.518	–	0.5	0.1	<0.001
	BP2	0.247	0.169	0.170	–	0.4	0.05	0.168
	PN	–	–	–	0.034	0.4	0.05	–
0 dB	BP1	0.843	0.668	0.551	–	0.5	0.1	<0.001
	BP2	0.228	0.206	0.195	–	0.4	0.05	0.019
	PN	–	–	–	0.053	0.4	0.05	–

dB, respectively. Thus, the bounded segmented regression method for finding onsets of BP1 and BP2 is clearly superior with respect to failure rate.

4.1.4.1.2 RMSEs for BP1, BP2 onsets and time of PN The root-mean-square errors for the onsets of BP1 and BP2 and the time of PN are given in Table 4.1. The error corresponding to each technique was calculated from successful cases only. The root-mean-square error for PN time was smallest, followed by BP2 and BP1 respectively. MRS performed poorly under all SNR conditions for both BP1 and BP2 onsets, thus, it was excluded from further analysis.

For BP1 onset, BSR produced smaller error under all three SNR conditions compared to CPM and these differences were also statistically significant ($p < 0.05$). Compared to simulated variation, BSR produced smaller error for BP1 onset at 6 dB, and larger error at 3 dB and 0 dB.

For BP2 onset, CPM produced smaller error at 6 dB and 3 dB compared to BSR. However, these differences were smaller than 0.001 seconds and also did not achieve statistical significance ($p > 0.05$). Whereas, at 0 dB, BSR had smaller ($p < 0.05$) error

compared to CPM. Compared to simulated variation, both BSR and CPM produced smaller error under all SNR conditions. These results suggest that BSR is superior in case of BP1 onset and both BSR and CPM detect very similar BP2 onsets. Thus, CPM was dropped from further analysis at this stage.

4.1.4.1.3 Model prediction Using the BP1, BP2 onsets and time of PN, the amplitudes at these time points were obtained from both the fitted model as given by Equation 4.1 and the simulated MRCP signals. The errors are shown in Figure 4.4 for BSR and LPM. The error for the fitted model was smaller for BP1 and BP2 across all three SNR conditions compared to amplitudes taken from the simulated MRCP signals. Whereas, the error for PN was smaller for the signal amplitudes across all three SNR conditions. All these differences were statistically significant ($p < 0.05$).

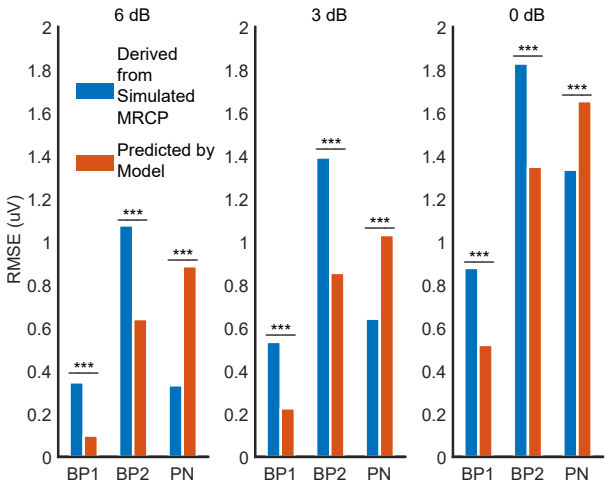

Figure 4.4: RMSEs for amplitudes at onsets of BP1, BP2 and time of PN
RMSEs for amplitudes at onsets of BP1, BP2 and time of PN taken from the simulated MRCP and the fitted models using BSR and LPM under three signal to noise ratios (6 dB, 3dB, 0 dB). '***' denote $p < 0.001$ for the null hypothesis that the two RMSEs are equal.

4.1.4.1.4 Comparison with an Expert on Simulated MRCPs Based on results from the previous sections, BSR was selected for identification of BP1 and BP2 onsets while LPM was selected for identification of the time of PN. These techniques were

applied to the simulated data to fit models as given in Equation 4.1. The amplitudes for BP1, BP2 onsets were computed from the fitted model. The amplitude for PN was calculated from the MRCP signal. The slopes were taken from the fitted model. The combination of these techniques is referred to as the proposed method in the text.

From simulated dataset II, the errors in the onsets of BP1, BP2, and time of PN identified by the proposed method are plotted against the error in labelling of these time points by an expert in Figure 4.5. This plot indicates that the errors from both the manual labelling and automated labelling were normally distributed.

The RMSE for onset of BP1 was 0.356 seconds for the expert and 0.478 seconds the proposed method, respectively. Similarly, the RMSE for BP2 onset was 0.195 seconds and 0.163 seconds for the expert and the proposed method, respectively. In case of PN, the RMSE for the expert and the proposed method was 0.096 seconds and 0.036 seconds, respectively. The p-values for null hypotheses corresponding to RMSE in onsets of BP1, BP2 and time of PN were 0.001, 0.010 and <0.001 respectively. These results suggest that the proposed method incurred smaller error in identifying the onset of BP2 and the time of PN compared to the expert. Whereas, the proposed method had larger error in identifying the onset of BP1 compared to the expert.

4.1.4.2 Evaluation on Experimental MRCPs

The proposed method was applied to the experimental data. The results for two of the MRCPs are shown in Figure 4.6. The proposed method successfully found all the features in all the cases.

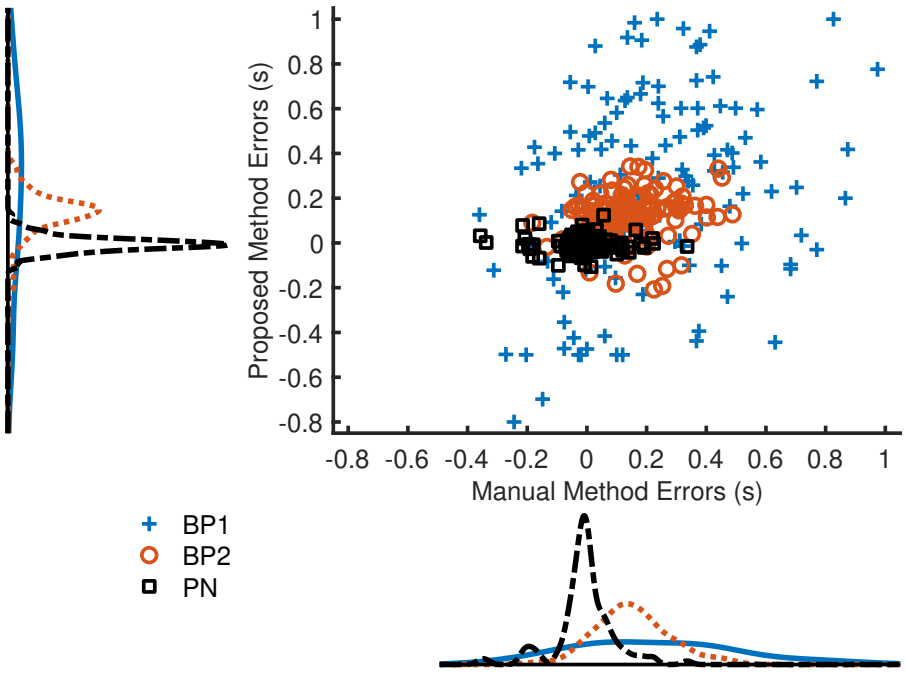

Figure 4.5: Distribution of errors for onsets of BP1, BP2 and time of PN
Distribution of errors for onsets of BP1, BP2 and time of PN for manual and automatic labelling of the simulated MRCPs.

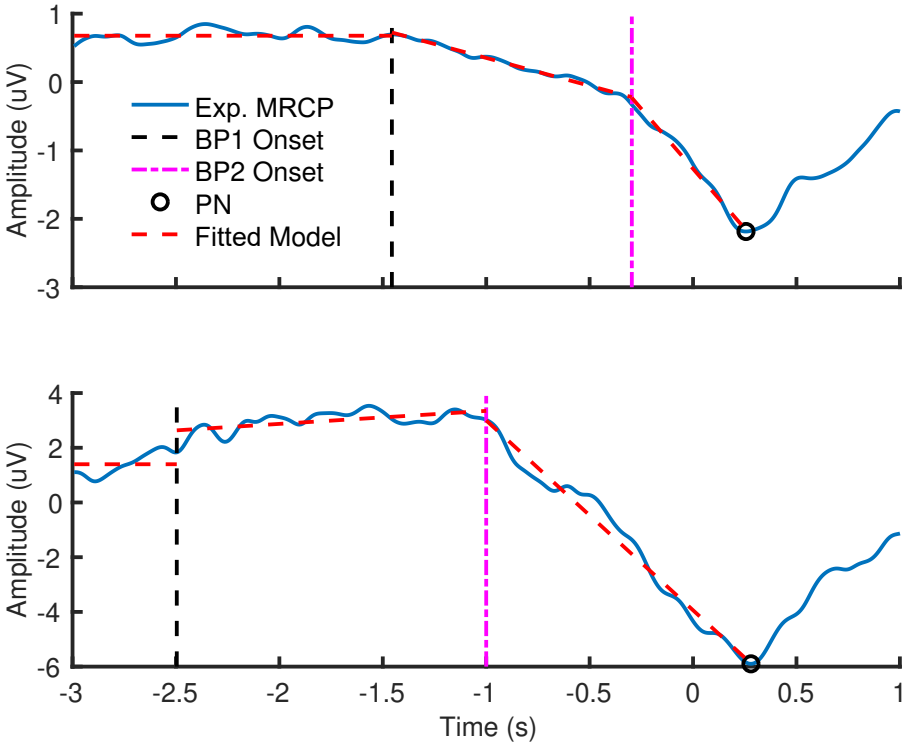

Figure 4.6: Experimental MRCPs from two different participants labelled by the proposed method
Note: The top MRCP had the lowest RMSE from the fitted model. Whereas, the bottom MRCP had the highest RMSE from the fitted model.

4.1.4.2.1 Absolute Reliability with Bland-Altman Plots The Bland-Altman plots for the features obtained for the MRCPs from two sessions are given in Figure 4.7. The Bland-Altman plots do not exhibit any systematic trends, except in case of onset of BP1 and time of PN where the error variability appears to be non-uniform. Furthermore, there was insufficient evidence to reject the null hypothesis that there was zero bias in any of the features. The coefficient of repeatability was smallest for the time of PN (0.279 seconds), followed by BP2 (0.571 seconds) and BP1 (1.279) respectively. On the other hand, for amplitudes an opposite trend in the size of CR was observed. CR was smallest for amplitude at onset of BP1 (1.988 uV), followed by amplitude at onset of BP2 (2.867 uV) and amplitude of PN (5.032 uV) respectively. Similarly, CR for slope of BP1 (3.016 uV/s) was smaller than that for BP2 (9.305 uV/s).

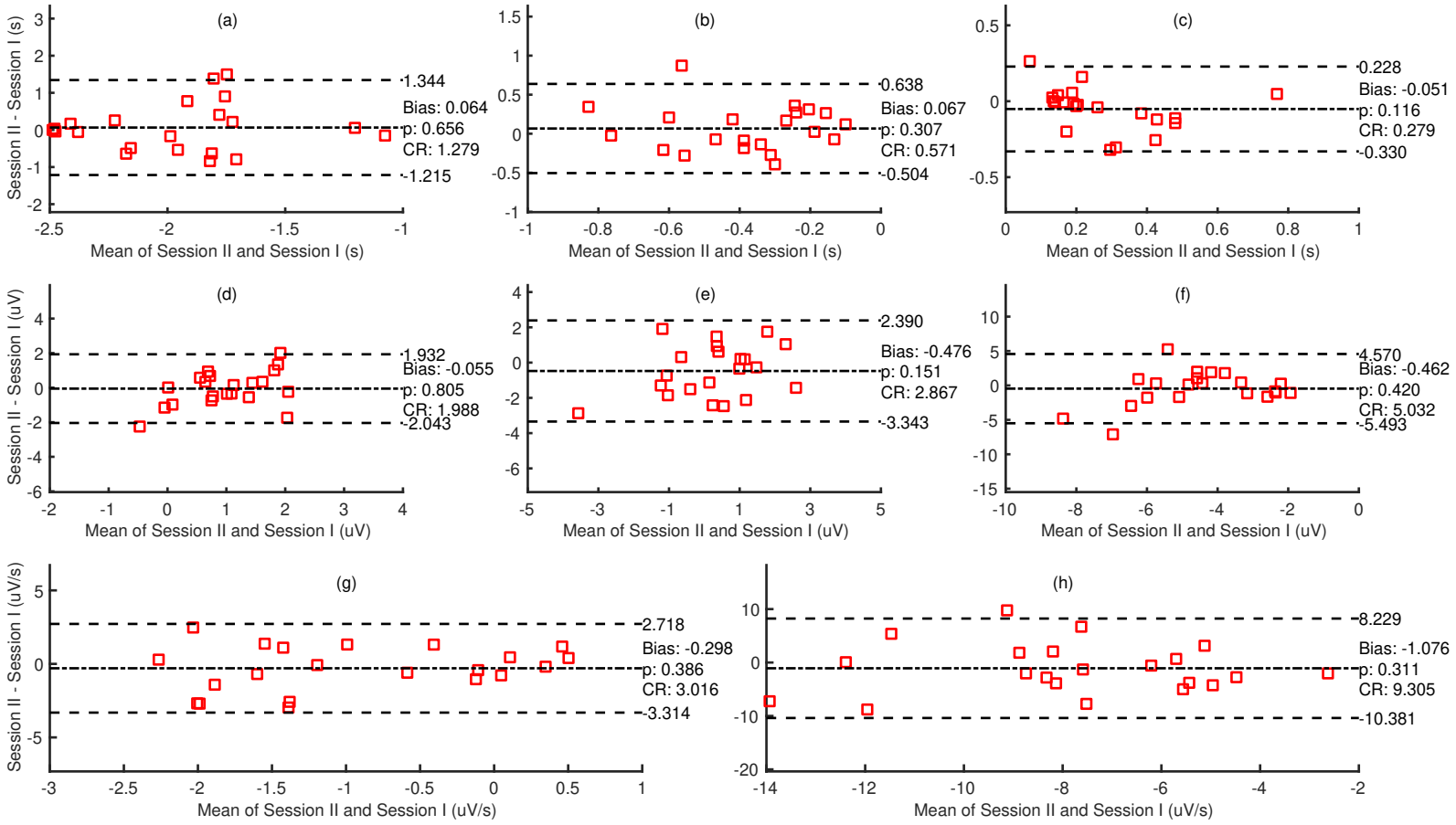

Figure 4.7: Bland-Altman plot for onset of BP1, onset of BP2, time of PN

Bland-Altman plot for onset of BP1 (a), onset of BP2 (b), time of PN (c), amplitude at onset of BP1 (d), amplitude at onset of BP2 (e), amplitude of PN (f), slope of BP1 (g), and slope of BP2 (h) for experimental MRCPs identified by the proposed method in session I and II.

4.1.4.2.2 Comparison with an Expert on Experimental MRCPs

The comparison of RMSE from the proposed method and manual labelling for onsets of BP1, BP2, time of PN, amplitudes at these time points, and slopes for BP1, BP2 is given in Table 4.2. There was not enough evidence ($p > 0.05$) to reject the null hypothesis that the two methods incurred same errors. Nonetheless, there were some notable differences in magnitude of the error across the two methods. The proposed method incurred larger RMSE in onset of BP1. Also, the proposed method achieved smaller error for the slopes of both BP1 and BP2.

Table 4.2: RMSEs for onsets of BP1, BP2, time of PN for experimental data
RMSEs for onsets of BP1, BP2, time of PN, amplitudes at these time points, and slopes for BP1, BP2. These errors were obtained from both the manual and automated labelling of experimental MRCPs from two sessions.

RMSE for	Potential	Method		p-value
		Manual	Proposed	
Time (s)	BP1	0.408	0.640	0.126
	BP2	0.225	0.292	0.338
	PN	0.174	0.148	0.585
Amplitude (uV)	BP1	1.655	0.991	0.064
	BP2	1.189	1.505	0.060
	PN	2.277	2.547	0.488
Slope (uV/s)	BP1	2.100	1.531	0.496
	BP2	6.325	4.756	0.648

4.1.4.3 Validation of Simulated MRCPs

Two experimental MRCPs along with their simulated counterparts in Set III, and the cosine similarity between the experimental MRCPs and their simulated versions is shown in Figure 4.8. The mean and standard deviation of the similarity index was 0.918 ± 0.078. These results suggest an excellent agreement between the experimental MRCPs and their simulated versions in majority of the cases.

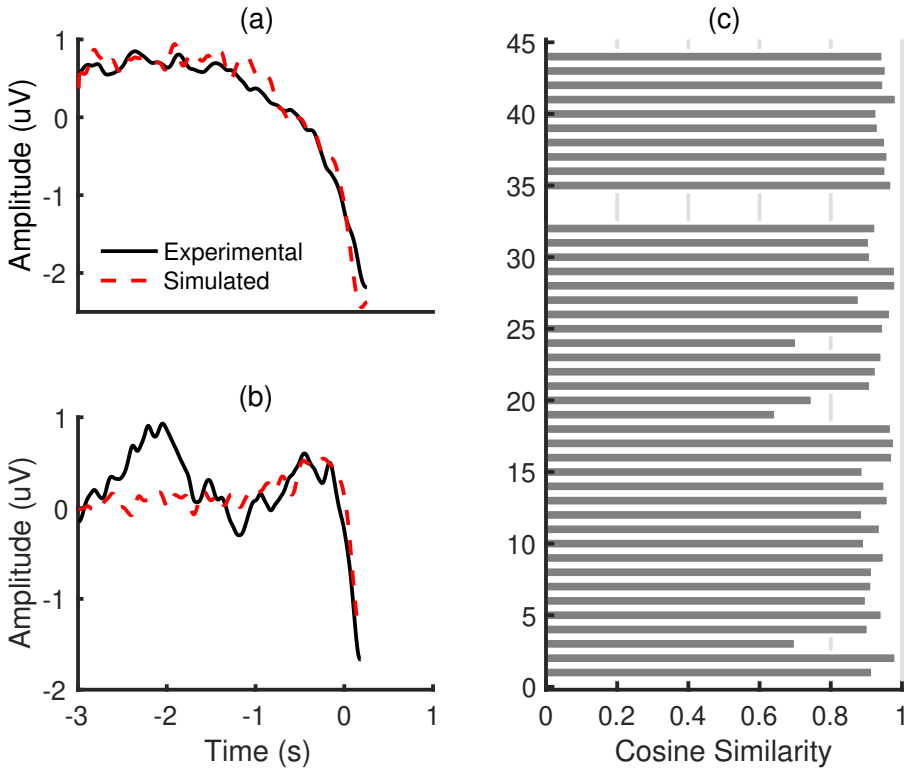

Figure 4.8: Examples of experimental MRCPs along with their simulated counterparts

Note: (a), (b) Examples of experimental MRCPs along with their simulated counterparts. (a) corresponds to the case with highest cosine similarity of 0.985. (b) corresponds to the case with lowest cosine similarity of 0.646. (c) The cosine similarity between the experimental MRCPs and their simulated versions. MRCPs at no. 33 and 34 correspond to the participant whose sEMG data was lost during recording.

4.1.5 Discussion

We have proposed and validated a method for automated labelling of movement-related cortical potentials. This method provides robust estimates of the MRCP features. On simulated MRCPs, BSR outperformed MSR and CPM in terms of failure rate, RMSEs in onsets of BP1, BP2, and time of PN. Also, simulation results showed that amplitudes obtained from fitted models result in smaller error compared to amplitudes directly taken from MRCP signals, except in the case of PN. Based on these results, BSR was selected for identification of BP1 and BP2 while LPM was selected for identification

of PN. When compared against labelling of onsets of BP1, BP2, and time of PN on simulated MRCPs by an expert; the proposed method had larger ($p < 0.05$) error in the onset of BP1 while it had a smaller ($p < 0.05$) error in the onset of BP2 and time of PN. On the experimental MRCPs, the proposed method did not show any systematic trends in Bland-Altman plots of the features with minor exceptions discussed in the following paragraphs. There was insufficient evidence ($p > 0.05$) to suggest the presence of bias in features across the two recording sessions. Compared to manual labelling of MRCPs, the proposed method had larger RMSE in onset of BP1 and smaller RMSEs in slopes of both BP1 and BP2. However, these differences did not achieve statistical significance.

4.1.5.1 Evaluation on Simulated MRCPs

In terms of RMSE for onset of BP1 the BSR performed better than the other two methods, whereas its performance for BP2 onset was comparable to that of CPM. We also evaluated the failure rate. For CPM it was generally higher compared to BSR and considerably higher (approx. 11%) under 0 dB SNR. The MSR method consistently performed poorly in terms of both the failure rate and RMSE. Thus, MSR and CPM were excluded from further analysis.

The RMSEs of the amplitudes predicted from the fitted models at BP1 and BP2 onsets were smaller compared to amplitudes derived directly from signals. This difference can be explained by the fact that the fitted model smooths local variability in the data. These results suggest that the MRCP amplitudes should not be measured directly from the signal at single time points. Rather, if necessary, the amplitudes predicted by the model should be used to reduce error due to local variability which can be a result of signal noise. However, for PN, opposite results were found. The error for the amplitude obtained from signal was smaller than that of the predicted amplitude. This can be explained by the fact that near PN, the MRCP signal violates the assumption that it can be modelled as a straight line. PN is a peak which deviates away from the fitted

straight line. Thus, in case of PN, the amplitude should be calculated from the signal itself. These results have implications for researchers interested in amplitudes at single time points or differences in amplitudes measured at multiple single time points from MRCPs (Kita et al., 2001). Furthermore, as highlighted in the introduction, amplitudes at single time points or differences across multiple time points do not fully capture the linear trends of BP1 and BP2, thus, we suggest the use of fitted slopes.

In comparison to manual labelling by an expert, the proposed method had smaller RMSEs in identifying the onset of BP2 and time of PN. However, it had larger errors in identifying the onset of BP1. One plausible explanation for this finding is that it is due to the break down of assumption 1 and 3 (refer to Section 4.1.3) at the onset of BP1. Under current assumptions, the onset is assumed to be an intersection point between two lines. Perhaps, the actual transition from baseline to BP1 is radically smoother than an edge and can only be correctly modelled by a spline. We suggest it is investigated in future research.

4.1.5.2 Evaluation on Experimental MRCPs

The Bland-Altman plots did not show any systematic trends except in case of the onset of BP1 and time of PN where the error variability was not uniform. The implication of this trend is that the CR obtained under the assumption of normally distributed errors are not true representations of the agreement limits (Vaz et al., 2013). The coefficient of repeatability was also reported for each feature which can be used to interpret pre and post intervention scores in a future study involving MRCPs (Vaz et al., 2013). For example, for an individual participant any change greater than 9.305 uV/s in the slope of BP2 from pre to post can be interpreted as a real difference with 95% confidence.

In comparison to manual labelling by an expert, the proposed method had larger error for onset of BP1. This can again be explained by the spline hypothesis suggested by the results of the comparison between the expert and the proposed method in

simulated MRCPs. The proposed method consistently achieved smaller measurement error in slopes of BP1 and BP2. These differences, however, did not achieve statistical significance and need further investigation in a larger sample.

4.1.5.3 Validation of Simulated MRCPs

The similarity between the experimental MRCPs and their simulated versions suggested an excellent agreement between the two in majority of the cases. Thus, the simulation method provided large test sets of valid MRCPs for which the ground truth was known. Additionally, simulated MRCPs gave us the ability to evaluate our proposed methods under large variations in time, amplitude and signal to noise ratio. Evaluation on experimental MRCPs under these variations would have not been possible without recording EEG data from a large number of participants from different populations.

The proposed simulation was based on findings of the past research. However, further work is required to adapt this simulation method to generate MRCPs at a single epoch level and demonstrate its validity.

4.1.5.4 Limitations

The findings of this research should be considered in light of a number of limitations. First, the MRCPs were labelled by a single expert. In some of the past studies, two experts labelled the MRCPs and the third expert selected the labelling of one of the experts. The reliability of these methods (single and multiple experts) has not yet been demonstrated. Second, the experimental MRCPs were recorded from 22 healthy participants. Thus, the estimates of measurement error and bias can not be applied across other populations without question. In future research, using large samples gathered from multiple populations, a full comparative analysis of the reliability of the proposed method and the different manual methods is needed.

4.1.5.5 Recommendations

1. The proposed method fully captures the two linear trends of BP1 and BP2 in the MRCP. Thus, we suggest that in future research, the slopes fitted by the proposed method be considered for studying the differences across conditions. Following our proposed method, one may automatically model MRCP parameters to quantify changes induced with an intervention or motor training paradigms (Mrachacz-Kersting et al., 2012; Jochumsen et al., 2017).

2. In studies where determining the onset of BP1 is of particular interest, we suggest the use of manual labelling. However, for the onset of BP2 and determining the time of PN; the use of the proposed method is suggested.

3. As the proposed method is fully automatic, a real-time implementation of particle swarm algorithm (Liu et al., 2008) can enable online neuroadaptive paradigms to support motor training (Zander et al., 2016).

4.1.5.6 Software Availability

The MATLAB based implementation of the proposed method, the graphical user interface tool for visual labelling of MRCPs and tools for Bland-Altman analysis have been made available online[3]. These tools can be used to automatically obtain features from MRCPs using the proposed method or manually label the MRCPs for calculating the features discussed in this research.

4.1.6 Conclusion

We have proposed a method for automated labelling of features in movement-related cortical potentials. The proposed method was formulated and validated using a large

[3]Available on Github at: https://github.com/GallVp/visualEEG

set of simulated MRCPs. Its absolute reliability was also evaluated on a set of experimental MRCPs. We conclude that the proposed method be used to automatically obtain robust estimates for the MRCP features with known measurement error in future studies involving MRCPs.

End of Published Manuscript 2

Start of Published Manuscript 3

4.2 Optimal Automatic Detection of Muscle Activation Intervals

4.2.1 Abstract

A significant challenge in surface electromyography (sEMG) is the accurate identification of onsets and offsets of muscle activations. Manual labelling and automatic detection are currently used with varying degrees of reliability, accuracy and time efficiency. Automatic methods still require significant manual input to set the optimal parameters for the detection algorithm. These parameters usually need to be adjusted for each individual, muscle and movement task. We propose a method to automatically identify optimal detection parameters in a minimally supervised way. The proposed method solves an optimisation problem that only require s as input the number of activation bursts in the sEMG in a given time interval. This approach was tested on an extended version of the widely adopted double thresholding algorithm, although the optimisation could be applied to any detection algorithm. sEMG data from 22 healthy participants performing a single (ankle dorsiflexion) and a multi-joint (step on/off) task were used for evaluation. Detection rate, concordance, F_1 score as an average of sensitivity and precision, degree of over detection, and degree of under detection were used as performance metrices. The proposed method improved the performance of the the double thresholding algorithm in multi-joint movement and had the same performance in single joint movement with respect to the performance of the double thresholding algorithm with task specific global parameters. Moreover, the proposed method was robust when an error of up to ±10% was introduced in the number of

activation bursts in the optimisation phase regardless of the movement. In conclusion, our optimised method has improved the automation of a sEMG detection algorithm which may reduce the time burden associated with current sEMG processing.

4.2.2 Introduction

Surface electromyography (sEMG) is widely used for measurement of muscle activity in biomechanics, biomedical and sports science areas (Hogrel, 2005; Reaz et al., 2006; Massó et al., 2010; Niazi et al., 2011; Ahmadian et al., 2013; Karimi et al., 2017; Chowdhury et al., 2013; Luca, 1997; Hermens et al., 2000). From sEMG recordings, the accurate identification of intervals of muscle activity has applications in the study of different pathologies such as neck or back pain (Falla et al., 2004; Larivière et al., 2010), in analysis of event-related brain signals (Boxtel et al., 1993) and in movement rehabilitation (Kawakami et al., 2016; Cauraugh et al., 2000; Hara et al., 2013) among others. The identification of these intervals is a multifaceted challenge, due to difficulty in defining *onsets* and *offsets* (Magda, n.d.), and large variability in the amplitude of the sEMG signal across different muscles, movement tasks and populations (Robichaud et al., 2009; Yang et al., 2017). Furthermore, different applications involving online or offline processing impose different constraints of time and computational complexity (Drapała et al., 2012).

When the sEMG is processed offline, onsets and offsets are identified either automatically using an algorithm (Chowdhury et al., 2013; Yang et al., 2017; J. A. Guerrero & Macías-Díaz, 2014; Staude et al., 2001; Merlo et al., 2003), or manually labelled by an expert (Falla et al., 2004; Worsley et al., 2013; Moseley et al., 2003; Vasseljen et al., 2006; Hodges et al., 2003). The limitations of the manual labelling method are the time needed to label individual onsets/offsets and the risk of subjective bias. Whereas, automatic methods use algorithms which dictate the amplitude and duration

of activity that should be classified as *on* or *off*. Nonetheless, the expert has to select an appropriate algorithm and a set of parameters for the algorithm, such as the number of standard deviations above baseline mean for sEMG activity to be classified as *on*. Fully automatic processing can be achieved by selecting a single set of parameters and applying it to the entire dataset. Such a single set of parameters is referred to as *global* parameters in this paper. The automatic method involving an algorithm along with a global set of parameters is time efficient but also prone to error (Jubany & Angulo-Barroso, 2016) and has poor repeatability (Hodges & Bui, 1996). Commonly researchers use a hybrid approach with an algorithm used initially, followed by visual inspection and manual adjustment of the detected sEMG bursts. However, this still requires the expert to manually adjust the parameters of the algorithm in response to varying signal characteristics, so that the algorithm detects muscle activity appropriately. To reduce this time burden, a method is needed to optimise the detection algorithm parameters with minimal additional input from the expert.

The aim of this research is to provide a simple and efficient method to optimise sEMG detection algorithms. We achieve this by exploiting the assumption that an expert can accurately visually identify the *number of bursts* in a sEMG signal. It is more difficult to visually identify the precise onsets and offsets since this requires inspecting the signals in detail. We propose an optimisation method which takes the estimated number of sEMG bursts in the signal as the only input from the expert and finds an optimal set of parameters for the sEMG detection algorithm. The proposed method can be used in two possible ways: (i) for finding an optimal set of parameters from a single trial that has a known number of bursts and then applying these obtained optimal parameters to subsequent trials, or (ii) for finding an optimal set of parameters for each trial separately. The advantage of the first technique is that the expert has to estimate the number of sEMG bursts only in one trial. The disadvantage is that the detection algorithm may not achieve desired performance on the subsequent trials with

parameters obtained from a single trial. The second technique overcomes this problem as an optimal set of parameters is obtained for each trial separately. When these optimal parameters are used to detect sEMG bursts from the same trial, it results in an optimal detection of onsets and offsets for that trial. The application of this technique may not be feasible with existing optimisation methods for which the expert has to manually select a number of different parameters some of which can be nonintuitive. With our proposed method the application of the second technique is feasible as the expert's initial input is reduced to estimating the number of bursts in the signal.

In theory the proposed optimisation method can be used with any detection algorithm which is deemed appropriate for a particular study. Here we use it in combination with an extended version of the widely adopted double thresholding algorithm (Bonato et al., 1998; Staude et al., 2001; Jubany & Angulo-Barroso, 2016). To evaluate our proposed method, we test it on sEMG data from two different lower limb tasks in a healthy population. We compare the quality of the activation bursts detected by the extended double thresholding algorithm optimised with the proposed method in each trial separately against the bursts manually labelled by an expert in that trial and the bursts detected by the extended double thresholding algorithm with task specific global parameters.

4.2.3 Methods

4.2.3.1 Proposed Optimisation Method

Given the number of muscle activations, an optimal set of parameters (P) was found by solving the following optimisation problem.

$$\begin{aligned} \min_{P} \quad & \|n(\Lambda(P_i, X)) - N_e\|_2 + \frac{N_A}{N} + \frac{E_B}{E} \\ & B^l \leq P \leq B^u \end{aligned} \tag{4.5}$$

Where $n(.)$ denoted the operation which gave the number of onset/offset pairs in the set returned by the detection algorithm (Λ). The algorithm took an initial set of parameters (P_i) and a sEMG signal (X). N_e was the estimated number of onset/offset pairs supplied by the expert as input. N_A and N denoted the number of samples contained by the detected onsets/offsets and total number of samples in the sEMG signal. E_B and E represented the energy outside the detected onsets/offsets and total energy of the sEMG signal. The Teager-Kaiser operator was used to find the energy from the sEMG signal (Solnik et al., 2010). B^l and B^u denoted the lower and the upper bounds on the parameters of the detection algorithm (Λ).

The proposed optimisation problem in Equation 4.5 is a heuristic optimisation problem (Gilli, 2004; Pearl, 1984). The heuristic based on the difference between the number of estimated bursts and the number of detected bursts directed the search strategy to the nearest minimum from the initial conditions in the solution space while disregarding the quality of the detected bursts. A very fast convergence (approximately $\leq$ 5 iterations) could be achieved by only using this heuristic, for achieving optimal quality for the detected bursts, the two balancing terms which minimise samples and maximise energy of the bursts were also used.

Solving the optimisation problem stated in Equation 4.5 with a traditional derivative based search strategy, such as gradient decent (Ruder, 2016), required mathematical derivation of the gradients. Such a derivation can only be performed if the detection algorithm (Λ) is known and its processing steps are differentiable. Furthermore, the convexity of the optimisation problem in Equation 4.5 has to be mathematically established for a given detection algorithm (Λ) so that a gradient based method can be used effectively. If the chosen detection algorithm (Λ) makes the optimisation problem non-convex, the quality of its solution depends heavily on the chosen initial parameters (P_i). To avoid these problems, we used the particle swarm algorithm described in (Eberhart & Kennedy, 1995) as the search strategy. A detailed tutorial explaining the particle

swarm algorithm along with practical examples can be found in (Marini & Walczak, 2015). The particle swarm algorithm is a global approach to optimisation and it can find a global or a near-global solution even when the optimisation problem is non-convex (Selvakumar & Thanushkodi, 2007; Parsopoulos & Vrahatis, 2002; Zhang et al., 2015; Rashid et al., 2019). Moreover, the particle swarm algorithm is a derivative-free method (Rios & Sahinidis, 2012) and the initial parameters (P_i) can be chosen randomly within the bounds (B^l and B^u). The optimisation problem proposed in Equation 4.5 is referred to as *nOptim* method in the subsequent sections.

4.2.3.2 Extended Double Thresholding Algorithm (eDTA)

The input to the algorithm was preprocessed sEMG data and a set of parameters. A low pass and a high pass filter were used to preprocess the data. Both the filters were zero-phase to avoid adding any time delay in the signal. Additional characteristics of the filters are discussed in Section 4.2.3.3 after introducing the experimental dataset. The output was a set of pairs of onsets and offsets. The parameters of the algorithms are listed below followed by the operations briefly explained in sequence. The last three operations (5, 6, 7) can be disabled when not required by appropriately setting the corresponding parameters.

L_b: Length of the baseline segment.

K_b^{th}: The rank of the moving average value which was used to select the baseline segment.

N_{sd}: Number of standard deviations of the baseline segment.

T_{on}: Time in seconds for detecting an onset.

T_{off}: Time in seconds for detecting an offset.

T_s: Time in seconds for the shortest sEMG burst.

N_{nt}: Number of standard deviations of the root mean square (RMS) values of the

detected bursts.

T_j: Time in seconds for the window in which two or more sEMG burst were joined into a single burst.

1. Baseline detection Given a preprocessed sEMG signal, the first step was the automatic selection of a baseline segment and estimation of baseline mean and standard deviation. This was achieved by first applying full wave rectification to the sEMG signal. This rectified signal was then passed through a moving average filter with a window length of L_b seconds. Using this moving average of the rectified signal, a baseline segment of length L_b seconds was selected from the rectified sEMG signal such that the rank of the corresponding moving average was K_b^{th}. The reason to select the K_b^{th} minimum value instead of the global minimum was that in some cases the rectified sEMG signal had a high noise content and choosing the quietest region as baseline was not the most suitable option. The baseline mean and standard deviation were estimated from the baseline segment of the rectified signal using sample mean and standard deviation formulae. It should be noted that the moving average filter was only used to select the baseline segment and the baseline mean and the standard deviation were computed from the preprocessed rectified signal without applying a moving average. Moreover, no moving average was applied to the signal in the subsequent operations of the algorithm.

2. *First* threshold using baseline parameters Thresholding with baseline mean plus a number of baseline standard deviations (N_{sd}) was applied to the rectified sEMG signal to detect bursts of muscle activity. This operation resulted in a train of 1's and 0's. A run of consecutive 1's corresponded to muscle activity and a run of consecutive 0's corresponded to a muscle resting state. This operation resulted in a large number of false positives. Most of these false positives were removed by applying a second threshold

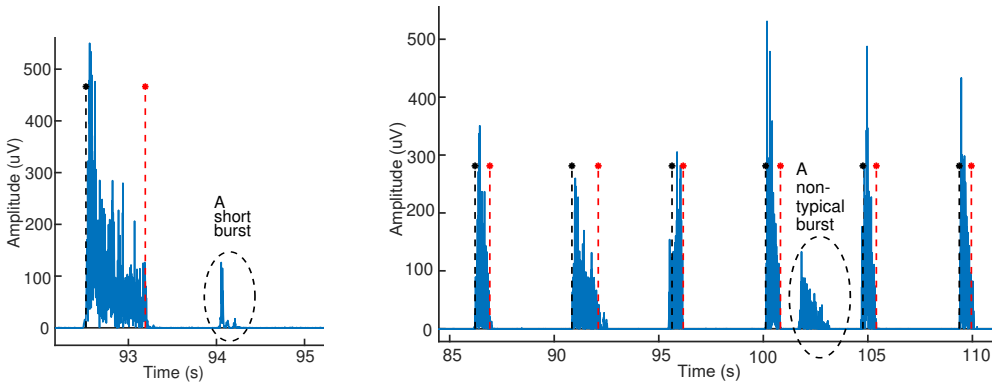

Figure 4.9: Example of a short burst and a non-typical burst

(Bonato et al., 1998).

3. *Second* threshold using on time In the train of 1's and 0's from the previous step, the first 1 in a run was considered the onset of muscle activity only if the run lasted for T_{on} seconds. And the last 1 in the run was considered the offset. This operation successfully removed very short runs, for example, burst trains of 1 or 2 consecutive ones. However, it also resulted in multiple onsets for a single movement.

4. *Third* threshold using off time To overcome the problem of multiple onsets, another threshold was applied along the time dimension. An offset from the last operation was only considered a true offset if it was not followed by another onset for at least T_{off} seconds.

5. Prune short events False positives resulting from short bursts in the sEMG signal were removed by applying another time threshold to all the onset/offset pairs (Merlo et al., 2003). An example of such a burst is shown in Figure 4.9. Thus, an onset/offset pair which had a time difference shorter than T_s seconds was removed.

This pruning operation was applied after onsets and offsets had been defined by the on time and the off time. This operation allowed the algorithm to have a sensitive threshold for the on time (T_{on}). If a larger on time threshold was used to remove the

short bursts of activity, such as the one shown in Figure 4.9, it resulted in delayed onset detection. This operation decoupled the sensitivity of the algorithm in detecting onsets and its ability to remove short bursts without decreasing the sensitivity. It gave the algorithm another degree of freedom.

6. Prune non-typical bursts In contrast to short bursts, there were situations when the sEMG signal had artefacts which last for a long time but had smaller amplitude compared to the typical bursts. An example non-typical burst is shown in Figure 4.9. These bursts were removed by applying a threshold on the root mean square (RMS) value. This can be done in two ways. Either by directly specifying a RMS threshold value, or, in the case of repeated movements, by specifying the number of standard deviations (N_{nt}) to create acceptable bounds around the mean RMS value of all the detected bursts. The latter approach was adopted in this study.

7. Join movement components Finally, this operation was introduced for situations where a movement had two components and it was desirable to represent the whole movement with one pair of an onset and an offset. For example, in case of a step on/off a step-stool, the movement had two components. The onset/offset pairs from the two components were joined together by specifying a time window of T_j seconds.

4.2.3.3 Experimental Dataset

The sEMG data used in this study was collected as part of a previously published study. Further details about the study and the experimental protocol can be found in (Rashid et al., 2018).

Participants Twenty two healthy participants (Average age: 36 ± SD 6 years, 10 Female) took part in the experiment conducted at Auckland University of Technology, New Zealand. Participants were excluded if they had a history of any neurological

disorders or epilepsy. All the participants signed a written consent form before data collection. The ethics for the study was approved by Central Health and Disability Ethics Committee (HDEC) (17/CEN/133), New Zealand in accordance with the Declaration of Helsinki.

Experimental protocol For each participant, data was collected in one session. The participants executed 50 single joint movements (right foot ballistic ankle dorsiflexions) while seated and 50 repetitions of multi-joint movements (right foot step on and off a step-stool which was approximately 23 cm high and placed at a comfortable distance) while standing. For ankle dorsiflexion, participants were seated in an ergonomic dentist-like chair with their back slightly reclined. Their legs were supported in approximately 25 degrees knee flexion and they had their ankle in a relaxed position. They were advised to look forward, flex their right ankle by pulling their toes towards their face in fast but controlled manner. For step on/off, participants were advised to place their right foot on the step-stool and immediately bring it back to the ground. They executed the tasks at their own pace while pausing for at least five seconds between each repetition. The order of the tasks was chosen at random.

Two surface electrodes (Ambu® BlueSensor N) were placed on the right tibialis anterior (TA) muscle. The electrodes were connected to a NuAmps (Compumedics Neuroscan) amplifier which was used for impedance measurement and data recording. Preparation included shaving, exfoliating with the Nuprep Gel (Weaver and Company, USA), subsequent cleansing with disposable alcohol swabs and accepting the electrode impedance below 10 kΩ. Data was recorded with the Acquire software (Compumedics Neuroscan). The sample-rate was set at 500 Hz. Examples of sEMG bursts for ankle dorsiflexion and step on/off are shown in Figure 4.10

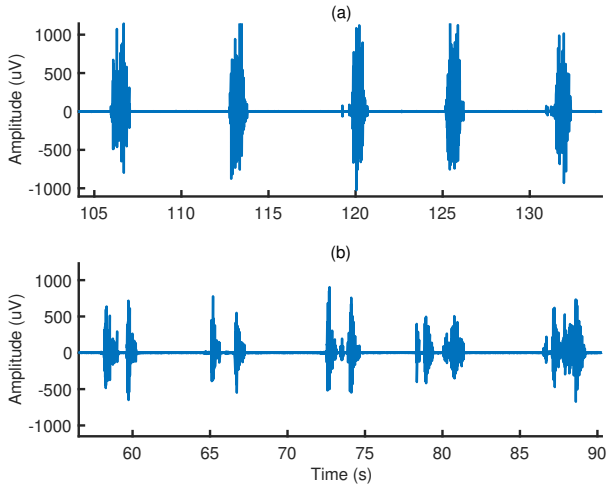

Figure 4.10: Example muscle activation bursts for ankle dorsiflexion (a) and step on/off (b)

Signal processing The data was processed on MATLAB 2017b (MathWorks, Inc.). The data from one sEMG electrode was subtracted from the other to form a single differential derivation. This channel was then filtered using a high pass and a low pass 2^{nd} order, zero-phase, Butterworth filter with cut-off at 10 Hz and 200 Hz respectively.

Manual labelling by an expert To conduct a comparison between the proposed nOptim method applied on eDTA and manual labelling, full wave rectified experimental data was manually labelled by an expert. The expert scrolled through the full wave rectified data using a custom graphical user interface (GUI) tool and manually placed onsets and offsets of muscle activity. The custom graphical user interface tool was developed on MATLAB 2017b.

4.2.3.4 Software Implementation

The MATLAB 2017b based graphical user interface tool developed as part of this study is shown in Figure 4.11 and has been made available online[4]. This toolbox includes the extended double thresholding algorithm and the proposed *nOptim* method. This

[4]https://github.com/GallVp/emgGO

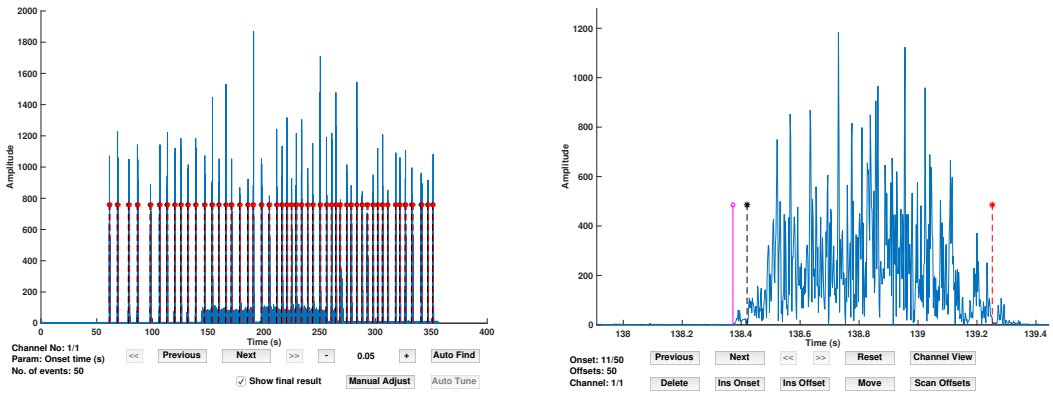

Figure 4.11: The graphical user interface (GUI) tool developed for processing of sEMG data
The graphical user interface (GUI) tool developed in this study. The left window shows the main GUI with options to find estimated number of onset/offset pairs. The right window shows one onset/offset pair with rectified sEMG signal. It allows the user to move, insert and delete individual events.

software can be used to visually estimate the number of bursts in multi-channel sEMG data and then obtain an optimal set of bursts using the *nOptim* method against that estimate. The individual onsets/offsets can be added, removed and moved. Other algorithms can easily be added to it and used with the *nOptim* method without the need to change any GUI related code. Although the toolbox allows processing of multi-channel data, each channel has to be processed separately as it keeps the algorithm parameters for each channel separate. This was implemented under the assumption that different channels may represent sEMG from different muscles with varied signal characteristics.

4.2.3.5 Global Parameters for eDTA

To conduct a comparison between the proposed nOptim method applied on eDTA and eDTA with global parameters, a separate set of global parameters was tuned for each task. Instead of obtaining the global parameters by manual tuning, an empirical approach was taken to select the best possible parameters. For each task, data from 6

participants was chosen at random as a training set. We chose 6 participants instead of all 22 for training as it represented a practical approach where data is manually labelled for a randomly chosen smaller set and algorithm parameters are obtained from this labelled data for use with the rest of the unseen unlabelled data. An optimal set of parameters was found for each participant in the training set by minimising the following cost function.

$$\begin{aligned} \min_{P} \quad & \|1 - C(\Lambda(P_i, X), R)\|_2 \\ & B^l \leq P \leq B^u \end{aligned} \tag{4.6}$$

Where R represented the set of onset/offset pairs manually labelled by the expert, and C denoted the concordance between the expert and the algorithm (see further details on concordance in Section 4.2.3.6.2). Particle swarm algorithm was used for optimisation. To avoid overfitting on a single participant, the obtained set of parameters was used to compute cross-validation cost, defined as $\|1 - C(\Lambda(P, X), R)\|_2$, for the remaining five participants in the training set. The set of task specific parameters which gave lowest mean leave-p-out cross-validation cost was selected and applied to all the 22 participants.

4.2.3.6 Statistical Analysis

Statistical analysis was performed in MATLAB 2017b. Four important questions needed to be answered with experimental data. First, what was the detection rate of the proposed *nOptim* method applied on eDTA and of the eDTA with global parameters, i.e., did these methods successfully produce as many onset/offset pairs as labelled by the expert? Second, what was the quality of their detections in comparison with the expert? Third, what was the quality of the detections of *nOptim* method applied on eDTA compared to the eDTA with global parameters? And fourth, what was the quality of the detections

of *nOptim* method applied on eDTA if there was an error in the estimated number of onset/offset pairs as compared to the actual number of sEMG bursts present in the signal. To answer these questions we ran the *nOptim* method on eDTA for each participant and task separately. The estimated number of onset/offset pairs (N_e in Section 4.2.3.1) was set equal to the number of onset/offset pairs manually labelled by the expert. For the eDTA, results were obtained using the task specific global parameters as explained in Section 4.2.3.5. The methods used to investigate these four questions are detailed in the following subsections.

4.2.3.6.1 Detection Rate Detection rate (DR) was obtained to quantify the difference in the number of detected pairs of onsets/offsets and the number of pairs manually labelled by the expert. It was defined as the percentage of the number of onset/offset pairs detected by the algorithm to the number of sEMG bursts labelled by the expert. It was obtained for both the *nOptim* method applied on eDTA and for eDTA with the global parameters. Statistical tests were performed to evaluate differences across the methods. Statistical tests are explained later in Section 4.2.3.6.3.

4.2.3.6.2 Comparison with the Expert To answer the second question we obtained concordance (CO), degree of over detection (OD), degree of under detection (UD) and F_1 score (a combined measure of sensitivity and precision). These measures were defined in terms of following quantities and expressed as percentages (Jubany & Angulo-Barroso, 2016).

- True positives (TPs): sEMG signal samples classified as burst by both the expert and the algorithm.
- False positives (FPs): Signal samples classified as burst by the algorithm and not by the expert.
- True negatives (TNs): Signal samples not classified as burst by both the algorithm

and the expert.

- False negatives (FNs): Signal samples not classified as burst by the algorithm and classified as burst by the expert.

CO was defined as the percentage of the sum of TPs and TNs to total number of signal samples. OD was defined as the percentage of FPs to the sum of TPs and FNs. UD was defined as the percentage of FNs to the sum of TNs and FPs. F_1 score was defined as the harmonic mean of the sensitivity and precision as follows:

$$\begin{aligned} F_1 &= 2 \times \frac{sensitivity \times precision}{sensitivity + precision} \times 100 \\ &= \frac{2 \times TPs}{2 \times TPs + FNs + FPs} \times 100 \end{aligned}$$

Where sensitivity (true positive rate) and precision (positive predictive value) were defined as follows.

$$\begin{aligned} Sensitivity &= \frac{TPs}{TPs + FNs} \times 100 \\ Precision &= \frac{TPs}{TPs + FPs} \times 100 \end{aligned}$$

CO was interpreted as the level of agreement between the algorithm and the expert in correctly classifying the signal as *on* or *off*. F_1 was interpreted as the combined measure of the sensitivity and the precision of the algorithm compared to the expert. OD/UD were interpreted as the degree to which the algorithm detected the onset early/late and detected the offset late/early with respect to the expert.

4.2.3.6.3 eDTA with nOptim versus eDTA with Global Parameters The third question was answered by comparing CO, F_1, UD and OD obtained with the proposed *nOptim* method applied on eDTA against eDTA with global parameters. Medians, inter quartile ranges, minimum and maximum values were reported for the measures as the

performance measures exhibited substantial skew and large number of outliers. We tested for the equality of medians across the two methods (*nOptim* vs. Global) within each task. For comparison of medians, Wilcoxon's signed rank test with *approximate* method was performed. Significance level was set at 0.05.

4.2.3.6.4 Sensitivity to Induced Error The fourth question was answered by running the proposed *nOptim* method on eDTA with an error introduced in the estimated number of onset/offset pairs for all the participants. Concordance was used for evaluation of its performance under $\pm 0\%$, $\pm 2\%$, $\pm 4\%$, $\pm 6\%$, $\pm 8\%$ and $\pm 10\%$ error. For example, if the expert had labelled 50 onset/offset pairs for a participant, an error of $\pm 10\%$ was induced by running the *nOptim* method on eDTA with the estimated number of onset/offset pairs (N_e in Section 4.2.3.1) set to either 45 or 55 chosen at random.

To test the statistical significance of the differences in concordance across different levels of induced error, we performed a Friedman's test with levels of error as the column factor and movement type as the block factor. Significance level was set at 0.05. One important limitation of the Friedman's test is that despite being a two-way model it does not test for the interaction effect or the row effects. It only tests the column effects after adjusting for the row effects (Hogg & Ledolter, 1987; Hollander et al., 2015). However, the advantage of using the Friedman's test is that it accounts for the repeated measures in the data (Bewick et al., 2004).

4.2.4 Results

4.2.4.1 Global Parameters for eDTA

The results for global parameter selection are shown in Figure 4.12. For dorsiflexion, parameters from the 2nd training set were selected as they produced lowest mean cross-validation cost. The parameters were {0.152, 5, 2, 0.01, 0.968, 0.012, 4, 0} in the

following order $\{L_b, K_b^{th}, N_{sd}, T_{on}, T_{off}, T_s, N_{nt}, T_j\}$. In the same order, parameters for step on/off were selected from the 3rd set, {0.28, 40, 2, 0.01, 1, 0.01, 7, 1.456}. The units of time parameters were seconds. These global parameters were used to detect onsets/offsets for all the 22 participants.

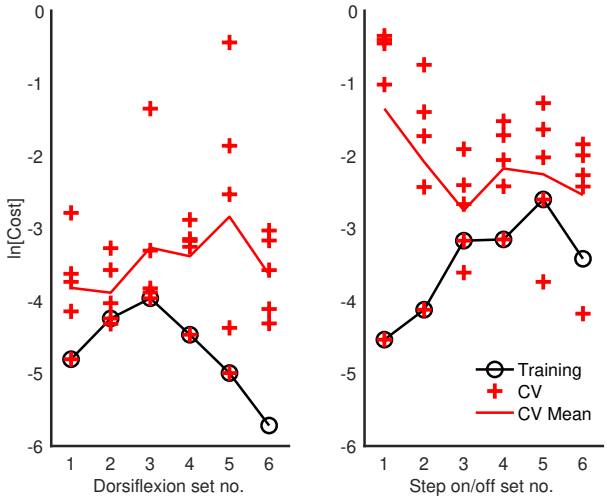

Figure 4.12: Training and cross-validation natural log costs for selection of global parameters for the extended double thresholding algorithm
Note: Cross-validation costs were computed using leave-p-out cross-validation. p was five in this case. Costs were plotted on the log scale as most of the individual cross-validation costs were too close to be distinguished from each other when plotted on a linear scale.

4.2.4.2 Detection Rate

The detection rate for the *nOptim* method applied on eDTA was 100% for all the participants in both tasks. On the other hand the detection rate with the global parameters ranged from 0 to 120% and 0 to 143% in dorsiflexion and step on/off respectively. However, there were no statistically significant ($p > 0.05$) differences in the median detection rate of two methods. Detailed results are presented in Table 4.3. These results indicate that *nOptim* method did always converge to the estimated number of onset/offset pairs.

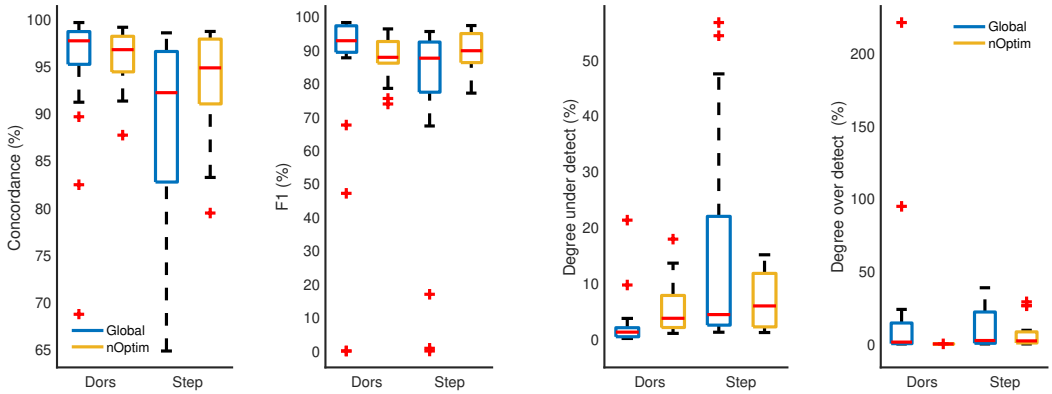

Figure 4.13: Movement wise results for concordance, F_1 score, degree of over detection and under detection
Note: Dors stands for dorsiflexion and Step for step on/off. Each box represent data from the 22 participants. The statistic line represents the median. The edges represent 1st and 3rd quartiles (Q_1 and Q_3). The lower and upper whiskers are at Q_1-1.5(Q_3-Q_1) and Q_3+1.5(Q_3-Q_1) respectively.

4.2.4.3 eDTA with nOptim versus eDTA with Global Parameters

Concordance, F_1 score, degree of under detection and over detection of eDTA against the expert with the *nOptim* method and the global parameters are shown in Figure 4.13. Medians, inter-quartile ranges, minimum and maximum values and results of significance tests for equality of medians are presented in Table 4.3. These results indicated that the *nOptim* parameters generally resulted in performance metrices with smaller variability compared to the global parameters.

Table 4.3: Medians, inter-quartile ranges, minimum and maximum values and results of significance tests for equality of medians

Note: M_g and M_n stand for median of the measure with global parameters and median of the measure with *nOptim* parameters. H_0 stands for the null hypothesis.

Measure	Movement	Median ± IQR [min, max] % With global	Median ± IQR [min, max] % With proposed *nOptim*	H_0: $M_g = M_n$ z-value, p-value
Detection rate	Dorsiflexion	100 ± 0 [0, 120]	100 ± 0 [100, 100]	-0.534, 0.594
	Step on/off	101.9 ± 4 [0, 142.9]	100 ± 0 [100, 100]	0.761, 0.447
Concordance	Dorsiflexion	97.7 ± 3.5 [68.7, 99.6]	96.7 ± 3.8 [87.7, 99.1]	1.055, 0.291
	Step on/off	92.2 ± 13.8 [64.9, 98.5]	94.8 ± 6.9 [79.5, 98.7]	-1.997, 0.046
F_1 score	Dorsiflexion	92.7 ± 7.9 [0, 98.1]	87.7 ± 6.5 [73.8, 96.2]	1.088, 0.277
	Step on/off	87.5 ± 15 [0, 95.5]	89.7 ± 8.7 [77.0, 97.2]	-1.997, 0.046
Degree under detect	Dorsiflexion	1.2 ± 1.6 [0.1, 21.3]	3.7 ± 5.7 [1, 17.9]	-2.841, 0.005
	Step on/off	4.4 ± 19.5 [1.2, 56.7]	5.9 ± 9.6 [1.2, 15.1]	0.666, 0.506
Degree over detect	Dorsiflexion	1.3 ± 14.2 [0, 221.2]	0 ± 0 [0, 0.1]	3.621, < 0.001
	Step on/off	2.4 ± 21.5 [0, 38.8]	2.1 ± 7.7 [0, 29]	0.643, 0.520

The differences in the median performance of the two methods were more subtle. In case of dorsiflexion, there were no statistically significant ($p > 0.05$) differences in the median concordance or F_1 score across the two methods. In case of step on/off, both the median concordance and the median F_1 score of the *nOptim* parameters were higher ($p < 0.05$) compared to the global parameters. These results indicated that the *nOptim* parameters resulted in same (ankle dorsiflexion) or better (step on/off) concordance and F_1 score compared to the global parameters. Thus, the *nOptim* method did not only produce the required number of onset/offset pairs, it also produced results which were in good agreement with the expert.

In case of dorsiflexion, the *nOptim* parameters resulted in higher ($p < 0.05$) degree of under detection and lower ($p < 0.05$) degree of over detection compared to the global parameters. In case of step on/off, there were no statistically significant ($p > 0.05$) differences across the two methods in both the degree of under detection and over detection. These results indicated that the *nOptim* method resulted in same (step on/off) or higher under detection (ankle dorsiflexion) compared to the global parameters. These results are further discussed later in Section 4.2.5.

4.2.4.4 Sensitivity to Induced Error

The percentage concordance with zero up to ± 10% error is shown in Figure 4.14. A smooth decrease in median concordance and increase in variability with an increase in error was observed. There was no statistically significant ($\chi^2 = 6.39$, $p = 0.27$) difference in median concordance across different levels of induced error. These results suggested that the *nOptim* method was robust to error in the estimated number of sEMG bursts.

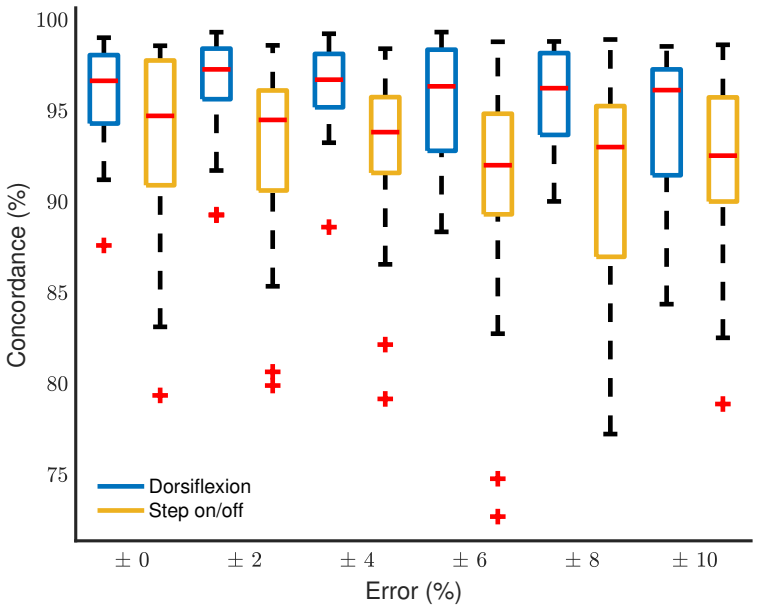

Figure 4.14: Concordance between the expert and the algorithm using the proposed *nOptim* method with increasing percentage of induced error
Note: Each box represent data from the 22 participants. The statistic line represents the median. The edges represent 1st and 3rd quartiles (Q_1 and Q_3). The lower and upper whiskers are at Q_1-1.5(Q_3-Q_1) and Q_3+1.5(Q_3-Q_1) respectively.

4.2.5 Discussion

We have proposed an optimisation method (*nOptim*) for sEMG detection algorithms. We have evaluated it as a method that can be used to obtain an optimised set of sEMG bursts from a trial given an estimate of the number of bursts in the trial. Its ability to optimise burst detection based on the estimated number of bursts is the key feature which stands out from previous optimisation methods in the sEMG literature (Staude et al., 2001). On sEMG data from 22 healthy participants executing single and multi-joint movements, the proposed *nOptim* method applied on an extended version of the double thresholding algorithm has shown good agreement with the bursts manually labelled by an expert in terms of concordance, F_1 score as an average of sensitivity and precision, degree of over detection and degree of under detection. When compared against bursts detected using eDTA with global parameters, the proposed *nOptim* method had same

(single joint movement) or better (multi-joint movement) performance in terms of concordance, sensitivity and precision. However, the proposed *nOptim* method had a tendency to under detect sEMG bursts in the single joint movement compared to the global parameters.

4.2.5.1 eDTA and Selection of Global Parameters

We have also extended the double thresholding algorithm and have proposed a method for selection of global parameters. The global parameter selection method can be used to tune parameters from a smaller set of data manually labelled by an expert and apply these parameters to the rest of the unseen unlabelled data. Although the performance of eDTA with global parameters selected using this method was less consistent compared to the *nOptim* method, it may be useful to researchers interested in deploying sEMG detection algorithms on small portable low power devices which can not afford to run an optimisation routine for each data recording (Balouchestani & Krishnan, 2014; Pashaei et al., 2015).

4.2.5.2 Detection Rate

The proposed method detected 100% of the number of sEMG bursts identified by the expert across all the participants in both single joint and multi-joint movements. These results are in agreement with the results of optimisation methods previously proposed (Staude et al., 2001). However, our proposed method only requires a single input from the user to perform the optimisation and minimal time in manually analysing the signal.

4.2.5.3 eDTA with nOptim versus eDTA with Global Parameters

Compared to the bursts detected by the extended double thresholding algorithm with the global parameters, the proposed *nOptim* method generally had smaller variability in concordance, F_1 score, degree of under detection and over detection. The worst case

outliers for concordance and F_1 score were above 70%, and below 20% for degree of under detection and over detection. A smaller variability in performance metrices suggests better consistency with implications for the amount of time spent by the expert on adjusting the onsets and offsets detected by using an algorithm.

The *nOptim* method had same median concordance and F_1 score in the single joint movement compared to the global parameters. Whereas it had higher concordance and F_1 score in the multi-joint movement. This difference may be explained by the fact that the *nOptim* method optimised the sEMG burst detection for each participant individually while the global parameters were applied under the assumption that sEMG signal has adequate similarity across participants. As multi-joint movements involve larger number of degrees of freedom, it is reasonable to expect that different participants used different strategies in performing these movements and recruiting their muscles. Thus, *nOptim* performed better in case of the multi-joint movement as it did not require the assumption that the sEMG signal from different participants was similar.

The degree of under detection with the proposed method was higher in the single joint movement compared to the extended double thresholding algorithm with the global parameters. This is perhaps due to the fact that the proposed method minimises the number of samples contained in the detected bursts while maximising the Teager-Kaiser energy. Although it requires further investigation, we hypothesise that the degree of under detection could be improved by adding weights to different terms in the cost function.

4.2.5.4 Sensitivity to Induced Error

We also investigated the sensitivity of the proposed method to induced error in the estimated number of onsets/offsets compared to the actual number of bursts present in the sEMG data. The results showed that with up to $\pm 10\%$ error in the estimated number of onset/offset pairs, the worst case outlier for concordance remained above

70%. However, a gradual decrease in median concordance and increase in variability was observed. These results suggest that the proposed method has a degree of tolerance to inaccuracy in the estimate of the number of sEMG bursts and its performance does not drop strikingly.

4.2.5.5 Limitations

The findings from this research should be considered in light of a number of factors. First, the cost function used for tuning the global parameters was based on the concordance measure which was also used for comparing the *nOptim* method against the global parameters. This favoured the performance of the global parameters as they were specifically optimised to perform better in terms of the concordance measure. Thus the comparison was likely conservative and aligned against the proposed *nOptim* method. Second, although particle swarm optimisation is a global approach to optimisation, a failure to detect the required number of onsets/offsets can be expected in some situations as the proposed method is not guaranteed to result in the global optimum. In such a case, running the optimisation with different initial conditions can help convergence to a more optimal solution. Third, a single expert manually labelled the sEMG data and their results were treated as the gold standard. This was done under the assumption that the results of manual labelling are reliable and repeatable (Jubany & Angulo-Barroso, 2016; Hodges & Bui, 1996). Fourth, the quantitative measures, such as concordance, used to evaluate the performance of the proposed methods do not measure the exact timing of the onsets and the offsets.

4.2.5.6 Recommendations for Future Work

The potential of the proposed *nOptim* method has not be fully evaluated yet. It may prove to be more useful with following future works.

1. A possible direction for future work is the use of the proposed *nOptim* method to obtain a global set of detection parameters that can be generalised across trials or within a long recording file. This might require adding a regularisation term to its cost function (Rakitianskaia & Engelbrecht, 2014). This approach may allow to optimize the parameters with the proposed *nOptim* method using a relatively short initial segment of the signal and then applying the optimised detection to the rest of the recording.
2. In this study we have used particle swarm optimisation as the search strategy for the proposed *nOptim* method. This allowed us to perform the optimisation without deriving the gradients of the cost function. The downside of this approach is that the particle swarm optimisation is a computationally expensive algorithm. This opens two possible directions for future work. First, to choose a detection algorithm which would allow derivation of gradients for the *nOptim* cost function and use a less computationally expensive search strategy such as gradient decent. Second, to evaluate the proposed *nOptim* method with a real-time implementation of the particle swarm algorithm (Liu et al., 2008).
3. sEMG data for both the single joint and the multi-joint movement in this study was processed as a single channel. Thus, a possible direction for future work is the evaluation of the proposed *nOptim* method on a movement, for example continuous walking, in which multi-channel data is recorded from different muscles which have different patterns of activation (Brantley et al., 2018). This, however, may also require using a detection algorithm other than the proposed extended double thresholding algorithm.

4.2.6 Conclusion

The proposed *nOptim* method can be used to obtain accurate estimates of onsets and offsets of muscle activity from a sEMG signal by simply inputting an estimate of the number of muscle activation bursts in the signal. The *nOptim* method exhibited good performance in terms of detection rate, concordance, F_1 score (sensitivity and precision), degree of under detection and over detection on sEMG data for both single joint and multi-joint movements manually labelled by an expert. This method may reduce the time burden associated with current sEMG processing.

End of Published Manuscript 3

4.3 Summary

In summary, computational methods are an integral part of modern medical devices. This chapter presented three computational methods for processing of MRCP and sEMG data. These methods were proposed to specifically address objectives numbered 4 and 5 in section 2.6 related to algorithms for a MRCP based rehabilitation medical device. However they were published in peer reviewed journals as general purpose methods for wider applicability. Additional work is required to implement and validate these method on a portable brain computer interface.

Chapter 5

Discussion

The research presented in this thesis was motivated by laboratory based evidence which suggests that the Movement-related Cortical Potentials (MRCPs) can be used to deliver a neuromodulatory intervention for post-stroke rehabilitation (Mrachacz-Kersting et al., 2012; Niazi et al., 2012). The importance of these findings is amplified by the fact that the MRCP based intervention does not require directly stimulating the brain with electric or magnetic potentials. This evidence, however, comes from laboratory based experimental studies. For further clinical investigation and for translating this evidence from the laboratory to clinical practice, research in development of mobile, affordable and usable medical devices is required. The primary aim of my PhD was to identify and address the key gaps in the scientific knowledge towards development of MRCP based rehabilitation medical devices. A secondary aim was to refine the computational methods which are currently used in processing of MRCPs in relation to post-stroke rehabilitation.

This chapter presents a summary of my contributions and discusses the implications of my findings in reference to the related scientific literature. Next the current state of the mobile BCI for MRCP based rehabilitation paradigms is summarised and avenues for future research are proposed. Finally this chapter concludes the thesis.

5.1 Summary and Wider Implications of my Contributions

I attempted to achieve the aims of my PhD by making following primary contributions.

Blueprint of a mobile BCI and research objectives for its development I undertook a detailed literature review of the existing scientific knowledge available on MRCP based rehabilitation paradigms, the current methods and equipment used to implement these paradigms, and the limitations of these methods. In light of these limitations, a blueprint for a Brain Computer Interface (BCI) which can be eventually developed into a mobile medical device for MRCP based rehabilitation was defined. With a further literature review, some of the components required for this BCI were identified and objectives for further research towards the selection or evaluation of the remaining components were also specified.

Performance assessment of a small footprint ADC My second contribution was to conduct a comprehensive experimental evaluation of Texas Instruments ADS1299 for its ability to record MRCPs. ADS1299 is a portable low power Analog to Digital Converter (ADC) which can be embedded in a mobile medical device. The main finding of my experimental study was that ADS1299 when coupled with wet state-of-the-art Ag/AgCl electrodes can record MRCPs at a quality analogous to that of a laboratory based system (Rashid et al., 2018). With this study, objective 2 identified in section 2.6 was fully achieved.

In the wider context, the fact that ADS1299 can be used for recording MRCPs at fairly high quality has implications for researchers involved in translation of BCIs based on low frequency EEG from laboratory to medical devices (Belwafi et al., 2018; McCrimmon et al., 2016). Similarly other BCI based rehabilitation paradigms which

require portable medical devices for their successful translation from research into clinical practice can benefit from these findings (Biasiucci et al., 2018).

Development of a prototype for exciteBCI Based on the findings of my experimental study investigating the performance of ADS1299, I undertook further prototyping in accordance with the BCI blueprint defined from the literature review. I created a prototype which consisted of Quick-Cap (Compumedics Neuroscan, Dresden, Germany), OpenBCI Cyton V3-32 board (OpenBCI, New York, NY, USA) which uses ADS1299 as its ADC, and an iPad application which could communicate with the rest of the hardware via Bluetooth. This prototype was capable of recording, cleaning and presenting MRCPs on an iPad. Based on this prototype, I together with team members from Auckland University of Technology (AUT) and Exsurgo Rehab Limited, successfully presented exciteBCI as a potential MRCP based medical device for post-stroke rehabilitation at a national technology challenge. Further development of exciteBCI is underway by Exsurgo Rehab Limited.

Automated labelling of MRCPs My fourth primary contribution was the first automated labelling method for MRCPs in self-paced movements. This method can be used to fully automate the extraction of important features of the MRCP which have been studied in the past for assessment of neurophysiological changes in response to motor training. With this method, objective 5 identified in section 2.6 was fully achieved.

In the wider context, the proposed method may be useful to researchers interested in online neuroadaptive paradigms to support motor training (Zander et al., 2016).

Computational methods for sEMG My fifth and sixth contributions were the two computational methods for processing of Surface Electromyography (sEMG) data. sEMG data is generally used to keep track of the timing of self-paced movements when recording MRCPs. The first method, the extended double thresholding algorithm, is

an extension of the already established double thresholding algorithm (Bonato et al., 1998). The extended version was specifically designed to detect muscle onsets and offsets in repeated functional movements. The second method is an optimisation technique, *nOptim*, which can be used in combination with any offline sEMG onset/offset detection algorithm to improve its detection performance without the need to change the parameters of the detection algorithm for each individual. With these method, objective 4 identified in section 2.6 was partially achieved.

In the wider context, these methods are particularly useful for researchers and clinicians who regularly employ sEMG to study timing of muscle activations (Chowdhury et al., 2013; Yang et al., 2017; J. A. Guerrero & Macías-Díaz, 2014; Staude et al., 2001; Merlo et al., 2003; Falla et al., 2004; Worsley et al., 2013; Moseley et al., 2003; Vasseljen et al., 2006; Hodges et al., 2003).

In addition to these six primary contributions, I made following two secondary contributions.

Simulation method for typical averaged MRCPs In order to evaluate the method for automated labelling of MRCPs in a large dataset with wide variability, I also proposed a method for simulating typical averaged MRCPs.

In the wider context, the proposed simulation method can also be valuable to researchers interested in algorithms for detection of movement intention from MRCPs (Yao et al., 2018; Karimi et al., 2017; Lin et al., 2016).

Publicly available documented source code The bulk of the code that I wrote during my PhD has been made available online in public repositories. I have also provided detailed documentation with this code and example data files where possible.

5.2 Current State of the Mobile BCI for MRCP based Rehabilitation Paradigms and Avenues for Future Work

The detailed literature review and the findings of my PhD have advanced the state of the mobile BCI for MRCP based rehabilitation paradigms in multiple directions. Research objectives numbered 2, 4 and 5 identified in section 2.6 have been fully or partially achieved. The current state of the BCI is summarised in Figure 5.1. The structure of the BCI in this figure is based on the blueprint BCI proposed in Chapter 2 and the components are based on my findings.

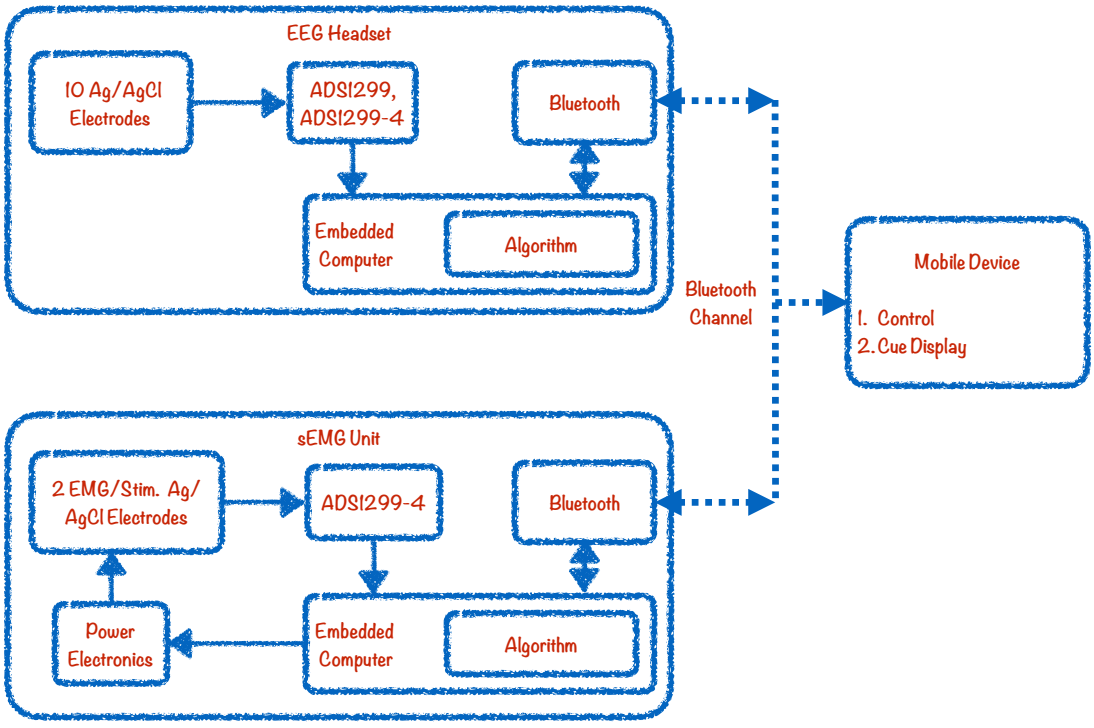

Figure 5.1: Current state of the mobile BCI for MRCP based rehabilitation paradigms

This figure suggests that a mobile BCI for MRCP based rehabilitation paradigms

can be built using Ag/AgCl wet electrodes, ADS1299 analogue to digital converter, bluetooth wireless communication, a set of algorithms, an embedded computer chosen for these algorithms and power electronics for electrical stimulation. Such a BCI may be usable for both the online and offline version of the MRCP based neuromodulatory intervention, and assessment of motor training. However complete prototyping of this type of general purpose BCI requires substantial work on selection of algorithms along with an embedded computer and extensive usability testing. In the following paragraphs, I have suggested avenues of future work which are necessary for its further development towards a mobile, affordable and usable medical device.

Performance assessment of dry electrodes for recording MRCPs Development and evaluation of dry EEG electrodes is an active area of research as these electrodes may lead to on-the-go and plug-n-play EEG based medical devices (Chi et al., 2010; Fiedler et al., 2014, 2016; Lopez-Gordo et al., 2014; Pedrosa et al., 2017; Oliveira et al., 2016; J. Xu et al., 2011). MRCPs are highly susceptible to movement noise and, therefore, one of the best test case signals for evaluation of dry electrodes. Availability of dry EEG electrodes which can record MRCP at high quality may increase adoption and usability of MRCP based rehabilitation medical devices.

Complexity analysis of BCI algorithms One important area for immediate future work is the time and memory complexity analysis of BCI algorithms (Wegener, 2005; Ahmadi et al., 2012). This analysis is missing from the past comparisons and reviews of BCI algorithms (Shakeel et al., 2015; Lotte et al., 2007; Garrett et al., 2003; Lotte et al., 2018). Without this analysis, it is difficult to determine which algorithm is best suited for deployment on a portable device and how powerful an embedded computer should be chosen for a particular BCI application.

Usability Testing of an MRCP based BCI The most important issue for successful adoption of a BCI in rehabilitation are related to its usability (Kübler et al., 2014; Maskeliunas et al., 2016; Ekandem et al., 2012; Holz et al., 2013; Rebolledo-Mendez et al., 2009; Zickler et al., 2013; Pasqualotto et al., 2012). A number of technological gaps were identified and addressed by this thesis towards the development of an MRCP based BCI rehabilitation medical device. Further prototyping of a medical device based on this thesis need to be carried out in parallel with its usability testing with clinicians and patients (Signal et al., 2019).

5.3 Conclusion

There is an increasing amount of evidence which supports a neuromodulatory rehabilitation intervention based on the movement-related cortical potential for a faster and greater post-stroke recovery. For successful translation of this research from the laboratory into clinical practice, research towards affordable, mobile and usable medical devices is required. In this thesis I have comprehensively examined the gaps in the scientific knowledge which hinder this translation. To address the key gaps, I proposed a blueprint brain computer interface which can be developed into a MRCP based rehabilitation medical device. The different components required for this brain computer interface were proposed and evaluated with experimental studies. This conceptual blueprint and the evidence generated by this research helped successful presentation of a potential MRCP rehabilitation medical device at a national technology challenge. Future research should focus how such a device will be embedded into clinical practice.

References

Adibifard, M., Bashiri, G., Roayaei, E. & Emad, M. A. (2016). Using particle swarm optimization (pso) algorithm in nonlinear regression well test analysis and its comparison with levenberg-marquardt algorithm. *International Journal of Applied Metaheuristic Computing (IJAMC)*, *7*(3), 1–23. doi: 10.4018/ijamc.2016070101

Adrian, E. D. & Matthews, B. H. C. (1934). The interpretation of potential waves in the cortex. *The Journal of Physiology*, *81*(4), 440–471. doi: 10.1113/jphysiol.1934.sp003147

Ahmadi, A., Dehzangi, O. & Jafari, R. (2012). Brain-computer interface signal processing algorithms: A computational cost vs. accuracy analysis for wearable computers. In *2012 ninth international conference on wearable and implantable body sensor networks* (pp. 40–45). doi: 10.1109/bsn.2012.19

Ahmadian, P., Cagnoni, S. & Ascari, L. (2013). How capable is non-invasive eeg data of predicting the next movement? a mini review. *Frontiers in human neuroscience*, *7*, 124. doi: 10.3389/fnhum.2013.00124

Balouchestani, M. & Krishnan, S. (2014). Effective low-power wearable wireless surface emg sensor design based on analog-compressed sensing. *Sensors*, *14*(12), 24305–24328. doi: 10.3390/s141224305

Bates, D., Mächler, M., Bolker, B. & Walker, S. (2015). Fitting linear mixed-effects models using lme4. *Journal of Statistical Software*, *67*(1), 1–48. doi: 10.18637/jss.v067.i01

Beauchene, C., Abaid, N., Moran, R., Diana, R. A. & Leonessa, A. (2016). The effect of binaural beats on visuospatial working memory and cortical connectivity. *PloS one*, *11*(11), e0166630. doi: 10.1371/journal.pone.0166630

Belwafi, K., Romain, O., Gannouni, S., Ghaffari, F., Djemal, R. & Ouni, B. (2018). An embedded implementation based on adaptive filter bank for brain–computer interface systems. *Journal of neuroscience methods*, *305*, 1–16. doi: 10.1016/j.jneumeth.2018.04.013

Berger, V. W. (2000). Pros and cons of permutation tests in clinical trials. *Statistics in medicine*, *19*(10), 1319–1328. doi: 10.1002/(sici)1097-0258(20000530)19:10<1319::aid-sim490>3.3.co;2-s

Bernhardt, J., Chan, J., Nicola, I. & Collier, J. M. (2007). Little therapy, little physical activity: Rehabilitation within the first 14 days of organized stroke unit care. *Journal of rehabilitation medicine*, *39*(1), 43–48. doi: 10.2340/16501977-0013

Bewick, V., Cheek, L. & Ball, J. (2004). Statistics review 10: further nonparametric methods. *Critical Care*, *8*(3), 196. doi: 10.1186/cc2857

Bezerra, E. A. & Gough, M. P. (2000). A guide to migrating from microprocessor to fpga coping with the support tool limitations. *Microprocessors and Microsystems*, *23*(10), 561–572. doi: 10.1016/s0141-9331(99)00063-0

Biasiucci, A., Leeb, R., Iturrate, I., Perdikis, S., Al-Khodairy, A., Corbet, T., ... d. R. Millán, J. (2018). Brain-actuated functional electrical stimulation elicits lasting arm motor recovery after stroke. *Nature communications*, *9*(1), 2421. doi: 10.1038/s41467-018-04673-z

Bonato, P., D'Alessio, T. & Knaflitz, M. (1998). A statistical method for the measurement of muscle activation intervals from surface myoelectric signal during gait. *IEEE Transactions on Biomedical Engineering*, *45*(3), 287–299. doi: 10.1109/10.661154

Boxtel, G. J. M., Geraats, L. H. D., Berg-Lenssen, M. M. C. & Brunia, C. H. M. (1993). Detection of emg onset in erp research. *Psychophysiology*, *30*(4), 405–412. doi: 10.1111/j.1469-8986.1993.tb02062.x

Brantley, J. A., Luu, T. P., Nakagome, S., Zhu, F. & Contreras-Vidal, J. L. (2018). Full body mobile brain-body imaging data during unconstrained locomotion on stairs, ramps, and level ground. *Scientific data*, *5*, 180133. doi: 10.1038/sdata.2018.133

Brodmann, K. (1909). *Vergleichende lokalisationslehre der grosshirnrinde in ihren prinzipien dargestellt auf grund des zellenbaues*. Barth. Retrieved from `https://archive.org/details/b28062449/page/n4`

Bulea, T. C., Prasad, S., Kilicarslan, A. & Contreras-Vidal, J. L. (2014). Sitting and standing intention can be decoded from scalp eeg recorded prior to movement execution. *Frontiers in neuroscience*, *8*, 376. doi: 10.3389/fnins.2014.00376

Butar, F. B. & Park, J.-W. (2008). Permutation tests for comparing two populations. *Journal of Mathematical Science & Mathematics Education V3*, *2*, 19–30. Retrieved from `https://www.researchgate.net/publication/265008252_Permutation_Tests_for_Comparing_Two_Populations`

Cauraugh, J., Light, K., Kim, S., Thigpen, M. & Behrman, A. (2000). Chronic motor dysfunction after stroke. *Stroke*, *31*(6), 1360–1364. doi: 10.1161/01.str.31.6.1360

Cervera, M. A., Soekadar, S. R., Ushiba, J., del R. Millán, J., Liu, M., Birbaumer, N. & Garipelli, G. (2018). Brain-computer interfaces for post-stroke motor rehabilitation: a meta-analysis. *Annals of clinical and translational neurology*, *5*(5), 651–663. doi: 10.1002/acn3.544

Chai, T. & Draxler, R. R. (2014). Root mean square error (rmse) or mean absolute error (mae)? – arguments against avoiding rmse in the literature. *Geoscientific model development*, *7*(3), 1247–1250. doi: 10.5194/gmd-7-1247-2014

Chi, Y. M., Jung, T.-P. & Cauwenberghs, G. (2010). Dry-contact and noncontact biopotential electrodes: Methodological review. *IEEE reviews in biomedical engineering*, *3*, 106–119. doi: 10.1109/rbme.2010.2084078

Chiesi, M., Guermandi, M., Placati, S., Scarselli, E. F. & Guerrieri, R. (2019). Creamino: A cost-effective, open-source eeg-based bci system. *IEEE Transactions on Biomedical Engineering*, *66*(4), 900–909. doi: 10.1109/tbme.2018.2863198

Chowdhury, R., Reaz, M., Ali, M., Bakar, A., Chellappan, K. & Chang, T. (2013). Surface electromyography signal processing and classification techniques. *Sensors*, *13*(9), 12431–12466. doi: 10.3390/s130912431

Clayton, E., Kinley-Cooper, S. K., Weber, R. A. & Adkins, D. L. (2016). Brain stimulation: Neuromodulation as a potential treatment for motor recovery following traumatic brain injury. *Brain research*, *1640*, 130–138. doi: 10.1016/j.brainres.2016.01.056

Cravo, A. M., Rohenkohl, G., Wyart, V. & Nobre, A. C. (2011). Endogenous modulation of low frequency oscillations by temporal expectations. *Journal of neurophysiology*, *106*(6), 2964–2972. doi: 10.1152/jn.00157.2011

Dang, X., Kang, B., Liu, X. & Cui, G. (2017). An interactive care system based on a depth image and eeg for aged patients with dementia. *Journal of healthcare engineering*, *2017*, 1–8. doi: 10.1155/2017/4128183

Das, D. P. & Webster, J. G. (1980). Defibrillation recovery curves for different electrode materials. *IEEE Transactions on Biomedical Engineering*, *BME-27*(4), 230–233. doi: 10.1109/tbme.1980.326728

Dehak, N., Dehak, R., Glass, J. R., Reynolds, D. A. & Kenny, P. (2010). Cosine similarity scoring without score normalization techniques. In *Odyssey* (p. 15). Retrieved from `https://groups.csail.mit.edu/sls/publications/2010/Dehak_Odyssey.pdf`

Delorme, A. & Makeig, S. (2004). Eeglab: an open source toolbox for analysis of single-trial eeg dynamics including independent component analysis. *Journal of neuroscience methods*, *134*(1), 9–21. doi: 10.1016/j.jneumeth.2003.10.009

Do Nascimento, O. F. & Farina, D. (2008, November). Movement-related cortical potentials allow discrimination of rate of torque development in imaginary isometric plantar flexion. *IEEE Transactions on Biomedical Engineering*, *55*(11), 2675–2678. doi: 10.1109/tbme.2008.2001139

Donnan, G. A., Fisher, M., Macleod, M. & Davis, S. M. (2008, May). Stroke. *The Lancet*, *371*(9624), 1612–1623. doi: 10.1016/s0140-6736(08)60694-7

Drapała, J., Brzostowski, K., Szpala, A. & Rutkowska-Kucharska, A. (2012). Two stage emg onset detection method. *Archives of Control Sciences*, *22*(4), 427–440. doi: 10.2478/v10170-011-0033-z

Dyall, L., Feigin, V., Brown, P. & Roberts, M. (2008, March). Stroke: A picture of health disparities in new zealand. *Social Policy Journal of New Zealand*, *33*, 178. Retrieved from `https://www.msd.govt.nz/about-msd-and-our-work/publications-resources/journals-and-magazines/social-policy-journal/spj33/33-stroke-a-picture-of-health-disparities-in-new-zealand-p178-191.html`

Eberhart, R. & Kennedy, J. (1995). A new optimizer using particle swarm theory. In *MHS'95. proceedings of the sixth international symposium on micro machine and human science* (pp. 39–43). IEEE. doi: 10.1109/mhs.1995.494215

Ekandem, J. I., Davis, T. A., Alvarez, I., James, M. T. & Gilbert, J. E. (2012). Evaluating the ergonomics of bci devices for research and experimentation. *Ergonomics*, *55*(5), 592–598. doi: 10.1080/00140139.2012.662527

Erdoğmuş, P. & Ekiz, S. (2016, November). Nonlinear regression using particle swarm optimization and genetic algorithm. *International Journal of Computer Applications*, *153*(6), 28–36. doi: 10.5120/ijca2016912081

Falla, D., Jull, G. & Hodges, P. W. (2004). Feedforward activity of the cervical flexor muscles during voluntary arm movements is delayed in chronic neck pain. *Experimental brain research*, *157*(1), 43–48. doi: 10.1007/s00221-003-1814-9

Fattapposta, F., Amabile, G., Cordischi, M. V., Venanzio, D. D., Foti, A., Pierelli, F., ... Morrocutti, C. (1996). Long-term practice effects on a new skilled motor learning: an electrophysiological study. *Electroencephalography and clinical Neurophysiology*, *99*(6), 495–507. doi: 10.1016/s0013-4694(96)96560-8

Feigin, V. L., Krishnamurthi, R. V., Barker-Collo, S., McPherson, K. M., Barber, P. A., Parag, V., ... and, R. B. (2015). 30-year trends in stroke rates and outcome in auckland, new zealand (1981-2012): A multi-ethnic population-based series of studies. *PloS one*, *10*(8), e0134609. doi: 10.1371/journal.pone.0134609

Ferree, T. C., Luu, P., Russell, G. S. & Tucker, D. M. (2001). Scalp electrode impedance, infection risk, and eeg data quality. *Clinical Neurophysiology*, *112*(3), 536–544. doi: 10.1016/s1388-2457(00)00533-2

Fiedler, P., Haueisen, J., Jannek, D., Griebel, S., Zentner, L., Vaz, F. & Fonseca, C. (2014). Comparison of three types of dry electrodes for electroencephalography. *Acta Imeko*, *3*(3), 33. doi: 10.21014/acta_imeko.v3i3.94

Fiedler, P., Strohmeier, D., Hunold, A., Griebel, S., Muhle, R., Schreiber, M., ... Haueisen, J. (2016, August). Modular multipin electrodes for comfortable dry eeg. In *Engineering in medicine and biology society (embc), 2016 ieee 38th annual international conference of the* (pp. 5705–5708). IEEE. doi: 10.1109/embc.2016.7592022

Formaggio, E., Storti, S. F., Galazzo, I. B., Gandolfi, M., Geroin, C., Smania, N., ... Manganotti, P. (2013). Modulation of event-related desynchronization in robot-assisted hand performance: brain oscillatory changes in active, passive and imagined movements. *Journal of neuroengineering and rehabilitation*, *10*(1), 24. doi: 10.1186/1743-0003-10-24

Fox, J. & Weisberg, S. (2011). *An R companion to applied regression* (Second ed.). Thousand Oaks CA: Sage. Retrieved from `http://socserv.socsci.mcmaster.ca/jfox/Books/Companion`

Friedman, J. H. (1991). Multivariate adaptive regression splines. *The annals of statistics*, *19*(1), 1–67. doi: 10.1214/aos/1176347963

Gabard-Durnam, L. J., Leal, A. S. M., Wilkinson, C. L. & Levin, A. R. (2018). The harvard automated processing pipeline for electroencephalography (happe): Standardized processing software for developmental and high-artifact data. *Frontiers in neuroscience*, *12*, 97. doi: 10.3389/fnins.2018.00097

Garrett, D., Peterson, D. A., Anderson, C. W. & Thaut, M. H. (2003). Comparison of linear, nonlinear, and feature selection methods for eeg signal classification. *IEEE Transactions on neural systems and rehabilitation engineering*, *11*(2), 141–144. doi: 10.1109/tnsre.2003.814441

Geddes, L. A. & Baker, L. E. (1977). *Principles of applied biomedical instrumentation* (Vol. 2). John Wiley & Sons. doi: 10.1097/00004669-197701000-00020

Gilli, M. (2004, September). An introduction to optimization heuristics. In *Seminar university of cyprus department of public and business administration.* Retrieved from `http://www.unige.ch/ses/dsec/static/gilli/CyprusLecture2004.pdf`

Gomez, C., Oller, J. & Paradells, J. (2012). Overview and evaluation of bluetooth low energy: An emerging low-power wireless technology. *Sensors*, *12*(9), 11734–11753. doi: 10.3390/s120911734

Gorelick, P. B. (2019). The global burden of stroke: Persistent and disabling. *The Lancet Neurology*, *18*(5), 417–418.

Gu, Y., Dremstrup, K. & Farina, D. (2009). Single-trial discrimination of type and speed of wrist movements from eeg recordings. *Clinical Neurophysiology*, *120*(8), 1596–1600. doi: 10.1016/j.clinph.2009.05.006

Guerrero, F. N. & Spinelli, E. M. (2018). A two-wired ultra-high input impedance active electrode. *IEEE transactions on biomedical circuits and systems*, *12*(2), 437–445. doi: 10.1109/tbcas.2018.2796581

Guerrero, J. A. & Macías-Díaz, J. E. (2014). A computational method for the detection of activation/deactivation patterns in biological signals with three levels of electric intensity. *Mathematical biosciences*, *248*, 117–127. doi: 10.1016/j.mbs.2013.12.010

Hallett, M. (1994). Movement-related cortical potentials. *Electromyography and clinical neurophysiology*, *34*(1), 5–13. Retrieved from `https://www.ncbi.nlm.nih.gov/pubmed/8168458`

Hamano, T., Lüders, H. O., Ikeda, A., Collura, T. F., Comair, Y. G. & Shibasaki, H. (1997). The cortical generators of the contingent negative variation in humans: a study with subdural electrodes. *Electroencephalography and Clinical Neurophysiology/Evoked Potentials Section*, *104*(3), 257–268. doi: 10.1016/s0168-5597(97)96107-4

Hara, Y. (2015). Brain plasticity and rehabilitation in stroke patients. *Journal of Nippon Medical School*, *82*(1), 4–13. doi: 10.1272/jnms.82.4

Hara, Y., Obayashi, S., Tsujiuchi, K. & Muraoka, Y. (2013). The effects of electromyography-controlled functional electrical stimulation on upper extremity function and cortical perfusion in stroke patients. *Clinical Neurophysiology*, *124*(10), 2008–2015. doi: 10.1016/j.clinph.2013.03.030

Hendricks, H. T., van Limbeek, J., Geurts, A. C. & Zwarts, M. J. (2002). Motor recovery after stroke: A systematic review of the literature. *Archives of physical medicine and rehabilitation*, *83*(11), 1629–1637. doi: 10.1053/apmr.2002.35473

Hermens, H. J., Freriks, B., Disselhorst-Klug, C. & Rau, G. (2000). Development of recommendations for semg sensors and sensor placement procedures. *Journal of electromyography and Kinesiology*, *10*(5), 361–374. doi: 10.1016/s1050-6411(00)00027-4

Hodges, P. W. & Bui, B. H. (1996). A comparison of computer-based methods for the determination of onset of muscle contraction using electromyography. *Electroencephalography and Clinical Neurophysiology/Electromyography and Motor Control*, *101*(6), 511–519. doi: 10.1016/s0921-884x(96)95190-5

Hodges, P. W., Moseley, G. L., Gabrielsson, A. & Gandevia, S. C. (2003). Experimental muscle pain changes feedforward postural responses of the trunk muscles. *Experimental Brain Research*, *151*(2), 262–271. doi: 10.1007/s00221-003-1457-x

Hogg, R. V. & Ledolter, J. (1987). *Engineering statistics*. Macmillan Pub Co.

Hogrel, J.-Y. (2005). Clinical applications of surface electromyography in neuromuscular disorders. *Neurophysiologie Clinique/Clinical Neurophysiology*, *35*(2-3), 59–71. doi: 10.1016/j.neucli.2005.03.001

Hollander, M., Wolfe, D. A. & Chicken, E. (2015). *Nonparametric statistical methods* (Vol. 751). John Wiley & Sons. doi: 10.1002/9781119196037

Holz, E. M., Höhne, J., Staiger-Sälzer, P., Tangermann, M. & Kübler, A. (2013). Brain–computer interface controlled gaming: Evaluation of usability by severely motor restricted end-users. *Artificial intelligence in medicine*, *59*(2), 111–120. doi: 10.1016/j.artmed.2013.08.001

Ichiro, N., Schunichi, O., Hiroiku, O. & Masafumi, Y. (2012). Movement-related cortical potentials associated with oral and facial functions in humans. In *Applications of emg in clinical and sports medicine.* InTech. doi: 10.5772/25860

Ikeda, A., Shibasaki, H., Kaji, R., Terada, K., Nagamine, T., Honda, M. & Kimura, J. (1997). Dissociation between contingent negative variation (cnv) and bereitschaft-spotential (bp) in patients with parkinsonism. *Electroencephalography and clinical neurophysiology*, *102*(2), 142–151. doi: 10.1016/s0921-884x(96)95067-5

Instruments, T. (2012). *Low-noise, 8-channel, 24-bit analog front-end for biopotential measurements ads1299.* Datasheet.

Ives, J. C. & Wigglesworth, J. K. (2003). Sampling rate effects on surface emg timing and amplitude measures. *Clinical Biomechanics*, *18*(6), 543–552. doi: 10.1016/s0268-0033(03)00089-5

Jankelowitz, S. & Colebatch, J. (2002, November). Movement-related potentials associated with self-paced, cued and imagined arm movements. *Experimental Brain Research*, *147*(1), 98–107. doi: 10.1007/s00221-002-1220-8

Jekabsons, G. (2016). *Areslab: Adaptive regression splines toolbox for matlab/octave.* Retrieved from `http://www.cs.rtu.lv/jekabsons/`

Jiang, N., Gizzi, L., Mrachacz-Kersting, N., Dremstrup, K. & Farina, D. (2015, January). A brain–computer interface for single-trial detection of gait initiation from movement related cortical potentials. *Clinical Neurophysiology*, *126*(1), 154–159. doi: 10.1016/j.clinph.2014.05.003

Jiang, N., Mrachacz-Kersting, N., Xu, R., Dremstrup, K. & Farina, D. (2014). An accurate, versatile, and robust brain switch for neurorehabilitation. In *Brain-computer interface research* (pp. 47–61). Springer. doi: 10.1007/978-3-319-09979-8_5

Jindal, U., Sood, M., Dutta, A. & Chowdhury, S. R. (2015). Development of point of care testing device for neurovascular coupling from simultaneous recording of eeg and nirs during anodal transcranial direct current stimulation. *IEEE journal of translational engineering in health and medicine*, *3*, 1–12. doi: 10.1109/jtehm.2015.2389230

Jochumsen, M. (2015). *Analysis of movement-related cortical potentials for brain-computer interfacing in stroke rehabilitation* (Doctoral dissertation). (Kim Dremstrup, Hovedvejleder) doi: 10.5278/vbn.phd.med.00007

Jochumsen, M., Cremoux, S., Robinault, L., Lauber, J., Arceo, J., Navid, M., ... Niazi, I. (2018). Investigation of optimal afferent feedback modality for inducing neural plasticity with a self-paced brain-computer interface. *Sensors*, *18*(11), 3761. doi: 10.3390/s18113761

Jochumsen, M., Navid, M. S., Nedergaard, R. W., Signal, N., Rashid, U., Hassan, A., ... Niazi, I. K. (2019). Self-paced online vs. cue-based offline brain–computer interfaces for inducing neural plasticity. *Brain Sciences*, *9*(6). Retrieved from `https://www.mdpi.com/2076-3425/9/6/127` doi: 10.3390/brainsci9060127

Jochumsen, M., Rovsing, C., Rovsing, H., Cremoux, S., Signal, N., Allen, K., ... Niazi, I. K. (2017, December). Quantification of movement-related eeg correlates associated with motor training: A study on movement-related cortical potentials and sensorimotor rhythms. *Frontiers in Human Neuroscience*, *11*, 604. doi: 10.3389/fnhum.2017.00604

Johnson, C. O., Nguyen, M., Roth, G. A., Nichols, E., Alam, T., Abate, D., ... others (2019). Global, regional, and national burden of stroke, 1990–2016: a systematic analysis for the global burden of disease study 2016. *The Lancet Neurology*, *18*(5), 439–458.

Jubany, J. & Angulo-Barroso, R. (2016, April). An algorithm for detecting emg onset/offset in trunk muscles during a reaction- stabilization test. *Journal of Back and Musculoskeletal Rehabilitation*, *29*(2), 219–230. doi: 10.3233/BMR-150617

Jukiewicz, M. & Cysewska-Sobusiak, A. (2016). Stimuli design for ssvep-based brain computer-interface. *International Journal of Electronics and Telecommunications*, *62*(2), 109–113. doi: 10.1515/eletel-2016-0014

Kamavuako, E. N., Jochumsen, M., Niazi, I. K. & Dremstrup, K. (2015). Comparison of features for movement prediction from single-trial movement-related cortical potentials in healthy subjects and stroke patients. *Computational Intelligence and Neuroscience*, *2015*, 1–8. doi: 10.1155/2015/858015

Kaongoen, N. & Jo, S. (2017). A novel hybrid auditory bci paradigm combining assr and p300. *Journal of neuroscience methods*, *279*, 44–51. doi: 10.1016/j.jneumeth.2017.01.011

Kaongoen, N., Yu, M. & Jo, S. (2017). Two-factor authentication system using p300 response to a sequence of human photographs. *IEEE Transactions on Systems, Man, and Cybernetics: Systems*, 1–8. doi: 10.1109/tsmc.2017.2756673

Karimi, F., Kofman, J., Mrachacz-Kersting, N., Farina, D. & Jiang, N. (2017). Detection of movement related cortical potentials from eeg using constrained ica for brain-computer interface applications. *Frontiers in neuroscience*, *11*, 356. doi: 10.3389/fnins.2017.00356

Kawakami, M., Fujiwara, T., Ushiba, J., Nishimoto, A., Abe, K., Honaga, K., ... Liu, M. (2016). A new therapeutic application of brain-machine interface (bmi) training followed by hybrid assistive neuromuscular dynamic stimulation (hands) therapy for patients with severe hemiparetic stroke: A proof of concept study. *Restorative neurology and neuroscience*, *34*(5), 789–797. doi: 10.3233/rnn-160652

Killick, R., Fearnhead, P. & Eckley, I. A. (2012). Optimal detection of changepoints with a linear computational cost. *Journal of the American Statistical Association*, *107*(500), 1590–1598. doi: 10.1080/01621459.2012.737745

Kim, K., Kim, J. S. & Chung, C. K. (2017). Increased gamma connectivity in the human prefrontal cortex during the bereitschaftspotential. *Frontiers in human neuroscience*, *11*, 180. doi: 10.3389/fnhum.2017.00180

Kita, Y., Mori, A. & Nara, M. (2001). Two types of movement-related cortical potentials preceding wrist extension in humans. *Neuroreport*, *12*(10), 2221–2225. doi: 10.1097/00001756-200107200-00035

Kleim, J. A. & Jones, T. A. (2008). Principles of experience-dependent neural plasticity: Implications for rehabilitation after brain damage. *Journal of speech, language, and hearing research*, *51*(1), S225–S239. doi: 10.1044/1092-4388(2008/018)

Knotkova, H. & Rasche, D. (Eds.). (2015). *Textbook of neuromodulation*. Springer New York. doi: 10.1007/978-1-4939-1408-1

Kornhuber, H. H. & Deecke, L. (1965). Hirnpotentialnderungen bei willkrbewegungen und passiven bewegungen des menschen: Bereitschaftspotential und reafferente potentiale. *Pflgers Archiv fr die Gesamte Physiologie des Menschen und der Tiere*, *284*(1), 1–17. doi: 10.1007/bf00412364

Krachunov, S. & Casson, A. (2016). 3d printed dry eeg electrodes. *Sensors*, *16*(10), 1635. doi: 10.3390/s16101635

Krames, E. S., Peckham, P. H., Rezai, A. & Aboelsaad, F. (2009). What is neuromodulation? In *Neuromodulation* (pp. 3–8). Elsevier. doi: 10.1016/b978-0-12-374248-3.00002-1

Kranczioch, C., Zich, C., Schierholz, I. & Sterr, A. (2014). Mobile eeg and its potential to promote the theory and application of imagery-based motor rehabilitation. *International Journal of Psychophysiology*, *91*(1), 10–15. doi: 10.1016/j.ijpsycho.2013.10.004

Krol, L. R., Pawlitzki, J., Lotte, F., Gramann, K. & Zander, T. O. (2018). Sereega: Simulating event-related eeg activity. *Journal of Neuroscience Methods*, *309*, 13–24. Retrieved from `http://www.sciencedirect.com/science/article/pii/S0165027018302395` doi: 10.1016/j.jneumeth.2018.08.001

Kübler, A., Holz, E. M., Riccio, A., Zickler, C., Kaufmann, T., Kleih, S. C., ... Mattia, D. (2014). The user-centered design as novel perspective for evaluating the usability of bci-controlled applications. *PLoS One*, *9*(12), e112392. doi: 10.1371/journal.pone.0112392

Lakens, D. (2013). Calculating and reporting effect sizes to facilitate cumulative science: a practical primer for t-tests and anovas. *Frontiers in psychology*, *4*, 863. doi: 10.3389/fpsyg.2013.00863

Lalor, E. C., Kelly, S. P., Finucane, C., Burke, R., Smith, R., Reilly, R. B. & McDarby, G. (2005). Steady-state vep-based brain-computer interface control in an immersive 3d gaming environment. *EURASIP Journal on Advances in Signal Processing*, *2005*(19), 706906. doi: 10.1155/asp.2005.3156

Lang, Lohse & Birkenmeier. (2015, December). Dose and timing in neurorehabilitation. *Current Opinion in Neurology*, *28*(6), 549–555. doi: 10.1097/wco.0000000000000256

Lang, W., Lang, M., Kornhuber, A., Deecke, L. & Kornhuber, H. H. (1983). Human cerebral potentials and visuomotor learning. *Pflügers Archiv*, *399*(4), 342–344. doi: 10.1007/bf00652762

Langan, J., Subryan, H., Nwogu, I. & Cavuoto, L. (2017, August). Reported use of technology in stroke rehabilitation by physical and occupational therapists. *Disability and Rehabilitation: Assistive Technology*, *13*(7), 641–647. doi: 10.1080/17483107.2017.1362043

Larivière, C., Forget, R., Vadeboncoeur, R., Bilodeau, M. & Mecheri, H. (2010, February). The effect of sex and chronic low back pain on back muscle reflex responses. *European Journal of Applied Physiology*, *109*(4), 577–590. doi: 10.1007/s00421-010-1389-7

Lavielle, M. (2005). Using penalized contrasts for the change-point problem. *Signal processing*, *85*(8), 1501–1510. doi: 10.1016/j.sigpro.2005.01.012

Lenth, R. V. (2016). Least-squares means: The R package lsmeans. *Journal of Statistical Software*, *69*(1), 1–33. doi: 10.18637/jss.v069.i01

Lew, E. (2012). Detection of self-paced reaching movement intention from eeg signals. *Frontiers in neuroengineering*, *5*, 13. doi: 10.3389/fneng.2012.00013

Lewis, P. M., Thomson, R. H., Rosenfeld, J. V. & Fitzgerald, P. B. (2016). Brain neuromodulation techniques. *The neuroscientist*, *22*(4), 406–421. doi: 10.1177/1073858416646707

Lin, C., Wang, B.-H., Jiang, N., Xu, R., Mrachacz-Kersting, N. & Farina, D. (2016). Discriminative manifold learning based detection of movement-related cortical potentials. *IEEE Trans. Neural Syst. Rehabilit. Eng*, *24*, 921–927. doi: 10.1109/tnsre.2016.2531118

Liu, L., Liu, W., Cartes, D. A. & Zhang, N. (2008). Real time implementation of particle swarm optimiation based model parameter identification and an application example. In *Evolutionary computation, 2008. cec 2008.(ieee world congress on computational intelligence). ieee congress on* (pp. 3480–3485). doi: 10.1109/cec.2008.4631268

Lopez-Gordo, M., Sanchez-Morillo, D. & Valle, F. (2014, July). Dry eeg electrodes. *Sensors*, *14*(7), 12847–12870. doi: 10.3390/s140712847

López-Larraz, E., Sarasola-Sanz, A., Irastorza-Landa, N., Birbaumer, N. & Ramos-Murguialday, A. (2018). Brain-machine interfaces for rehabilitation in stroke: A review. *NeuroRehabilitation*, *43*(1), 77–97. doi: 10.3233/nre-172394

Lotte, F., Bougrain, L., Cichocki, A., Clerc, M., Congedo, M., Rakotomamonjy, A. & Yger, F. (2018). A review of classification algorithms for eeg-based brain–computer interfaces: a 10 year update. *Journal of neural engineering*, *15*(3), 031005. doi: 10.1088/1741-2552/aab2f2

Lotte, F., Congedo, M., Lécuyer, A., Lamarche, F. & Arnaldi, B. (2007). A review of classification algorithms for eeg-based brain–computer interfaces. *Journal of neural engineering*, *4*(2), R1-R13. doi: 10.1088/1741-2560/4/2/r01

Lu, M.-K., Arai, N., Tsai, C.-H. & Ziemann, U. (2011, March). Movement related cortical potentials of cued versus self-initiated movements: Double dissociated modulation by dorsal premotor cortex versus supplementary motor area rTMS. *Human Brain Mapping*, *33*(4), 824–839. doi: 10.1002/hbm.21248

Lu, N., Zhou, J., He, Y. & Liu, Y. (2009). Particle swarm optimization for parameter optimization of support vector machine model. In *Intelligent computation technology and automation, 2009. icicta'09. second international conference on* (Vol. 1, pp. 283–286). doi: 10.1109/icicta.2009.76

Luan, S., Williams, I., Nikolic, K. & Constandinou, T. G. (2014). Neuromodulation: present and emerging methods. *Frontiers in neuroengineering*, *7*, 27.

Luca, C. J. D. (1997). The use of surface electromyography in biomechanics. *Journal of applied biomechanics*, *13*(2), 135–163. doi: 10.1123/jab.13.2.135

Luck, S. J. (2014). *An introduction to the event-related potential technique* (Vol. 2). MIT press.

Magda, M. (n.d.). *Emg onset detection–development and comparison of algorithms* (mathesis, Faculty of Computing, Blekinge Institute of Technology, SE-371 79 Karlskrona, Sweden). Retrieved from https://www.diva-portal.org/smash/get/diva2:840646/FULLTEXT02.pdf

Makeig, S., Bell, A. J., Jung, T.-P. & Sejnowski, T. J. (1996). Independent component analysis of electroencephalographic data. In *Advances in neural information processing systems*. Retrieved from https://dl.acm.org/citation.cfm?id=2998849

Marini, F. & Walczak, B. (2015). Particle swarm optimization (pso). a tutorial. *Chemometrics and Intelligent Laboratory Systems*, *149*, 153–165. doi: 10.1016/j.chemolab.2015.08.020

Maskeliunas, R., Damasevicius, R., Martisius, I. & Vasiljevas, M. (2016). Consumer grade eeg devices: are they usable for control tasks? *PeerJ*, *4*, e1746. doi: 10.7717/peerj.1746

Massó, N., Rey, F., Romero, D., Gual, G., Costa, L. & Germán, A. (2010). Surface electromyography applications. *Apunts Medicina de l" Esport (English Edition)*, *45*(165), 121–130.

McCrimmon, C. M., Fu, J. L., Wang, M., Lopes, L. S., Wang, P. T., Karimi-Bidhendi, A., ... Do, A. H. (2017). Performance assessment of a custom, portable, and low-cost brain–computer interface platform. *IEEE Transactions on Biomedical Engineering*, *64*(10), 2313–2320. doi: 10.1109/tbme.2017.2667579

McCrimmon, C. M., Wang, M., Lopes, L. S., Wang, P. T., Karimi-Bidhendi, A., Liu, C. Y., ... Do, A. H. (2016). A small, portable, battery-powered brain-computer interface system for motor rehabilitation. In *Engineering in medicine and biology society (embc), 2016 ieee 38th annual international conference of the* (pp. 2776–2779). doi: 10.1109/embc.2016.7591306

McFarland, D. J., McCane, L. M., David, S. V. & Wolpaw, J. R. (1997). Spatial filter selection for eeg-based communication. *Electroencephalography and clinical Neurophysiology*, *103*(3), 386–394. doi: 10.1016/s0013-4694(97)00022-2

McLaren, R., Signal, N., Lord, S., Taylor, S., Henderson, J. & Taylor, D. (2019). The volume and timing of upper limb movement in acute stroke rehabilitation: still room for improvement. *Disability and Rehabilitation*, 1–6. doi: 10.1080/09638288.2019.1590471

Merlo, A., Farina, D. & Merletti, R. (2003). A fast and reliable technique for muscle activity detection from surface emg signals. *IEEE Transactions on Biomedical Engineering*, *50*(3), 316–323. doi: 10.1109/tbme.2003.808829

Mihajlovic, V., Patki, S. & Grundlehner, B. (2014). The impact of head movements on eeg and contact impedance: An adaptive filtering solution for motion artifact reduction. In *Engineering in medicine and biology society (embc), 2014 36th annual international conference of the ieee* (pp. 5064–5067). doi: 10.1109/embc.2014.6944763

Miller, J., Patterson, T. & Ulrich, R. (1998, January). Jackknife-based method for measuring LRP onset latency differences. *Psychophysiology*, *35*(1), 99–115. doi: 10.1111/1469-8986.3510099

Ministry of Health. (2009). *Report on new zealand cost-of-illness studies on long-term conditions* (Tech. Rep.). Retrieved from https://www.health.govt.nz/publication/report-new-zealand-cost-illness-studies-long-term-conditions

Mora, N., Munari, I. D., Ciampolini, P. & del R. Millán, J. (2016, November). Plug&play brain–computer interfaces for effective active and assisted living control. *Medical & Biological Engineering & Computing*, *55*(8), 1339–1352. doi: 10.1007/s11517-016-1596-4

Mordkoff, J. T. & Gianaros, P. J. (2000). Detecting the onset of the lateralized readiness potential: A comparison of available methods and procedures. *Psychophysiology*, *37*(3), 347–360. doi: 10.1111/1469-8986.3730347

Morone, G., Paolucci, S., Cherubini, A., Angelis, D. D., Venturiero, V., Coiro, P. & Iosa, M. (2017). Robot-assisted gait training for stroke patients: current state of the art and perspectives of robotics. *Neuropsychiatric disease and treatment*, *Volume 13*, 1303–1311. doi: 10.2147/ndt.s114102

Moseley, G. L., Hodges, P. W. & Gandevia, S. C. (2003). External perturbation of the trunk in standing humans differentially activates components of the medial back muscles. *The Journal of physiology*, *547*(2), 581–587. doi: 10.1113/jphysiol.2002.024950

Mrachacz-Kersting, N. & Aliakbaryhosseinabadi, S. (2018). Comparison of the efficacy of a real-time and offline associative brain-computer-interface. *Frontiers in neuroscience*, *12*, 455. doi: 10.3389/fnins.2018.00455

Mrachacz-Kersting, N., Jiang, N., Stevenson, A. J. T., Niazi, I. K., Kostic, V., Pavlovic, A., ... Farina, D. (2016). Efficient neuroplasticity induction in chronic stroke patients by an associative brain-computer interface. *American Journal of Physiology-Heart and Circulatory Physiology*, *115*(3), 1410–1421. doi: 10.1152/jn.00918.2015

Mrachacz-Kersting, N., Kristensen, S. R., Niazi, I. K. & Farina, D. (2012). Precise temporal association between cortical potentials evoked by motor imagination and afference induces cortical plasticity. *The Journal of physiology*, *590*(7), 1669–1682. doi: 10.1113/jphysiol.2011.222851

Mrachacz-Kersting, N., Stevenson, A. J. T., Jørgensen, H. R. M., Severinsen, K. E., Aliakbaryhosseinabadi, S., Jiang, N. & Farina, D. (2019). Brain state-dependent stimulation boosts functional recovery following stroke. *Annals of Neurology*, *85*(1), 84–95. doi: 10.1002/ana.25375

Nascimento, O. F. D., Nielsen, K. D. & Voigt, M. (2004, July). Relationship between plantar-flexor torque generation and the magnitude of the movement-related potentials. *Experimental Brain Research*, *160*(2), 154–165. doi: 10.1007/s00221-004-1996-9

Nathan, V. & Jafari, R. (2015). Design principles and dynamic front end reconfiguration for low noise eeg acquisition with finger based dry electrodes. *IEEE transactions on biomedical circuits and systems*, *9*(5), 631–640. doi: 10.1109/tbcas.2015.2471080

Niazi, I. K., Jiang, N., Tiberghien, O., Nielsen, J. F., Dremstrup, K. & Farina, D. (2011). Detection of movement intention from single-trial movement-related cortical potentials. *Journal of neural engineering*, *8*(6), 066009. doi: 10.1088/1741-2560/8/6/066009

Niazi, I. K., Mrachacz-Kersting, N., Jiang, N., Dremstrup, K. & Farina, D. (2012). Peripheral electrical stimulation triggered by self-paced detection of motor intention enhances motor evoked potentials. *IEEE transactions on neural systems and rehabilitation engineering*, *20*(4), 595–604. doi: 10.1109/tnsre.2012.2194309

Niedermeyer, E. & da Silva, F. H. L. (2005). *Electroencephalography: basic principles, clinical applications, and related fields*. Lippincott Williams & Wilkins.

Niemann, J., Winker, T., Gerling, J., Landwehrmeyer, B. & Jung, R. (1991). Changes of slow cortical negative dc-potentials during the acquisition of a complex finger motor task. *Experimental brain research*, *85*(2), 417–422. doi: 10.1007/bf00229418

Nunez, P. L. & Srinivasan, R. (2006). *Electric fields of the brain*. Oxford University Press. doi: 10.1093/acprof:oso/9780195050387.001.0001

Oishi, M., Mochizuki, Y., Du, C. & Takasu, T. (1995). Contingent negative variation and movement-related cortical potentials in parkinsonism. *Electroencephalography and clinical Neurophysiology*, *95*(5), 346–349. doi: 10.1016/0013-4694(95)00084-c

Ojeda, A., Klug, M., Kreutz-Delgado, K., Gramann, K. & Mishra, J. (2019). A bayesian framework for unifying data cleaning, source separation and imaging of electroencephalographic signals. *bioRxiv*, 559450. doi: 10.1101/559450

Oliveira, A. S., Schlink, B. R., Hairston, W. D., König, P. & Ferris, D. P. (2016, May). Proposing metrics for benchmarking novel eeg technologies towards real-world measurements. *Frontiers in human neuroscience*, *10*, 188. doi: 10.3389/fnhum.2016.00188

Olsen, S., Signal, N., Niazi, I. K., Christensen, T., Jochumsen, M. & Taylor, D. (2017, June). Paired associative stimulation delivered by pairing movement-related cortical potentials with peripheral electrical stimulation: An investigation of the duration of neuromodulatory effects. *Neuromodulation: Technology at the Neural Interface*, *21*(4), 362–367. doi: 10.1111/ner.12616

O'Regan, S., Faul, S. & Marnane, W. (2013). Automatic detection of eeg artefacts arising from head movements using eeg and gyroscope signals. *Medical engineering and Physics*, *35*(7), 867–874. doi: 10.1016/j.medengphy.2012.08.017

Parsopoulos, K. & Vrahatis, M. (2002). Recent approaches to global optimization problems through particle swarm optimization. *Natural Computing*, *1*(2-3), 235–306. doi: 10.1023/a:1016568309421

Pashaei, A., Yazdchi, M. R. & Marateb, H. R. (2015). Designing a low-noise, high-resolution, and portable four channel acquisition system for recording surface electromyographic signal. *Journal of medical signals and sensors*, *5*(4), 245–252.

Pasqualotto, E., Federici, S. & Belardinelli, M. O. (2012). Toward functioning and usable brain–computer interfaces (bcis): A literature review. *Int J Bioelectromagn*, *7*, 121–122. doi: 10.3109/17483107.2011.589486

Patil, A. L., Sood, S. K., Goyal, V. & Kochhar, K. P. (2017). Cortical potentials prior to movement in parkinson's disease. *Journal of clinical and diagnostic research*. doi: 10.7860/jcdr/2017/25520.9598

Pearl, J. (1984). Heuristics: intelligent search strategies for computer problem solving.

Pedrosa, P., Fiedler, P., Schinaia, L., Vasconcelos, B., Martins, A. C., Amaral, M. H., ... Fonseca, C. (2017, August). Alginate-based hydrogels as an alternative to electrolytic gels for rapid eeg monitoring and easy cleaning procedures. *Sensors and Actuators B: Chemical*, *247*, 273–283. doi: 10.1016/j.snb.2017.02.164

Qian, X., Chen, Y., Feng, Y., Ma, B., Hao, H. & Li, L. (2017). A method for removal of deep brain stimulation artifact from local field potentials. *IEEE Transactions on Neural Systems and Rehabilitation Engineering*, *25*(12), 2217–2226. doi: 10.1109/tnsre.2016.2613412

Radüntz, T. (2018). Signal quality evaluation of emerging eeg devices. *Frontiers in physiology*, *9*, 98. doi: 10.3389/fphys.2018.00098

Rakitianskaia, A. & Engelbrecht, A. (2014). Weight regularisation in particle swarm optimisation neural network training. In *Swarm intelligence (sis), 2014 ieee symposium on* (pp. 1–8). doi: 10.1109/sis.2014.7011773

Ramos-Murguialday, A. & Birbaumer, N. (2015). Brain oscillatory signatures of motor tasks. *Journal of neurophysiology*, *113*(10), 3663–3682. doi: 10.1152/jn.00467.2013

Ramos-Murguialday, A., Schürholz, M., Caggiano, V., Wildgruber, M., Caria, A., Hammer, E. M., ... Birbaumer, N. (2012). Proprioceptive feedback and brain computer interface (bci) based neuroprostheses. *PloS one*, *7*(10), e47048. doi: 10.1371/journal.pone.0047048

Rashid, U., Niazi, I. K., Jochumsen, M., Krol, L. R., Signal, N. & Taylor, D. (2019). Automated labelling of movement-related cortical potentials using segmented regression. *IEEE Transactions on Neural Systems and Rehabilitation Engineering*, 1–1. doi: 10.1109/tnsre.2019.2913880

Rashid, U., Niazi, I. K., Signal, N. & Taylor, D. (2018). An eeg experimental study evaluating the performance of texas instruments ads1299. *Sensors*, *18*, 3721. doi: 10.3390/s18113721

Reaz, M. B. I., Hussain, M. S. & Mohd-Yasin, F. (2006). Techniques of emg signal analysis: detection, processing, classification and applications. *Biological procedures online*, *8*(1), 11–35. doi: 10.1251/bpo115

Rebolledo-Mendez, G., Dunwell, I., Martínez-Mirón, E. A., Vargas-Cerdán, M. D., de Freitas, S., Liarokapis, F. & García-Gaona, A. R. (2009). Assessing neurosky's usability to detect attention levels in an assessment exercise. In *International conference on human-computer interaction* (pp. 149–158). doi: 10.1007/978-3-642-02574-7_17

Reinkensmeyer, D. J., Emken, J. L. & Cramer, S. C. (2004). Robotics, motor learning, and neurologic recovery. *Annu. Rev. Biomed. Eng.*, *6*, 497–525. doi: 10.1146/annurev.bioeng.6.040803.140223

Ries, A. J., Touryan, J., Vettel, J., McDowell, K. & Hairston, W. D. (2014, February). A comparison of electroencephalography signals acquired from conventional and mobile systems. *Journal of Neuroscience and Neuroengineering*, *3*(1), 10–20. doi: 10.1166/jnsne.2014.1092

Rios, L. M. & Sahinidis, N. V. (2012, July). Derivative-free optimization: a review of algorithms and comparison of software implementations. *Journal of Global Optimization*, *56*(3), 1247–1293. doi: 10.1007/s10898-012-9951-y

Robichaud, J. A., Pfann, K. D., Leurgans, S., Vaillancourt, D. E., Comella, C. L. & Corcos, D. M. (2009). Variability of emg patterns: A potential neurophysiological marker of parkinson's disease? *Clinical neurophysiology*, *120*(2), 390–397. doi: 10.1016/j.clinph.2008.10.015

Rohrbaugh, J., Syndulko, K. & Lindsley, D. (1976). Brain wave components of the contingent negative variation in humans. *Science*, *191*(4231), 1055–1057. doi: 10.1126/science.1251217

Rohrbaugh, J. W. & Gaillard, A. W. K. (1983). Sensory and motor aspects of the contingent negative variation. , *10*, 269–310. doi: 10.1016/s0166-4115(08)62044-0

Rossi, S., Hallett, M., Rossini, P. M. & Pascual-Leone, A. (2009). Safety, ethical considerations, and application guidelines for the use of transcranial magnetic stimulation in clinical practice and research. *Clinical neurophysiology*, *120*(12), 2008–2039. doi: 10.1016/j.clinph.2009.08.016

Ruder, S. (2016, September). An overview of gradient descent optimization algorithms. *arXiv e-prints*. Retrieved from `https://ui.adsabs.harvard.edu/abs/2016arXiv160904747R`

Sakamoto, K., Nakata, H., Honda, Y. & Kakigi, R. (2009). The effect of mastication on human motor preparation processing: A study with cnv and mrcp. *Neuroscience research*, *64*(3), 259–266. doi: 10.1016/j.neures.2009.03.008

Sburlea, A. I., Montesano, L., de la Cuerda, R. C., Diego, I. M. A., Miangolarra-Page, J. C. & Minguez, J. (2015). Detecting intention to walk in stroke patients from pre-movement eeg correlates. *Journal of neuroengineering and rehabilitation*, *12*(1), 113. doi: 10.1186/s12984-015-0087-4

Schwarzenau, P., Falkenstein, M., Hoormann, J. & Hohnsbein, J. (1998). A new method for the estimation of the onset of the lateralized readiness potential (lrp). *Behavior Research Methods, Instruments, & Computers*, *30*(1), 110–117. doi: 10.3758/bf03209421

Schweizer, T. A. & Macdonald, R. L. (2014). *The behavioral consequences of stroke*. Springer.

Selvakumar, A. I. & Thanushkodi, K. (2007, February). A new particle swarm optimization solution to nonconvex economic dispatch problems. *IEEE Transactions on Power Systems*, *22*(1), 42–51. Retrieved from `http://adsabs.harvard.edu/abs/2007ITPSy..22...42S` doi: 10.1109/tpwrs.2006.889132

Shakeel, A., Navid, M. S., Anwar, M. N., Mazhar, S., Jochumsen, M. & Niazi, I. K. (2015). A review of techniques for detection of movement intention using movement-related cortical potentials. *Computational and mathematical methods in medicine*, *2015*, 1–13. doi: 10.1155/2015/346217

Shibasaki, H., Barrett, G., Halliday, E. & Halliday, A. M. (1981). Cortical potentials associated with voluntary foot movement in man. *Clinical Neurophysiology*, *52*(6), 507–516. doi: 10.1016/0013-4694(81)91426-7

Shibasaki, H. & Hallett, M. (2006). What is the bereitschaftspotential? *Clinical neurophysiology*, *117*(11), 2341–2356. doi: 10.1016/j.clinph.2006.04.025

Shumway-Cook, A. & Woollacott, M. H. (2007). *Motor control: translating research into clinical practice*. Lippincott Williams & Wilkins.

Signal, N. E. J., Scott, K., Taylor, D. & Kayes, N. M. (2019). What helps or hinders the uptake of new technologies into rehabilitation practice? In *International conference on neurorehabilitation* (pp. 265–268). doi: 10.1007/978-3-030-01845-0_53

Simpson, S. L., Lyday, R. G., Hayasaka, S., Marsh, A. P. & Laurienti, P. J. (2013). A permutation testing framework to compare groups of brain networks. *Frontiers in computational neuroscience*, *7*, 171. doi: 10.3389/fncom.2013.00171

Smulders, F. T. Y. (2010). Simplifying jackknifing of erps and getting more out of it: Retrieving estimates of participants' latencies. *Psychophysiology*, *47*(2), 387–392. doi: 10.1111/j.1469-8986.2009.00934.x

Solnik, S., Rider, P., Steinweg, K., DeVita, P. & Hortobágyi, T. (2010). Teager–kaiser energy operator signal conditioning improves emg onset detection. *European journal of applied physiology*, *110*(3), 489–498. doi: 10.1007/s00421-010-1521-8

Solodkin, A., Hlustik, P. & Buccino, G. (2007). Handbook of psychophysiology. In (pp. 507–539). Cambridge University Press. Retrieved from `https://www.cambridge.org/core/books/handbook-of-psychophysiology/anatomy-and-physiology-of-the-motor-system-in-humans/C8987071D7D6FE40F8C2A0E4D3146978`

Ssentongo, P., Robuccio, A. E., Thuku, G., Sim, D. G., Nabi, A., Bahari, F., … Schiff, S. J. (2017). A murine model to study epilepsy and sudep induced by malaria infection. *Scientific reports*, *7*, 43652. doi: 10.1038/srep43652

Staude, G., Flachenecker, C., Daumer, M. & Wolf, W. (2001). Onset detection in surface electromyographic signals: A systematic comparison of methods. *EURASIP Journal on Applied Signal Processing*, *2001*(1), 67–81. doi: 10.1155/s1110865701000191

Suppa, A., Quartarone, A., Siebner, H., Chen, R., Lazzaro, V. D., Giudice, P. D., … Classen, J. (2017). The associative brain at work: Evidence from paired associative stimulation studies in humans. *Clinical Neurophysiology*, *128*(11), 2140–2164. doi: 10.1016/j.clinph.2017.08.003

Sur, S. & Sinha, V. K. (2009). Event-related potential: An overview. *Industrial psychiatry journal*, *18*(1), 70. doi: 10.4103/0972-6748.57865

Symeonidou, E.-R., Nordin, A., Hairston, W. & Ferris, D. (2018). Effects of cable sway, electrode surface area, and electrode mass on electroencephalography signal quality during motion. *Sensors*, *18*(4), 1073. doi: 10.3390/s18041073

Tallgren, P., Vanhatalo, S., Kaila, K. & Voipio, J. (2005). Evaluation of commercially available electrodes and gels for recording of slow eeg potentials. *Clinical Neurophysiology*, *116*(4), 799–806. doi: 10.1016/j.clinph.2004.10.001

Taylor, M. J. (1978). Bereitschaftspotential during the acquisition of a skilled motor task. *Electroencephalography and clinical neurophysiology*, *45*(5), 568–576. doi: 10.1016/0013-4694(78)90157-8

Trammell, J. P., MacRae, P. G., Davis, G., Bergstedt, D. & Anderson, A. E. (2017). The relationship of cognitive performance and the theta-alpha power ratio is age-dependent: An eeg study of short term memory and reasoning during task and resting-state in healthy young and old adults. *Frontiers in aging neuroscience*, *9*, 364. doi: 10.3389/fnagi.2017.00364

Uktveris, T. & Jusas, V. (2018, July). Development of a modular board for EEG signal acquisition. *Sensors*, *18*(7), 2140. doi: 10.3390/s18072140

van Deursen, J. A., Vuurman, E. F. P. M., Smits, L. L., Verhey, F. R. J. & Riedel, W. J. (2009). Response speed, contingent negative variation and p300 in alzheimer's disease and mci. *Brain and cognition*, *69*(3), 592–599. doi: 10.1016/j.bandc.2008.12.007

Vasseljen, O., Dahl, H. H., Mork, P. J. & Torp, H. G. (2006). Muscle activity onset in the lumbar multifidus muscle recorded simultaneously by ultrasound imaging and intramuscular electromyography. *Clinical biomechanics*, *21*(9), 905–913. doi: 10.1016/j.clinbiomech.2006.05.003

Vaz, S., Falkmer, T., Passmore, A. E., Parsons, R. & Andreou, P. (2013). The case for using the repeatability coefficient when calculating test–retest reliability. *PLoS One*, *8*(9), e73990. doi: 10.1371/journal.pone.0073990

von Bernhardi, R., von Bernhardi, L. E. & Eugenín, J. (2017). What is neural plasticity? In *The plastic brain* (pp. 1–15). Springer. doi: 10.1007/978-3-319-62817-2_1

von Lühmann, A., Wabnitz, H., Sander, T. & Müller, K.-R. (2017). M3ba: A mobile, modular, multimodal biosignal acquisition architecture for miniaturized eeg-nirs-based hybrid bci and monitoring. *IEEE Transactions on Biomedical Engineering*, *64*(6), 1199–1210. doi: 10.1109/tbme.2016.2594127

Vos, M. D., Gandras, K. & Debener, S. (2014). Towards a truly mobile auditory brain–computer interface: Exploring the p300 to take away. *International journal of psychophysiology*, *91*(1), 46–53. doi: 10.1016/j.ijpsycho.2013.08.010

Walter, W. G., Cooper, R., Aldridge, V. J., Mccallum, W. C. & Winter, A. L. (1964). Contingent negative variation : An electric sign of sensori-motor association and expectancy in the human brain. *Nature*, *203*(4943), 380–384. doi: 10.1038/203380a0

Webster, J. G. (2009). *Medical instrumentation application and design*. John Wiley & Sons.

Wegener, I. (2005). *Complexity theory: exploring the limits of efficient algorithms*. Springer Science & Business Media.

Winter, B. (2013). Linear models and linear mixed effects models in r with linguistic applications. *arXiv preprint arXiv:1308.5499*. Retrieved from `https://arxiv.org/abs/1308.5499`

Winter, B. B. & Webster, J. G. (1983). Driven-right-leg circuit design. *IEEE Transactions on Biomedical Engineering*, *BME-30*(1), 62–66. doi: 10.1109/tbme.1983.325168

Wolpaw, J. R., Birbaumer, N., McFarland, D. J., Pfurtscheller, G. & Vaughan, T. M. (2002). Brain–computer interfaces for communication and control. *Clinical neurophysiology*, *113*(6), 767–791. doi: 10.1016/s1388-2457(02)00057-3

Worsley, P., Warner, M., Mottram, S., Gadola, S., Veeger, H. E. J., Hermens, H., ... Stokes, M. (2013). Motor control retraining exercises for shoulder impingement: effects on function, muscle activation, and biomechanics in young adults. *Journal of Shoulder and Elbow Surgery*, *22*(4), e11-e19. doi: 10.1016/j.jse.2012.06.010

Wright, D. J., Holmes, P., Russo, F. D., Loporto, M. & Smith, D. (2012b). Reduced motor cortex activity during movement preparation following a period of motor skill practice. *PloS one*, *7*(12), e51886. doi: 10.1371/journal.pone.0051886

Wright, D. J., Holmes, P. S., Russo, F. D., Loporto, M. & Smith, D. (2012a). Differences in cortical activity related to motor planning between experienced guitarists and non-musicians during guitar playing. *Human movement science*, *31*(3), 567–577. doi: 10.1016/j.humov.2011.07.001

Wright, D. J., Holmes, P. S. & Smith, D. (2011). Using the movement-related cortical potential to study motor skill learning. *Journal of motor behavior*, *43*(3), 193–201. doi: 10.1080/00222895.2011.557751

Xu, J., Yazicioglu, R. F., Grundlehner, B., Harpe, P., Makinwa, K. A. A. & Hoof, C. V. (2011). A $160\ \mu\mathrm{w}$ 8-channel active electrode system for eeg monitoring. *IEEE Transactions on Biomedical circuits and systems*, *5*(6), 555–567. doi: 10.1109/tbcas.2011.2170985

Xu, R., Jiang, N., Dosen, S., Lin, C., Mrachacz-Kersting, N., Dremstrup, K. & Farina, D. (2016). Endogenous sensory discrimination and selection by a fast brain switch for a high transfer rate brain-computer interface. *IEEE Transactions on Neural Systems and Rehabilitation Engineering*, *24*(8), 901–910. doi: 10.1109/tnsre.2016.2523565

Yang, D., Zhang, H., Gu, Y. & Liu, H. (2017, March). Accurate emg onset detection in pathological, weak and noisy myoelectric signals. *Biomedical Signal Processing and Control*, *33*, 306–315. doi: 10.1016/j.bspc.2016.12.014

Yao, L., Sheng, X., Mrachacz-Kersting, N., Zhu, X., Farina, D. & Jiang, N. (2018). Performance of brain–computer interfacing based on tactile selective sensation and motor imagery. *IEEE Transactions on Neural Systems and Rehabilitation Engineering*, *26*(1), 60–68. doi: 10.1109/tnsre.2017.2769686

Zander, T. O., Krol, L. R., Birbaumer, N. P. & Gramann, K. (2016). Neuroadaptive technology enables implicit cursor control based on medial prefrontal cortex activity. *Proceedings of the National Academy of Sciences*, *113*(52), 14898–14903. doi: 10.1073/pnas.1605155114

Zhang, Y., Wang, S. & Ji, G. (2015). A comprehensive survey on particle swarm optimization algorithm and its applications. *Mathematical Problems in Engineering*, *2015*, 1–38. doi: 10.1155/2015/931256

Zhao, X., Zhao, D., Wang, X. & Hou, X. (2017). A ssvep stimuli encoding method using trinary frequency-shift keying encoded ssvep (tfsk-ssvep). *Frontiers in human neuroscience*, *11*, 278. doi: 10.3389/fnhum.2017.00278

Zickler, C., Halder, S., Kleih, S. C., Herbert, C. & Kübler, A. (2013). Brain painting: Usability testing according to the user-centered design in end users with severe motor paralysis. *Artificial intelligence in medicine*, *59*(2), 99–110. doi: 10.1016/j.artmed.2013.08.003

Zou, Y., Nathan, V. & Jafari, R. (2016). Automatic identification of artifact-related independent components for artifact removal in eeg recordings. *IEEE journal of biomedical and health informatics*, *20*(1), 73–81. doi: 10.1109/jbhi.2014.2370646

Appendix A

Ethics Documents

Ethics approval letter from Health and Disability Ethics Committees (HDEC), the participant information sheet and the consent form are pasted on the following pages.

A.1 Ethics Approval Letter

Health and Disability Ethics Committees
Ministry of Health
133 Molesworth Street
PO Box 5013
Wellington
6011

0800 4 ETHICS
hdecs@moh.govt.nz

02 August 2017

Mr. Usman Rashid
23 Akoranga Drive
NorthShore 0627

Dear Mr. Rashid

Re:	**Ethics ref:**	**17/CEN/133**
	Study title:	Using Electroencephalography data for Brain Computer Interfaces in Physical Rehabilitation.

I am pleased to advise that this application has been *approved* by the Central Health and Disability Ethics Committee. This decision was made through the HDEC-Expedited Review pathway.

Conditions of HDEC approval

HDEC approval for this study is subject to the following conditions being met prior to the commencement of the study in New Zealand. It is your responsibility, and that of the study's sponsor, to ensure that these conditions are met. No further review by the Central Health and Disability Ethics Committee is required.

Standard conditions:

1. Before the study commences at *any* locality in New Zealand, all relevant regulatory approvals must be obtained.

2. Before the study commences at *a given* locality in New Zealand, it must be authorised by that locality in Online Forms. Locality authorisation confirms that the locality is suitable for the safe and effective conduct of the study, and that local research governance issues have been addressed.

After HDEC review

Please refer to the *Standard Operating Procedures for Health and Disability Ethics Committees* (available on www.ethics.health.govt.nz) for HDEC requirements relating to amendments and other post-approval processes.

Your **next progress report** is due by **01 August 2018.**

Participant access to ACC

The Central Health and Disability Ethics Committee is satisfied that your study is not a clinical trial that is to be conducted principally for the benefit of the manufacturer or distributor of the medicine or item being trialled. Participants injured as a result of treatment received as part of your study may therefore be eligible for publicly-funded compensation through the Accident Compensation Corporation (ACC).

Please don't hesitate to contact the HDEC secretariat for further information. We wish you all the best for your study.

Yours sincerely,

Mrs Helen Walker
Chairperson
Central Health and Disability Ethics Committee

Encl: appendix A: documents submitted
appendix B: statement of compliance and list of members

Appendix A
Documents submitted

Document	*Version*	*Date*
CV for CI	1	04 July 2017
Evidence of scientific review: Peer review confirmation by research team member.	1	08 March 2017
Protocol	1	04 July 2017
PIS/CF	1	04 July 2017
Evidence of scientific review: Review of the overall project by independent reviewer.	1	21 May 2017
Evidence of scientific review: Independent review of the overall project.	1	21 May 2017
Written consent form.	1	04 July 2017
Application		

Appendix B
Statement of compliance and list of members

Statement of compliance

The Central Health and Disability Ethics Committee:

- is constituted in accordance with its Terms of Reference
- operates in accordance with the *Standard Operating Procedures for Health and Disability Ethics Committees*, and with the principles of international good clinical practice (GCP)
- is approved by the Health Research Council of New Zealand's Ethics Committee for the purposes of section 25(1)(c) of the Health Research Council Act 1990
- is registered (number 00008712) with the US Department of Health and Human Services' Office for Human Research Protection (OHRP).

List of members

Name	*Category*	*Appointed*	*Term Expires*
Mrs Helen Walker	Lay (consumer/community perspectives)	01/07/2015	01/07/2018
Dr Angela Ballantyne	Lay (ethical/moral reasoning)	30/07/2015	30/07/2018
Dr Melissa Cragg	Non-lay (observational studies)	30/07/2015	30/07/2018
Dr Peter Gallagher	Non-lay (health/disability service provision)	30/07/2015	30/07/2018
Mrs Sandy Gill	Lay (consumer/community perspectives)	30/07/2015	30/07/2018
Dr Patries Herst	Non-lay (intervention studies)	27/10/2015	27/10/2018
Dr Dean Quinn	Non-lay (intervention studies)	27/10/2015	27/10/2018
Dr Cordelia Thomas	Lay (ethical/moral reasoning)	20/05/2017	20/05/2020

Unless members resign, vacate or are removed from their office, every member of HDEC shall continue in office until their successor comes into office (HDEC Terms of Reference)

http://www.ethics.health.govt.nz

A.2 Participant Information Sheet

Participant Information Sheet

Date Information Sheet Produced:

28 February 2017

Project Title

Performance Assessment of a Brain Computer Interface in Healthy People

An Invitation

Kia ora and Hello! My name is Usman and I am a PhD student at AUT. You are invited to take part in a study aiming to assess the performance of a device which detects brain-waves. This device is being developed for physical rehabilitation of people with stroke.

Please remember that:

- Your participation in this study is entirely voluntary (your choice). You do not have to take part in this study.
- If you do agree to take part you are free to withdraw at any time, without having to give a reason.

This information sheet will explain the research study. Please feel free to discuss with others and ask about anything that you do not understand.

What is the purpose of this research?

Human brain is made up of 100 billion small units called neurons. These neurons process information and generate commands. They communicate with each other by electrical waves. We can record these waves and relate them with our state of mind and responses. This method is called electroencephalography. One such wave is Motor Related Cortical Potential (MRCP). It can be recorded from the brain during the planning and execution of a movement. Thus, using this technique it is possible to tell when a person is planning a movement and is just about to execute the movement. You can say it is a very rudimentary form of 'Mind Reading'.

This 'Mind Reading' has potential applications in rehabilitation of people with stroke. Recent rehabilitation research has shown that by repeatedly stimulating the effected limb of a stroke patient while their brain is planning to move it, we can help them regain their ability to actually move that limb.

The problem, however, is that the devices currently used for detecting these brain waves are very expensive with a price tag of 31,000 NZ Dollars. In my PhD, I have proposed and prototyped a low cost device after consulting with experienced physiotherapists working in neurorehabilitation. However, we don't know yet how it performs in comparison to state-of-the-art devices. To assess its performance, I need your help.

The findings of this study will inform us whether our device is reliable enough to be used for detection of brain waves and at a later stage for rehabilitation purposes. The outcomes of this study will be presented to rehabilitation health professionals and researchers at conferences and published in rehabilitation and neuroscience journals.

How was I identified and why am I being invited to participate in this research?

You will have made contact with myself and your participation in this study is voluntary. You may be eligible for this study if you meet the following entry criteria:

- Aged over 18 years,
- Do not have any neurological disorders,
- Do not have epilepsy or history of seizures,
- Do not have a skull fracture or other known skull defects,
- Have not had a head injury or concussion within the last six months,
- Are not taking any medications that lower seizure threshold.

We will be recruiting 15 people to participate in the study.

How do I agree to participate in this research?

You can contact us on the details below if you wish to take part in the study. You will need to undergo a brief screening assessment and complete a consent form before participating in the research study.

What will happen in this research?

You will be contacted by us to make an appointment to attend the laboratory at the Health & Rehabilitation Research Institute, AUT North Campus, Akoranga Drive, Northcote. The study involves participating in 4 sessions, at least 48 hours apart.

In each session lasting about 45 minutes, the EEG Cap will be placed on your head. The cap can be seen in the below figure. A conductive gel made up of 'Table Salt' will be inserted into the electrodes. Two electrodes will be placed on your right leg after shaving, lightly abrading, and swiping with alcohol a small patch. Afterwards, you will have to perform 50 repetitions of right ankle dorsiflexion while sitting on a chair and 50 repetitions of stepping on a small pedestal placed in front of you while standing.

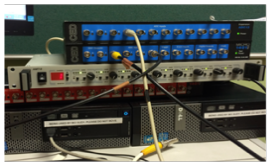


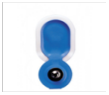

What are the discomforts and risks?

There is a small chance that the procedures being used in this study may make some people anxious. We will minimise this chance by making sure you are fully informed about what to expect prior to any procedure. We will monitor how you are feeling throughout each procedure and you are able to stop the session at any stage.

Small areas of skin on the leg will need to be shaved, lightly exfoliated and wiped with alcohol before the electrodes can be applied. This can cause a temporary stinging sensation and may cause minor, temporary skin reddening. Aloe Vera lotion will be offered as required.

The EEG Cap needs the conductive gel. Very small amount of gel will be applied to each electrode. This gel is made up of 'Table Salt' and is completely harmless. However, after removing the Cap, small patches of dried gel are left in your hair which can be removed by a usual hair wash.

How will these discomforts and risks be alleviated?

Disposable razors for hair removal and disposable blunt needles for application of gel will be used to minimize the risk of infection.

What are the benefits?

There are no direct benefits to you. However, by taking part in this study you are acting, as co-researcher and your contribution will help to develop a low cost rehabilitation device for people with stroke. You will also have the experience of participating in a modern research laboratory project.

What compensation is available for injury or negligence?

In the unlikely event of a physical injury as a result of your participation in this study, rehabilitation and compensation for injury by accident may be available from the Accident Compensation Corporation, providing the incident details satisfy the requirements of the law and the Corporation's regulations.

How will my privacy be protected?

Your confidentiality will be maintained in the following ways. Results will be identified by a code number only. Researchers will only have access to coded data, which will exclude their knowing your identity. All results will be pooled, so no names or any material that could identify you will be published or presented. Consent forms are locked away in a separate location from the data, so no association can be made between the results and the consent forms. After ten years, this data will be destroyed.

What are the costs of participating in this research?

The cost to you is your time. This would be a total of 3:30 hours over 4 separate sessions, excluding your travel time. Travel vouchers will be provided on each visit to compensate for your time and to assist with travel costs incurred for traveling to and from the laboratory.

What opportunity do I have to consider this invitation?

You are encouraged to take time to consider this invitation and to discuss it with family/whanau. If you have any questions, please feel free to contact one of the researchers listed below. If you would like to be considered for the study, please respond to this invitation within two weeks.

Will I receive feedback on the results of this research?

Yes. If you wish, a copy of your results and a short summary of the overall findings will be sent to you when the study is completed. It is usual for there to be substantial delay between the time of your participation and the time of receiving these results.

What do I do if I have concerns about this research?

Any concerns regarding the nature of this project should be notified in the first instance to the Project Supervisor, Dr Denise Taylor, denise.taylor@aut.ac.nz, 921 9680.

Concerns regarding the conduct of the research should be notified to the Executive Secretary of AUTEC, Kate O'Connor, *ethics@aut.ac.nz* , 921 9999 ext 6038.

Whom do I contact for further information about this research?

Researcher Contact Details:

Usman Rashid

Health & Rehabilitation Research Institute

AUT University

Private Bag 92006

Auckland 1142

urashid@aut.ac.nz

Project Supervisor Contact Details:

Dr Denise Taylor

Health & Rehabilitation Research Institute

AUT University

Private Bag 92006

Auckland 1142

921 9680

Denise.taylor@aut.ac.nz

A.3 Consent Form

Consent Form

Project title: ***Performance Assessment of a Brain Computer Interface in Healthy People***

Project Supervisor: **Professor Denise Taylor**

Researcher: **Usman Rashid, Dr Nada Signal, Dr Imran Khan Niazi.**

- ○ I have read and understood the information provided about this research project in the Information Sheet dated 28 February 2017.
- ○ I have had an opportunity to ask questions and to have them answered.
- ○ I understand that taking part in this study is voluntary (my choice) and that I may withdraw from the study at any time without being disadvantaged in any way.
- ○ I understand that if I withdraw from the study then I will be offered the choice between having any data or tissue that is identifiable as belonging to me removed or allowing it to continue to be used. However, once the findings have been produced, removal of my data may not be possible.
- ○ I am not suffering from any neurological disorders including epilepsy and seizures among others. Furthermore, I do not have a skull fracture, did not have had a head injury within the last six months and I'm not taking any medicine that lowers seizure threshold.
- ○ I agree to take part in this research.
- ○ I wish to receive a summary of the research findings (please tick one): Yes○ No○

Participant's signature : .....

Participant's name : .....

Date : .....

Note: The Participant should retain a copy of this form